CRIF1 and its Function in Anti-Viral Immunity

Debra Stefanie Lietke

München 2017

Aus der Abteilung für Klinische Pharmakologie
Leiter: Prof. Dr. med. S. Endres
Medizinische Klinik und Poliklinik IV
Klinikum der Ludwig-Maximilians-Universität München
Direktor: Prof. Dr. med. M. Reincke

CRIF1 and its Function in Anti-Viral Immunity

Debra Stefanie Lietke

Dissertation
zum Erwerb des Doktorgrades der Medizin
an der Medizinischen Fakultät
der Ludwig–Maximilians–Universität zu München

vorgelegt von
Debra Stefanie Lietke
aus Hannover

Mit Genehmigung der Medizinischen Fakultät
der Universität München

Berichterstatter: Prof. Dr. med Simon Rothenfußer

Mitberichterstatter: Prof. Dr. Anne Krug
Priv. Doz. Dr. Ursula Zimber-Strob

Mitbetreuung durch die
promovierten Mitarbeiter: Dr. rer. nat. Andreas Schmidt

Dekan: Prof. Dr. med. dent. Reinhard Hickel
Tag der mündlichen Prüfung: 27.04.2017

Contents

List of Figures

List of Tables

Chapter 1

Introduction

1.1 Background

1.1.1 The Human Immune System

Throughout evolution, humans and all their ancestors had to fight infection with different, similarly evolving pathogens in order to survive. Over time, a very powerful system developed to protect our tissue from the danger of invading microbes, virus-infected cells, or tumor cells. To achieve this protection, the immune system has to be able to distinguish between self and non-self, mounting a destructive response only against foreign microbes and malignant cells while keeping healthy tissue intact. Excess activation of the immune response can have disastrous consequences as autoimmune diseases illustrate. Therefore, precise recognition and a fine-tuned modulation of the triggered signal is necessary.

1.1.2 Innate and Adaptive Immunity

How does the immune system achieve powerful protection and precise modulation?
The immune system can be divided into two branches: innate and adaptive immunity.
The innate immune system was discovered as the first line of defense comprised on the cellular level of phagocytes like macrophages and neutrophils which effectively ingest and kill invading microbes [1].
Adaptive immunity is executed by lymphocytes that acquire highly specific antigen receptors through somatic rearrangement and hypermutation and clonal selection. Lymphocytes include CD4+ and cytotoxic T cells as well as B cells that turn into antibody producing plasma cells. Their selected receptors, each specific for one antigen, are stored for reactivation in the form of B and T memory cells.
Both branches were thought of as independent systems at first, one being unspecific and the other specific and generally sequential in order, until evidence suggested a costimulatory signal is necessary for lymphocytes to be activated [2].
In 1989, Charles Janeway proposed that conserved microbial products activating germline encoded receptors induce this costimulatory signal [3].

This pattern recognition theory was substantiated by the discovery of Toll-like receptors (TLRs) which both induce cytokines [4] and react to microbial stimuli [5]. Over the years, many more pattern recognition receptors (PRRs) that recognize so-called pathogen associated molecular patterns (PAMPs) were described [6]. These PRRs activate signaling cascades that lead to the production of inflammatory cytokines and chemokines. These in turn induce an anti-microbial response in both immune and non-immune cells. As a result, depending on the activated innate PRRs, different PAMPs initiate different types of adaptive response and modulate their magnitude and duration [7].

1.1.3 Cytokines and Interferons

Cytokines as Mediators of Immunity

Cytokines comprise a heterogeneous group of small proteins that are secreted by immune or non-immune cells to mediate an inflammatory reaction.

This reaction includes the induction of fever necessary to efficiently fight infection and protect host tissue. Induction of fever is mainly mediated by tumor necrosis factor-alpha (TNFα), interleukin (IL)-1, and IL-6. These cytokines also initiate the so-called acute-phase response which involves the production of inflammatory effector proteins in the liver, especially in response to bacterial infection. Acute-phase proteins like C-reactive protein (CRP) mimic the actions of antibodies, such as opsonization and complement activation, but have a broad specificity and require only cytokines for their production. TNFα, IL-1, and IL-6 also mobilize neutrophils from bone marrow to ingest (phagocytose) microbes, mobilize energy from fat and muscle cells to fight infection and induce dendritic cell maturation.

TNFα is produced by macrophages, natural killer cells (NK cells) and T cells to promote inflammation and endothelial activation. It triggers local containment of infection, but can also induce shock when released systemically.

IL-1 is secreted by macrophages and epithelial cells. It enables leukocyte transmigration and induces T cell and macrophage activation.

IL-6 is secreted by T cells, macrophages and endothelial cells and can, among other functions, induce T and B cell growth and differentiation.

Binding of interleukins to their receptors activates the JAK-STAT signal transduction pathway. This involves tyrosine kinase Janus kinases (JAKs)-mediated dimerization of signal transducer and activator of transcriptions (STATs) and their translocation to the nucleus, where they activate transcription of target genes [8].

As viruses use their host's replication machinery to replicate within host cells, a specific type of immune response is necessary to restrain infection. In mammals, birds and fish, interferons, aptly named for their ability to interfere with the viral replication cycle, play a major role for this response [9].

Antiviral Immunity and the Interferon System

Interferons can be separated into three groups; type I, II, and III IFNs.
The group of type I IFNs consists of several subtypes of interferon-α (IFN-α) and one interferon-β (IFN-β) and is expressed ubiquitously upon viral infection, for example in fibroblasts and epithelial cells. Leukocytes, especially plasmacytoid dendritic cells (pDCs), are responsible for producing systemic levels of IFN-α [10].
The three type III IFNs called interferon-λ (IFN-λ), IL-28A, and B are also ubiquitously expressed upon viral infection, their respective receptors being limited to specific tissue types [10].

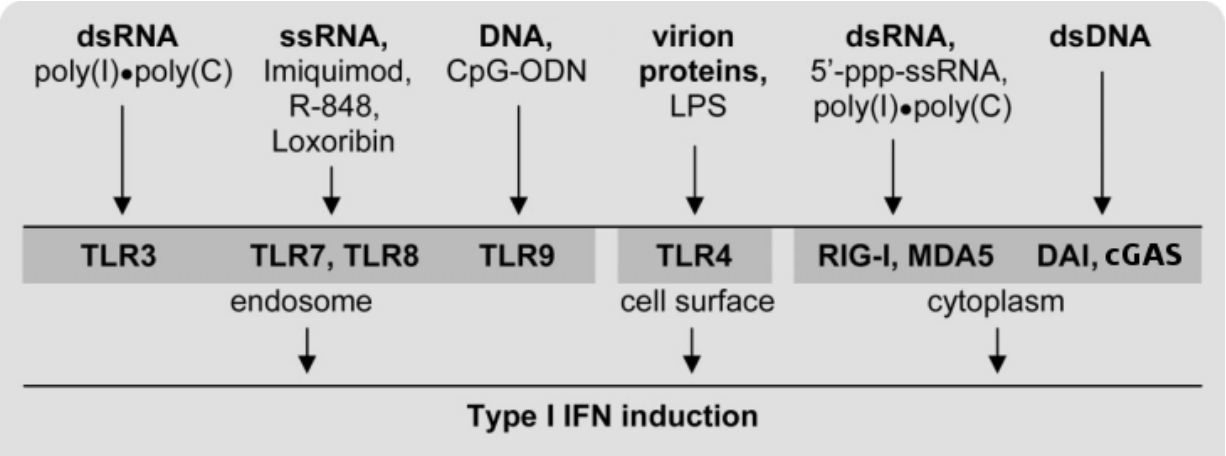

Figure 1.1: Type I IFN Induction by Different PAMPs

Viral pathogen associated molecular patterns or synthetic analogues induce interferon expression by binding to cytosolic receptors or Toll-like receptors on the cell surface or in endosomes (adapted from [10]).

Type I interferons are induced by PAMPs, especially by viral nucleic acids or their synthetic analogues (Figure 1.1).
Type II IFNs include only interferon-γ (IFN-γ), which is expressed by T cells and NK cells upon activation of their antigen receptor and stimulation with IL-12 and IL-18 [10].
For IFN-α and -β, induction requires signaling via IFN regulatory factor (IRF)-3 and -7. While IRF-3 is constitutively expressed at low levels, IRF-7 is induced by IFN-β, establishing a positive feedback loop of type I interferon induction [11] (Figure 1.2, right).
Both type I IFNs bind to the ubiquitously expressed dimeric IFN-α receptor (IFNAR). When assembled, IFNAR brings two Janus tyrosine kinases called JAK-1 and tyrosine kinase (TYK)-2 in close proximity so they phosphorylate each other as well as the transcription factors STAT-1 and -2. These transcription factors associate with IRF-9 to form a complex called interferon stimulated gene factor (ISGF)-3. This transcription factor translocates into the nucleus and activates transcription of interferon stimulated genes (ISGs) by binding to the interferon stimulated responsive element (ISRE) in their promoter region [12] (Figure 1.2, left).

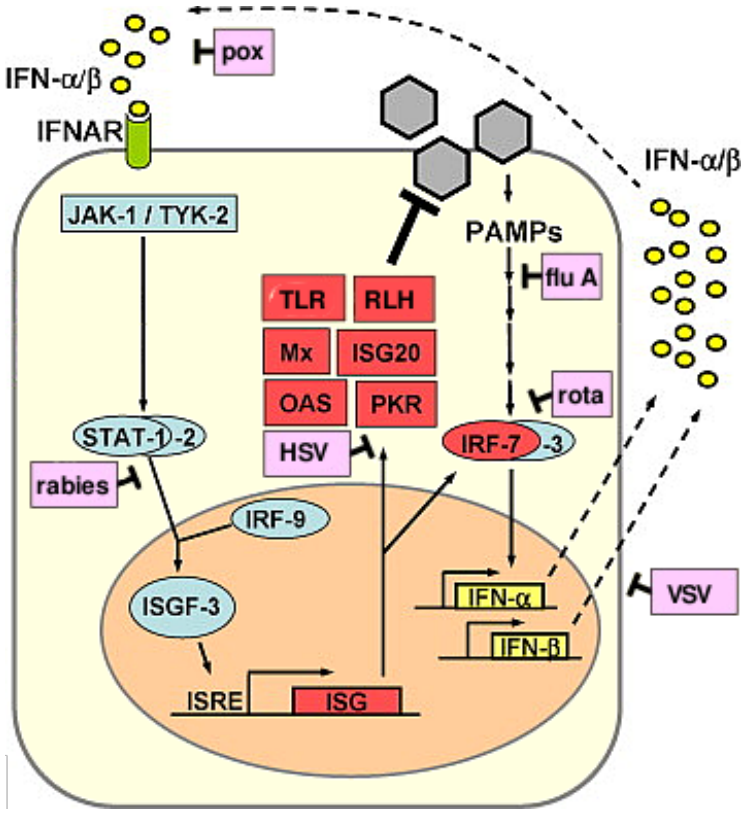

Figure 1.2: Type I Interferon Synthesis and Signaling

PAMPs induce IFN-α and -β via IRF-3 and -7. Both activate the IFN-α receptor and signal via a JAK/STAT-pathway to induce hundreds of ISGs to generate an antiviral state. Among these ISGs are antiviral signaling proteins like TLRs, RLHs and IRF-7 to boost viral recognition as well as antiviral effector genes like PKR and OAS. Pink boxes indicate points of viral interference (adapted from [13]).

Effects of Type I Interferons

There are hundreds of ISGs mediating the diverse context-specific effects of interferons. In uninfected cells without costimulation by PRRs, an antiviral state is induced to prevent the spread of infection. In infected cells, tumor suppressor p53 and other mechanisms induce apoptosis [14] and suppress proliferation [15].

The antiviral state includes upregulation of antiviral signaling proteins like TLRs, RIG-I-like helicases and IRF-7 to promote viral recognition [10]. Other ISGs are antiviral effector proteins like the myxovirus resistance (Mx) family, ISG20, OAS, or PKR (Figure 1.2, middle).

Mx proteins detect and bind viral nucleocapsid proteins, rendering them unavailable for viral replication [16].

OAS is activated by double-stranded RNA (dsRNA) and in turn activates the endoribonuclease RNase L, which cleaves viral genomic and messenger RNA as well as cellular messenger RNA (mRNA). This cleavage blocks viral replication, produces immunogenic stretches of ribonucleic acid (RNA) and even induces apoptosis [17].

Similarly, ISG20 is an exonuclease which cleaves single-stranded RNA (ssRNA) [18].

dsRNA activates PKR, which inhibits translation of viral and cellular mRNA and induces apoptosis [19].

In addition to these cell-intrinsic effects, type I IFNs have diverse effects on adaptive immune cells when combined with signaling via T cell receptor (TCR) or TLRs. In this context, they regulate NK cell and cytotoxic T cell function, thereby aiding the elimination of infected cells, and facilitate presentation of viral antigens to cytotoxic T cells by dendritic cells [15].

Viral Evasion Strategies

Viruses inhibit IFN signaling in a variety of ways. They can minimize stimulation of PRRs, block IFN induction, signaling or ISG activity, and even block host gene expression or protein synthesis altogether [20].

For example, influenza A virus NS1 protein inhibits IFN induction by sequestration of dsRNA [20], and rotavirus NSP1 protein degrades IRF-3 [21]. Vesicular stomatitis virus (VSV) matrix (M) protein blocks transcription unless a point mutation attenuates it, in which case efficient IFN production is restored [22]. Poxviruses secrete soluble IFN-binding proteins [23], rabiesvirus P protein inhibits STAT-1 and -2 [24], and Herpes simplex virus-1 protein US11 inhibits PKR [25].

The numerous strategies viruses have evolved to impede with the IFN response underline its importance for the infected host.

In conclusion, type I interferons are essential mediators linking innate and adaptive immunity for the eradication of viruses. Their induction by PRRs is discussed in the next section.

1.1.4 Pathogen Recognition by the Innate Immune System

The heterogenous group of PRRs can be divided into membrane-bound and cytoplasmic receptors.
Membrane-bound PRRs include the family of TLRs, which can be found on both the outer cell membrane and the endosomal membrane. TLRs can recognize both extracellular and endocytosed pathogens. Since they identify a wide range of pathogens, they play an important role in the activation of both innate and adaptive immune responses.
C-type lectin receptors (CLRs) comprise soluble and transmembrane proteins expressed by myeloid cells that can recognize pathogenic carbohydrate structures and danger-associated self molecules [26].
Cytoplasmic PRRs include NOD-like receptors (NLRs), which recognize different bacterial components [27], and cGAMP synthase (cGAS), which recognizes deoxyribonucleic acid (DNA) [28], and RLHs.

1.1.5 Toll-like Receptors and their Signaling

The family of TLRs comprises ten members in the human genome, nine of which are conserved in both humans and mice and have been well described, namely TLR1-9. They recognize a wide variety of bacterial, viral, fungal and protozoal compounds, a selection of which is summarized in table 1.1. Both their structure and activation process have been described in much detail. While TLR1, 2, 4, 5, and 6 reside on the cell surface, where they recognize PAMPs from bacteria, fungi, and protozoa and induce mainly inflammatory cytokines, TLR3, 7, 8, and 9 recognize mainly nucleic acid PAMPs from viruses and bacteria and are able to induce type I interferons in response to activation by their ligands [29].
When activated by their respective ligand, TLRs signal by recruiting different TIR-domain containing molecules which comprise myeloid differentiation factor 88 (MyD88), MyD88-adaptor like (MAL), TIR-domain-containing adaptor protein inducing IFN-beta (TRIF) and TRIF-related adaptor molecule (TRAM). These adaptor molecules activate a signaling cascade that culminates in the activation of transcription factors like nuclear factor kappa B (NF-κB), IRF-3 and -7 and mitogen-activated protein kinases (MAPKs). NF-κB and MAPK induce a large number of inflammatory cytokines like IL-6, IL-12p40 and TNFα. IRF-3 and -7 collaborate with NF-κB in the induction of type I interferons [29].

1.1.6 The Family of RIG-I-like Helicases

While TLRs and CLRs are only expressed in specialized immune cells, RLHs are ubiquitously expressed and enable non-immune cells to combat viral infection.
RIG-I, melanoma-differentiation-associated protein 5 (MDA5), and laboratory of genetics and physiology 2 (LGP2) form the family of RLHs.

TLR	ligand	origin
TLR1/2	triacyl lipopeptides	bacteria, mycobacteria, mycoplasma
TLR2	peptidoglycan	gram-positive bacteria
	lipoarabinomannan	mycobacteria
	alkylacylglycerol, lipophosphoglycan	protozoa
TLR2/dectin-1	β-glucans	fungi
TLR3	ssRNA, dsRNA	viruses
	poly(I:C) RNA	synthetic
TLR4	LPS	gram-negative bacteria
	glycoinositolphospholipids	protozoa
TLR4/CD14	glucuronoxylomannan	fungi
TLR5	flagellin	flagellated bacteria
TLR6/2	diacyl lipopeptides	mycoplasma
	lipoteichoic acid	gram-positive bacteria
TLR7	ssRNA	viruses, bacteria
	R848	synthetic
TLR8	ssRNA, dsRNA	RNA viruses
	R848	synthetic
TLR9	DNA with unmethylated CpG motifs	viruses, bacteria, protozoa

Table 1.1: TLRs and Their Ligands

Structure and Activation of RLHs

The structure and activation process of RIG-I were recently uncovered in more detail by crystallography. RIG-I is a large multidomain protein containing a DExD/H box RNA helicase domain and a C-terminal domain (CTD) connected via bridging helices [30]. Two caspase-recruitment domains (CARDs) required for downstream signaling make up the N-terminus. MDA5 and LGP2 share a similar structure, except that LGP2 lacks the CARDs. Lacking CARDs, LGP2 has been proposed as both a negative and a positive regulator of RIG-I and MDA5 signaling in different experimental settings [31, 32].

In order to efficiently detect viral RNA among an abundance of cellular or host RNA, binding of RIG-I or MDA5 requires characteristics unique to viral RNA. MDA5 is activated by long viral dsRNA or its synthetic analog polyinosinic:polycytidylic acid (poly(I:C)) [33]. The properties of synthetic or viral RNA to activate RIG-I have been the subject of extensive research. The minimal requirement seems to be a blunt-ended base-paired oligonucleotide of 10-20 base pairs (bps) with a 5'triphosphate. Some longer (>200bp) dsRNAs seem to bind as well, even without a triphosphate end, possibly by translocation of RIG-I along the RNA strand [30]. Host RNA is usually single-stranded and further secured from recognition by RIG-I through addition of a cap at the 5'-end before it is exported from the nucleus into the cytosol.

In the absence of a ligand, RIG-I is in an auto-repressed state characterized by an open and flexible conformation. Only the two CARDs form a rigid unit with the inner CARD

attached to the helicase domain (Figure 1.3). The CTD is flexibly linked to the helicase domain and free to bind its RNA ligand with high affinity.
Once it binds the RNA, it induces the closed conformation of the RIG-I molecule in which the helicase domain cooperatively binds the RNA strand and adenosine triphosphate (ATP). The tandem CARDs are released and become accessible for downstream signaling, but also for ubiquitination. Once they are ubiquitinated by tripartite motif E3 ligase (TRIM25) [34], reversion to the repressed state is blocked even if ATP is hydrolyzed or removed [30] (Figure 1.3).

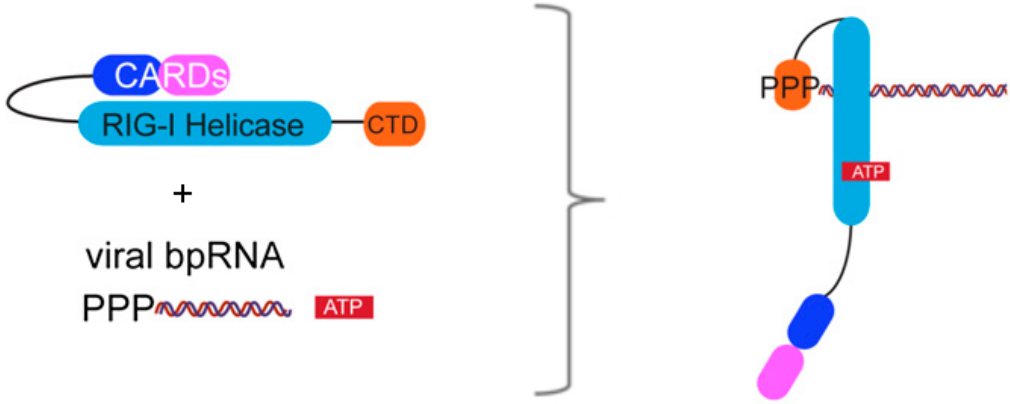

Figure 1.3: RIG-I Structure and Activation

The RIG-I molecule comprises a helicase domain, a CTD and two N-terminal CARDs attached to the helicase domain. Upon binding of triphosphate RNA and ATP, the CTD binds the 5' triphosphate containing end and, together with the helicase domain, binds the RNA. The CARDs are released from their binding to the helicase domain to activate downstream signaling (adapted from [30]).

Different viruses are differentially recognized by RIG-I and MDA5. While paramyxoviruses, VSV, influenza virus as well as the flaviviruses Japanese encephalitis virus and hepatitis C virus are recognized by RIG-I, picornaviruses such as encephalomyocarditis virus (EMCV) and Theiler's virus are sensed via MDA5 [35].
RIG-I has also been found to recognize RNA transcribed from viral DNA by cellular RNA polymerase III, thus it is able to sense not only RNA viruses, but also DNA viruses like Epstein-Barr virus (EBV) [36].

Signaling of RLHs

Upon activation by their respective ligand, RIG-I and MDA5 bind via homotypic CARD-CARD interaction to mitochondrial antiviral signaling protein (MAVS), also known as IPS1, Cardif, or VISA. MAVS is a transmembrane protein in the outer mitochondrial membrane that also contains a CARD on the cytosolic side. Intact mitochondrial function including a stable membrane potential $\Delta\Psi_m$ is necessary for MAVS signaling to occur [37] (Figure 1.4).

MAVS recruits TNF-receptor-associated factor (TRAF) family members TRAF2, 3 and 6. TRAF3, in concert with NF-κB essential modulator (NEMO), activates a kinase complex comprising of two kinases named TANK-binding kinase 1 (TBK1) and inducible IαB kinase (IKK)ϵ. These two kinases can phosphorylate IRF3 and 7, resulting in their formation of homo- or heterodimers and translocation to the nucleus, where they induce the expression of type I interferon (Figure 1.4, right).
TRAF2 and 6 activate a kinase complex composed of IKKα, IKKβ and NEMO, which phosphorylates the inhibitory protein inhibitor of NF-κBα (IκBα), thereby marking it for ubiquitin-dependent proteasomal degradation. This loss of inhibition enables the two NF-κB subunits p65 and p50 to translocate to the nucleus and induce the production of inflammatory cytokines (Figure 1.4, left).
These seemingly separate pathways leading to induction of type I IFNs and inflammatory cytokines intertwine. NF-κB is required for the initial induction of IFN-β, which in turn induces IRF-7 to create a positive feedback loop [38].

1.1.7 Mitochondria

Mitochondria are dynamic organelles that are vital for a wide range of cellular processes in virtually all eucaryotic cells. In addition to a number of important functions in metabolism and homeostasis, mitochondria are involved in various signaling cascades, including cell cycle control, apoptosis, and innate immune signaling [39].
According to the now widely recognized endosymbiotic theory, mitochondria developed from α-proteobacteria that became incorporated into eucaryotic cells in a symbiotic relationship [40]. This theory is substantiated by a number of mitochondrial characteristics that mark their bacterial origin: they possess a double membrane, their own circular genome, and 70S ribosomes similar to those of bacteria. Mitochondrial DNA encodes 13 proteins of the oxidative phosphorylation complex; however, most of the approximately 1500 proteins in the mitochondrial proteome are encoded in the nucleus [39].

Regulation of Metabolism

Mitochondria are well known for their critical role in providing energy to the cell in the form of ATP. The energy is transformed by the oxidation of nutrients through the five complexes of the respiratory chain located in the inner mitochondrial membrane (Figure 1.5). Complex I and II obtain electrons from NADH or $FADH_2$, respectively, and pass them on to complex III via coenzyme Q (CoQ). Complex III relays them via cytochrome C to complex IV, where the electrons react with O_2 and H^+ ions to form water. This electron transport chain is coupled to the movement of H^+ ions across the inner mitochondrial membrane at complexes I, III and IV, creating a proton gradient across the membrane. The energy of this proton gradient is utilized by complex V to phosphorylate adenosine diphosphate (ADP) to ATP, thus completing the process of oxidative phosphorylation (Figure 1.5).

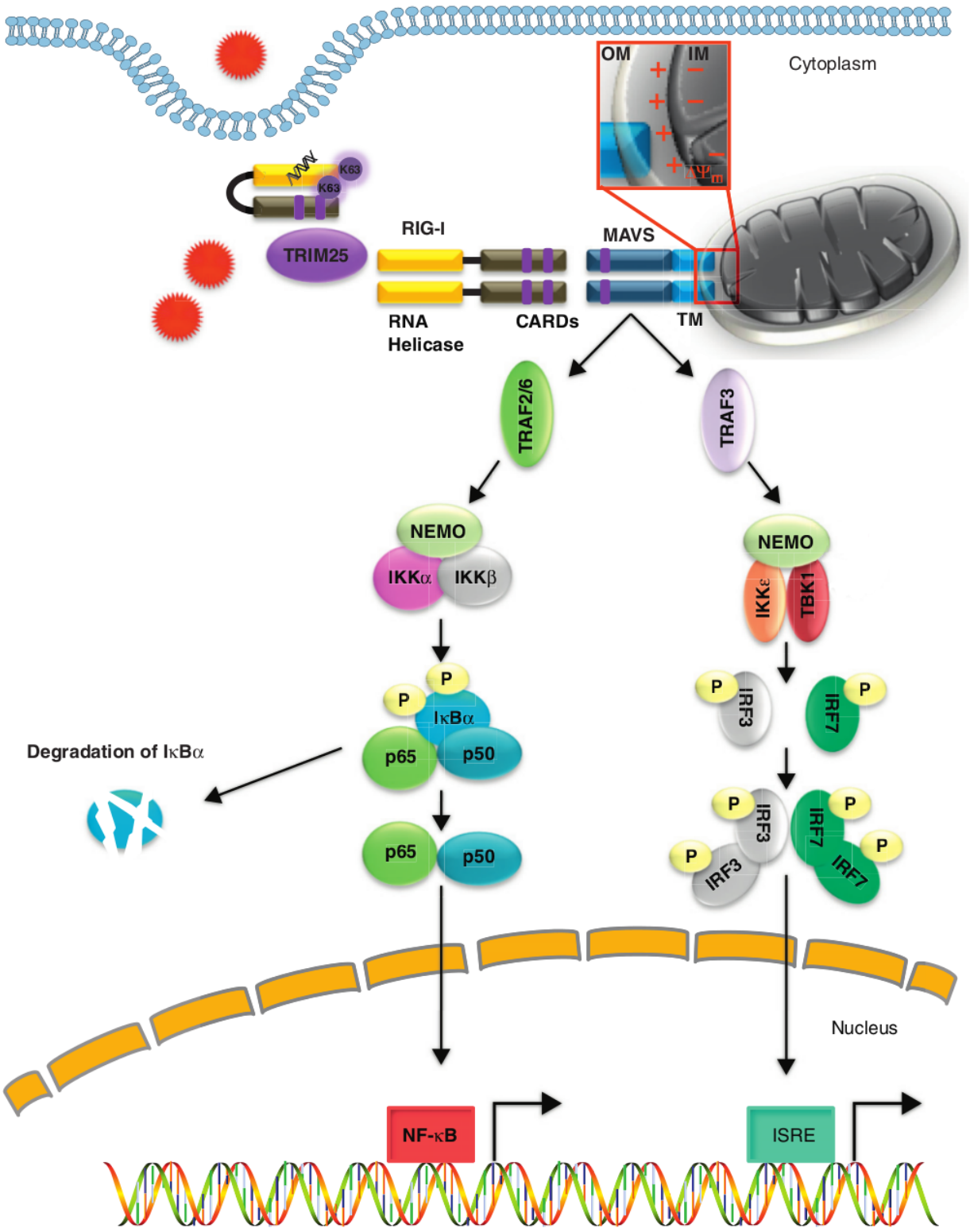

Figure 1.4: RLH-Mediated Signaling

Upon activation by viral RNA, RIG-I and MDA5 associate with MAVS through their CARDs. MAVS in turn activates TRAF3, which together with NEMO enables TBK1 and IKK-ϵ to phosphorylate IRF3 and 7, leading to the expression of type I interferon. TRAF2 and 6 induce inflammatory cytokines via NEMO, IKKα, IKKβ, and NF-κB ([38], simplified).

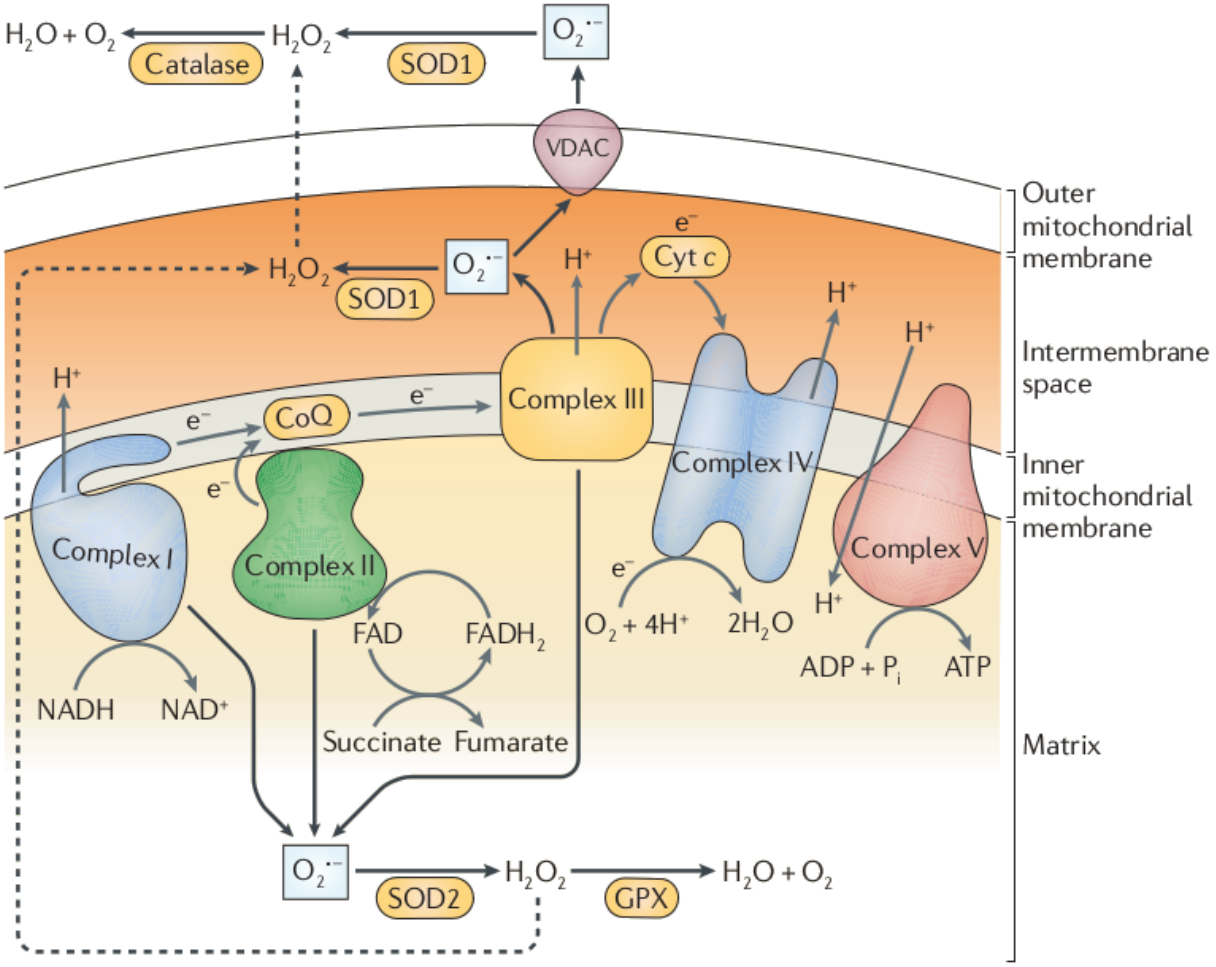

Figure 1.5: Mitochondrial Oxidative Phosphorylation and ROS Generation

Oxidative phosphorylation takes place at the inner mitochondrial membrane complexes I-V. These complexes transfer electrons from NADH or $FADH_2$ onto O_2 and H^+, yielding H_2O. Complexes I, III, and IV also expel H^+ across the inner membrane, creating a protein gradient that is used by complex V to create ATP. Superoxide ($O_2^{\cdot -}$) is produced by complexes I, II, and III and inactivated by mitochondrial or cytosolic enzymes ([41], simplified).

reactive oxygen species (ROS) like superoxide ($O_2^{\cdot -}$) are produced by electron leakage at complexes I, II, and III (Figure 1.5). They are inactivated by superoxide dismutase (SOD)1 and 2 together with cytosolic catalase and mitochondrial glutathione peroxidase (GPX). Interestingly, ROS are not merely a toxic byproduct, but have also been found to be tightly regulated signaling molecules with diverse functions [42].
Nutrient supply regulates metabolic rates [43], but mitochondrial dynamics also seem to play a role [44]. Mitochondrial dynamics include mitochondrial motility within the cell as well as two opposite processes called fusion and fission (Figure 1.6). Fusion is regulated by mitofusin (Mfn)1 and 2, while dynamin related protein 1 (Drp1) achieves fission. Both Mfn1 and 2 have been implicated in the control of metabolic rates [39].

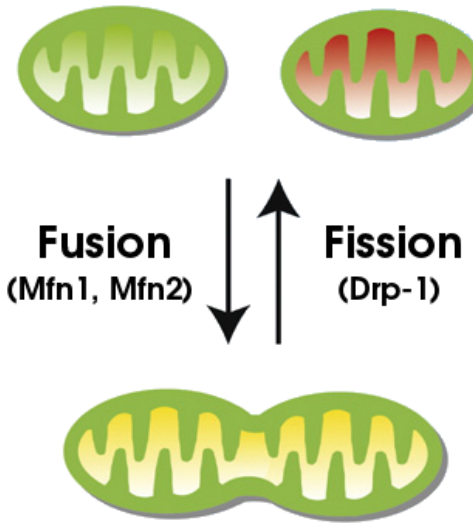

Figure 1.6: Mitochondrial Dynamics

Mitochondrial fusion and fission and involved mediator proteins (adapted from [45]).

In addition to their role in providing ATP, mitochondria are also involved in calcium homeostasis and a number of biosynthetical pathways such as the production of amino acids, lipids, nucleotides, and haem [41].

Mitochondria in Apoptosis and Cell Cycle Control

Mitochondria play a central role in the execution of programmed cell death also called apoptosis. For apoptosis, cell intrinsic or extrinsic signals activate a signaling network that recruits a family of cysteine proteases called caspases. These caspases initiate the breakdown of cells, by a process including DNA condensation and nuclear fragmentation, cell shrinkage and blebbing [46]. In the extrinsic activation pathway mediated by death receptors, mitochondria create an amplification loop, whereas in the intrinsic pathway initiated by cellular deprival or stress, mitochondria are the central regulators [46]. This regulation is achieved by the translocation of proapoptotic factors of the Bcl-2 family to the

mitochondria. There, they mediate the release of apoptogenic factors like cytochrome c, a caspase activator, from the mitochondria into the cytosol [39]. Mitochondrial fragmentation occurs during cell death, but seems to be a necessary step as well, as inhibiting Drp1 delays or inhibits cell death [47].

In addition to orchestrating apoptosis, mitochondria are tightly linked to cell cycle control. Mitochondria fragment before cell division [48]. Conversely, overexpression of Mfn2 not only stimulates mitochondrial fusion, but also induces cell cycle arrest via a Ras-dependent pathway [49], while many of the downstream signaling partners are also located at the mitochondria [39]. Furthermore, low energy conditions characterized by a high adenosine monophosphate (AMP) concentration induce a p53-dependent cell cycle arrest [50].

A reason for the involvement of mitochondria in several diverse signaling pathways might be their unique membrane composition. Formation of microdomains by lipid rafts or actin patches has been hinted to be an essential part of many signaling cascades [39].

Mitochondria in Innate Immunity

Mitochondrial integrity and function is essential for innate immune signaling and effector functions. The central adaptor protein for RLH-signaling, MAVS, is not only located on the outer mitochondrial membrane, but the mitochondrial environment seems to be essential for its function, as cytosolic mislocalization abrogates its signaling function [51].

Upon activation, MAVS self-assembles into large prion-like aggregates on the surface of the mitochondria that activate IRF-3 and induce assembly in native MAVS proteins [52].

A number of mitochondrial cofactors create the environment essential for MAVS signaling. For example, translocase of the outer membrane (TOM)70 and heat-shock protein (HSP)90 interact with and enable signaling of MAVS and TBK1 [53]. HSP90 might be necessary for assembly of MAVS into prion-like structures [52].

In addition to its role in mitochondrial fusion, Mfn2 has been shown to inhibit MAVS signaling [54]. Mfn1-induced fusion also appears to be necessary for assembling MAVS signaling complexes, suggesting a role for mitochondrial dynamics in antiviral signaling [55]. Elongation of mitochondria has been shown to occur during RLH signaling. Conversely, inhibiting fission boosts signaling, while inhibiting fusion stops it [56].

As some viruses replicate near mitochondrial membranes [57], antiviral signaling might have evolved around mitochondria to be in close proximity of viral replication and thereby increasing the likelihood to detect viral invasion early [41].

Furthermore, mitochondrial membrane potential has been reported as a requirement for the activation and signaling of MAVS [37].

The presence of ROS also appears to be a component of efficient signaling [58]. A rise in cellular ROS, caused by diminished autophagy for example, can augment RLH signaling [59]

In summary, mitochondria form a unique environment and establish an essential platform for antiviral signaling.

1.2 Objectives and Aims

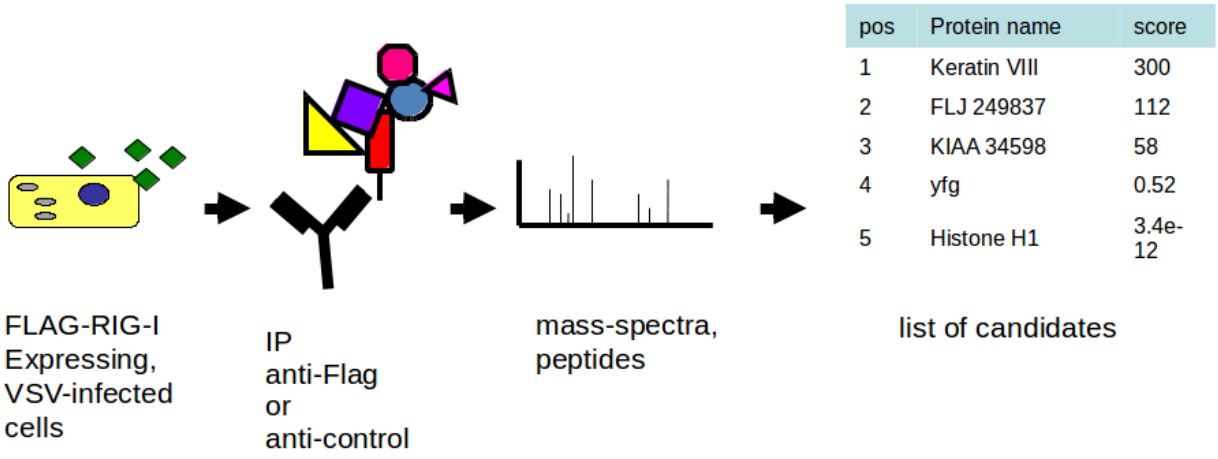

pos	Protein name	score
1	Keratin VIII	300
2	FLJ 249837	112
3	KIAA 34598	58
4	yfg	0.52
5	Histone H1	3.4e-12

Figure 1.7: Co-Immunoprecipitation and Analysis by Mass Spectrometry

Cells expressing flag-tagged RIG-I were infected with VSV, lysed and immunoprecipitated with anti-flag antibodies. The eluate was analyzed via mass spectrometry to produce a list of candidate RIG-I interacting proteins.

In order to identify new factors possibly involved in the RIG-I-dependent detection of viral infection, our group previously performed immunoprecipitation and subsequent analysis by mass spectrometry of proteins that co-immunoprecipitated with overexpressed RIG-I-FLAG in VSV-infected human embryonic kidney 293 (HEK293) cells (Dominik Höchter, data not shown).
These experiments (Figure 1.7) identified a list of potential RIG-I-interacting proteins. After eliminating known interactors, known artefacts, and viral proteins, two proteins, cytokine-responsive protein CR6-interacting factor 1 and RNA binding motif 10 remained as previously unknown, possibly new interactors of RIG-I.
RBM proteins contain an RNA recognition motif (RRM) which can perform various functions within the cell, like pre-mRNA processing, RNA stability, and translation. RNA binding motif 10 (RBM10) shows high sequence similarity to RBM5, which has been described as a cell cycle regulator. However, further functional data for RBM10 were lacking thus far [60].
CRIF1 is a functionally elusive protein for which different subcellular localizations and diverse interacting proteins had been described at the beginning of this project.
CRIF1 was first shown to interact with members of the growth arrest and DNA damage inducible protein 45 (GADD45) protein family and was therefore suggested to influence cell cycle progression and cell growth [61].
Further studies suggested a role in cell proliferation [62]. In addition, research found interactions with nuclear proteins including nuclear receptor 77 (NUR77) [63], androgen receptor [64], and nuclear respiratory factor 2 (NRF2) [65], thus claiming an essential

role for intestinal development [66]. Furthermore, CRIF1 was suggested to be a specific coactivator of STAT3 [67].
In preliminary experiments, both proteins had shown antiviral effects. Therefore, the aim of the present study was to investigate if CRIF1 or RBM10 indeed had a function in antiviral immunity and if so, by what mechanism. To this purpose, the following questions were explored:

- Do CRIF1 or RBM10 influence viral infection or cytokine response to infection?
- Are CRIF1 or RBM10 levels influenced by viral infection?
- How can CRIF1 or RBM10 exert an influence on antiviral signaling?
- Do CRIF1 or RBM10 specifically interact with RIG-I?

Chapter 2

Materials and Methods

2.1 Materials

2.1.1 Equipment

Technical equipment and instruments used in this study are listed in table 2.1. Reagents for molecular biology methods are listed in table 2.2, reagents for cell biology methods in table 2.3, and reagents for biochemical methods in table 2.4.
Plastic material for cell culture was obtained from Greiner (Frickenhausen, D), Falcon (Heidelberg, D), Becton Dickinson (Le Pont de Claix, F), Bibby Sterrilin (Stone, Staffordshire, GB) and Corning (Corning, USA).
Assays and kits used for the described experiments are listed in table 2.5.

Table 2.1: Technical Equipment and Instruments

Instrument	Vendor
AlphaImager HP®	Alpha Innotech (San Leandro, CA, USA)
Balance SBC 21®	Scaltec Instruments (Heiligenstadt, D)
Centrifuge 5415 R®	Eppendorf (Hamburg, D)
FACSCalibur® flow cytometer	BD Biosciences (San Diego, CA, USA)
FACSCanto II® flow cytometer	BD Biosciences (San Diego, CA, USA)
Ice machine	Ziegra (Isernhagen, D)
Incubator	Heraeus (Hanau, D)
ImageQuant® biomolecular imager	GE Healthcare (Little Chalfont, UK)
Lamin Air® (HB2448)	Heraeus (Hanau, D)
Leica LAS AF® microscope	Leica Microsystems (Wetzlar, D)
LightCycler 480®	Roche (Basel, CH)
Macrovue 2011® transilluminator	LKB (Bromma, SE)
Mini centrifuge MCF-2360	LMS (Löwen, B)
Multifuge 3L-R centrifuge	Heraeus (Hanau, D)
Multiplate reader Mithras LB940®	Berthold Technologies (Bad Wildbach, D)
NanoPhotometer®	Implen (München, D)

pH meter SB70P sympHony®	VWR (Darmstadt, D)
PowerPac 200® Power Supply	Bio-Rad (München, D)
Thermocycler T3®	Biometra (Göttingen, D)
Thermomixer® compact	Eppendorf (Hamburg, D)
Vortex mixer	Janke & Kunkel (Staufen, D)
Water filter	Millipore (Schwalbach, D)

Table 2.2: Reagents for Molecular Biology Methods

Reagents	Company
Real-time PCR	
LightCycler 480 Probes Master®	Roche (Basel, CH)
Reverse transcriptase H-	Fermentas (St. Leon-Roth, D)
Universal Probe Library® rt-PCR probes	Roche (Basel, CH)
In-vitro transcription	
Chloroform	Roth (Karlsruhe, D)
Ethanol	Roth (Karlsruhe, D)
Mini quick spin oligo columns	Roche (Mannheim, D)
Roti®-phenol/chloroform/isoamylalkohol	Roth (Karlsruhe, D)
Exo-Minus klenow DNA polymerase	Fermentas (St. Leon-Roth, D)
Exo-Minus klenow buffer	Fermentas (St. Leon-Roth, D)
RNase inhibitor	Fermentas (St. Leon-Roth, D)
Gel electrophoresis	
Agarose	Sigma-Aldrich (Steinheim, D)
Tris acetate	Roth (Karlsruhe, D)
Ethidium bromide	Sigma-Aldrich (Steinheim, D)
6x loading dye	Thermo Fisher (Waltham, MA, USA)
O'GeneRuler® DNA ladder mix	Thermo Fisher (Waltham, MA, USA)
PCR and quick change PCR	
Pfu polymerase and buffer	Fermentas (St. Leon-Roth, D)
DpnI	Fermentas (St. Leon-Roth, D)
Desoxyribonucleotides	Fermentas (St. Leon-Roth, D)
Plasmid construction	
AscI restriction enzyme	New England Biolabs (Ipswich, MA, USA)
FseI restriction enzyme	New England Biolabs (Ipswich, MA, USA)
NEBuffer 4	New England Biolabs (Ipswich, MA, USA)
Calf intestine alkaline phosphatase	Promega (Madison, WI, USA)
T4 DNA ligase	Fermentas (St. Leon-Roth, D)
DH5α	Invitrogen (Carlsbad, CA, USA)

Luria Bertani (LB) broth	Roth (Karlsruhe, D)
Potassium acetate (KAc)	Roth (Karlsruhe, D)
Manganese chloride ($MnCl_2$)	Roth (Karlsruhe, D)
Rubidium chloride (RbCl)	Roth (Karlsruhe, D)
Calcium chloride ($CaCl_2$)	Roth (Karlsruhe, D)
Morpholinepropanesulfonic acid (MOPS)	Thermo Fisher (Waltham, MA, USA)
LB agar	Roth (Karlsruhe, D)
Ampicillin	Roth (Karlsruhe, D)
Kanamycin	Sigma-Aldrich (Steinheim, D)

Table 2.3: Reagents for Biochemical Methods

Reagents	Vendor
Immunoprecipitation and western blot	
Monoclonal anti-flag antibody clone M2 (mouse)	Sigma-Aldrich (Steinheim, D)
Anti-cMYC antibody 9E10	Gentaur (Kampenhout, B)
Rb pAB to RBM10 ab72423	Abcam (Cambridge, UK)
Anti-rabbit IgG, HRP-linked Ab	Cell Signaling Technology (Danvers, MA, USA)
Anti-mouse IgG, HRP-linked Ab	Cell Signaling Technology (Danvers, MA, USA)
Anti-FLAG M2 Affinity Gel beads	Sigma-Aldrich (Steinheim, D)
Ammonium persulfate (APS)	Sigma-Aldrich (Steinheim, D)
Beta-mercaptoethanol	Bio-Rad (München, D)
Blotting paper	Schleicher & Schuell (Düsseldorf, D)
Ethylenediaminetetraacetic acid (EDTA)	Roth (Karlsruhe, D)
Glycin	Roth (Karlsruhe, D)
Laemmli sample buffer	Bio-Rad (München, D)
Magnesium chloride ($MgCl_2$)	Roth (Karlsruhe, D)
Methanol	Merck (Darmstadt, D)
Milk powder	Roth (Karlsruhe, D)
Prestained protein molecular weight marker	Fermentas (St. Leon-Roth, D)
Immobilon-P® PVDF transfer membrane	Millipore (Schwalbach, D)
Rotiphorese® Gel 30	Roth (Karlsruhe, D)
Sodium chloride (NaCl)	Roth (Karlsruhe, D)
sodium dodecyl sulfate (SDS)	Roth (Karlsruhe, D)
Tetramethylethylenediamine (TEMED)	Roth (Karlsruhe, D)
Tris(hydroxymethyl)aminomethane (Tris)	Roth (Karlsruhe, D)
Tris-hydrochloride (Tris-HCl)	Roth (Karlsruhe, D)
Polysorbate 20 (Tween 20)	Roth (Karlsruhe, D)
WB substrate reagent A, B	BD Biosciences (San Diego, CA, USA)
Cell lysis	
Beta-glycerophosphate	Sigma-Aldrich (Steinheim, D)
Glycerol	Roth (Karlsruhe, D)

Sodium orthovanadate	Sigma-Aldrich (Steinheim, D)
Nonidet P-40 (NP40)	Fluka Biochemika (Buchs, CH)
Protease inhibitor cocktail	Sigma-Aldrich (Steinheim, D)
Phenylmethylsulfonyl fluoride (PMSF)	Fluka Biochemika (Buchs, CH)
ELISA	
Bovine serum albumine (BSA)	Roth (Karlsruhe, D)
Phosphate-buffered saline (PBS)	PAA (Linz, A)
Substrate reagent	BD Biosciences (San Diego, CA, USA)
Luciferase assay	
Passive lysis buffer	Promega (Mannheim, D)
Luciferin	Biosynth (Staad, CH)
Tricine	Sigma-Aldrich (Steinheim, D)
Magnesium sulfate ($MgSO_4$)	Sigma-Aldrich (Steinheim, D)
Sodium hydroxide (NaOH)	Roth (Karlsruhe, D)
Magnesium carbonate hydroxide ($(MgCO_3)4Mg(OH)2.5H_2O$)	Sigma-Aldrich (Steinheim, D)
Dithiothreitol (DTT)	Roth (Karlsruhe, D)
Adenosine triphosphate (ATP)	Sigma-Aldrich (Steinheim, D)
Acetyl coenzyme A	Sigma-Aldrich (Steinheim, D)

Table 2.4: Reagents for Cell Biology Methods

Reagents	Vendor
Cell culture	
Aqua ad iniectabilia	Braun (Melsungen, D),
Dulbecco's modified eagle medium (DMEM)	Sigma-Aldrich (Steinheim, D)
fetal bovine serum (FBS)	GibcoBRL (Paisley, GB)
L-Glutamine	PAA (Linz, A)
OptiMEM®	Invitrogen (Carlsbad, CA, USA)
Penicillin	PAA (Linz, A)
Phosphate-buffered saline (PBS)	PAA (Linz, A)
Streptomycin	PAA (Linz, A)
Trypan blue	Sigma-Aldrich (Steinheim, D)
Cryoconservation	
Dimethyl sulfoxide (DMSO)	Roth (Karlsruhe, D)
Isopropanol	Roth (Karlsruhe, D)
Mr. Frosty® freezing container	Thermo Fisher (Waltham, MA, USA)
Viability assay	
CellTiter-Blue® cell viability assay	Promega (Madison, WI, USA)

Transfection	
GeneJuice® transfection reagent	EMD chemicals (San Diego, CA, USA)
Lipofectamine RNAiMax®	Invitrogen (Carlsbad, CA, USA)
Poly(I:C)	Amersham/GE Healthcare
Flow cytometric cell cycle analysis	
Methanol	Merck (Darmstadt, D)
Propidium iodide (PI)	Sigma-Aldrich (Steinheim, D)
Ribonuclease A	Sigma-Aldrich (Steinheim, D)
Plaque assay	
LE agarose	Biozym Scientific (Hessisch Oldendorf, D)
Crystal violet	Sigma-Aldrich (Steinheim, D)
Formaldehyde	Roth (Karlsruhe, D)
Ethanol	Roth (Karlsruhe, D)
Immunofluorescence microscopy	
Crif1 antibody M-222	Santa Cruz Biotechnology (Santa Cruz, CA, USA)
Alexa Fluor® 488 chicken anti-rabbit IgG	Invitrogen (Carlsbad, CA, USA)
DAPI	Sigma-Aldrich (Steinheim, D)
HardSet mounting medium	Vector Laboratories (Burlingame, CA, USA)
Hoechst 33342 nucleic acid stain	Invitrogen (Carlsbad, CA, USA)
MitoTracker® Green FM	Invitrogen (Carlsbad, CA, USA)
MitoTracker® Red CMXRos	Invitrogen (Carlsbad, CA, USA)

Table 2.5: Assays and Kits

Assay	Vendor
ELISA Substrate Solution	BD Biosciences (San Diego, CA, USA)
GeneJet Plasmid Miniprep Kit	Thermo Fisher (Waltham, MA, USA)
JETQuick Spin Columns	GENOMED (Löhne, D)
Human IP-10 ELISA	BD Biosciences (San Diego, CA, USA)
Human IL-6 ELISA	BD Biosciences (San Diego, CA, USA)
Luciferase Assay Kit	BioThema (Handen, S)
MEGAscript T7 Kit	Ambion (Kassel, D)
PeqGOLD total RNA kit	PEQLAB (Erlangen, D)
Plasmid Maxi Kit	QIAGEN (Hilden, D)
RNeasy mini RNA extraction kit	QIAGEN (Hilden, D)

2.1.2 Media, Solutions and Buffers

Cell lines were cultured in DMEM medium containing 100IU/mL penicillin, 100μg/mL streptomycin, 1.5mM L-glutamine and 10% FBS.
DH5α (Invitrogen) were cultured in LB broth or on LB agar, with 100μg/mL ampicillin or 50μg/mL kanamycin if required for selection.
Other solutions or buffers are listed in table 2.6.

Table 2.6: Solutions and Buffers

Running Buffer 192mM glycin 25mM tris-base 0.1% SDS in aqua dest.	Wet transfer Buffer 192mM glycin 25mM tris-base 20% methanol in aqua dest.	TBE Buffer 89mM tris 89mM boric acid 2mM EDTA pH 8.3 in aqua dest.
Lysis Buffer 20mM tris-HCl (pH 7.5) 150mM NaCl 1.5mM MgCl2 10% glycerol 0.2% NP40 0.5mM EDTA 20MM beta-glycerophosphate 1mM sodium orthovanadate 1mM PMSF 10g/L Protease Inhibitor Cocktail	PBSTween 0.1% Tween 20 in PBS Hybridization Buffer 10mM tris-base 1mM EDTA pH 7.4 in aqua dest	Blocking Buffer 5% milk powder in PBSTween Crystal Violet Solution 0.5% crystal violet 0.8% NaCl 0.5% formaldehyde 50% ethanol in aqua dest.
tris-buffered saline (TBS) 50 mM Tris-Cl, pH 7.5 150 mM NaCl in aqua dest.	TFB1 30mM KAc 50mM $MnCl_2$ 100mM RbCl 10mM $CaCl_2$ 15% glycerol in aqua dest. to pH 5.8 with HAc	TFB2 10mM MOPS/NaOH (pH 7) 75mM $CaCl_2$ 10mM RbCl 15% glycerol in aqua dest.

2.1.3 Cells and Viruses

The human embryonic kidney cell line Hek293 was acquired from the American type culture collection (ATCC).

The human melanoma cell line 1205Lu was obtained from M. Herlyn (Wistar Institute, Philadelphia, PA, USA).
Baby hamster kidney fibroblast cell line BHK-21 was kindly provided by Prof. Conzelmann (Max von Pettenkofer Institute (MPI), Munich, D)
TLR7- and TLR9- cells used for luciferase assays are HEK293 cell lines stably overexpressing TLR-7 or -9, respectively, as well as an NF-κB-controlled firefly luciferase reporter gene. Both stable cell lines were kindly provided by Prof. Simon Rothenfusser, Ludwig-Maximilians-Universität (LMU), Germany.
Wildtype VSV Indiana strain expressing green fluorescent protein (GFP) [68] and IFN-inducing VSV mutant M51R (VSV M) [69] expressing GFP were kindly provided by Dr. Oliver Ebert from Technical University Munich (TUM), Germany.
Modified vaccinia Ankara (MVA) GFP virus [70] was kindly provided by Dr. Gerd Sutter, TUM, Germany.
Sendai virus (SeV) Cantell strain was purchased from Charles River Laboratories (Wilmington, MA, USA).

2.1.4 Oligonucleotides

So-called small interfering RNAs (siRNAs) are short double-stranded RNA molecules that interfere with the expression of specific genes with a complementary sequence. Synthetical siRNAs are used to induce RNA interference (RNAi) — the knockdown of almost any protein when transfected to the cytoplasm of mammalian cells. siRNAs used in this study were obtained from Eurofins MWG (Ebersberg, D). Table 2.7 lists their sequences and target proteins. If not stated otherwise, siRNAs were designed using the Dharmacon siRNA center (now Thermo Fisher).
In addition, polymerase chain reaction (PCR) primers used to clone protein inserts from one expression vector to another are listed in table 2.8. FA primers were designed to produce a recognition site for the restriction enzymes FseI at the 5' end and AscI at the 3' end so that the insert could be easily transferred to vectors containing these two restriction sites while M primers are primers for site-directed mutagenesis (also see plasmids listed in table 2.10).
In order to quantify RNA levels of a gene of interest in a cell population relative to a housekeeping gene, quantitative real time reverse transcription PCR (qRT-PCR) was used. Primers were designed using the Roche Universal Probe Library system. Table 2.9 summarizes their targets and sequences.

2.1.5 Plasmids

All plasmids used are listed in table 2.10.
Empty pCS2 and pcDNA5 vectors were kindly provided by Prof. Olaf Stemmann, Department of Genetics, University of Bayreuth, Germany. pEGFP-CRIF1-C3 was obtained from Dr. Martin Müller from the German Cancer Research Center, Heidelberg, Germany [77]. pOTB7-RBM10 was purchased from imaGenes (Berlin, D).

Table 2.7: siRNAs

SiRNA	Target	Sequence 5'-3'	Reference
CO4	none	GCG CUA UCC AGC UUA CGU A	[71]
siLamin A	Human Lamin A	AAC UGG ACU UCC AGA AGA ACA	[72]
siMRE11	Human MRE11	UGG CUA AUG ACU CUG AUG AUA	
siGL2	Luciferase GL2	CGU ACG CGG AAU ACU UCG A	[73]
siRIG-I	Human RIG-I 3'UTR	CCU UAA CAA UCU ACU GAA A	[74]
siRIG-I	Human RIG-I	AUC ACG GAU UAG CGA CAA A	[71]
siMAVS	Human MAVS	CCA CCU UGA UGC CUG UGA A	[75]
siMDA5	Human MDA5	GUA UCG UGU UAU UGG AUU A	[75]
siCRIF1	Human CRIF1	GCA GAG UGC AUG GCC AAG A	
siCRIF1-2	Human CRIF1	CCA CAG AUG AUU GUG AAC U	
siCRIF1-3	Human CRIF1 3'UTR	CUU UGU CCC UUC CCA AUA A	
siRBM10	Human RBM10	GCC AGU CGU AUA CCA UCA U	
siRBM10-2	Human RBM10	CCU GGC AUC UAC CAA CAA U	
siIFNAR 0534	Human IFNα receptor	UCC UCC AGA AGU ACA UUU A	[74]
siIRF3	Human IRF3	AAA UCU ACG AGU UUG UGA A	
siSTAT3	Human STAT3	GGG ACC UGG UGU GAA UUA U	
siCKII	Human CKII	GAU CCA CGU UUC AAU GAU A	[76]
siGADD45γ	Human GADD45γ	CAG CCA AAG UCU UGA ACG U	

The sequence depicted is the 19-nt portion in the sense strand of the targeted mRNA. 3' overhangs were dTdT.

Table 2.8: PCR Primers

Primer	Target	Sequence 5'-3'
FA211	Human RBM10 variant 1 forward	attaGGCCGGCCaATGGAGTATGAAAGACGTGG
FA212	Human RBM10 variant 1 reverse	attaGGCGCGCCaCTGGGCCTCGTTGAAGC
FA213	Human CRIF1 forward	attaGGCCGGCCaATGGCGGCGTCCGTGC
FA214	Human CRIF1 reverse	attaGGCGCGCCaGGAGCTGGGTGCCCCA
Cl281	Human δ MTS CRIF1 forward	attaGGCCGGCCaatgGGACCCCGGTGGCCAG
M284	Human CRIF1 mutation R26A forward	GGCCCCGGGTTCCCGTGGCTACgcGGCGCGGCCGCCCCCGCGC
M285	Human CRIF1 mutation R26A reverse	GCGCGGGGGCGGCCGCGCCgcGTAGCCACGGGAACCCGGGGCC

Upper-case letters indicate sequences coding for restriction sites or target annealing. Lower-case letters mark base pairs added for methodological reasons.

Table 2.9: qRT-PCR Primers

Primer	Target	Sequence 5'-3'	Probe #
3_huIFNbeta_left	Human IFNβ	cgacactgttcgtgttgtca	25
4_huIFNbeta_right	Human IFNβ	gaggcacaacaggagagcaa	
91_RBM10_left	Human RBM10	ccaagcccaagatcaatgag	76
92_RBM10_right	Human RBM10	ttctctcggcgtttgaagtt	
93_MAVS_left	Human MAVS	tgtctgccagcacagtcc	32
94_MAVS_right	Human MAVS	gagctgctggggtctcct	
95_CRIF1_left	human CRIF1	ctggccgaagagcagaag	32
96_CRIF1_right	Human CRIF1	tcttggccatgcactctg	
113_huRIG-I left	Human RIG-I	tggaccctacctacatcctga	69
114_huRIG-I right	Human RIG-I	ggcccttgttgtttttctca	
119_huSTAT3 left	Human STAT3	cccttggattgagagtcaaga	14
120_huSTAT3 right	Human STAT3	aagcggctatactgctggtc	
129_huCKII left	Human CKII	gcgccaatatgatgtcagg	74
130_huCKII right	Human CKII	tggaacaggcatcccaag	

Plasmids containing RIG-I, MAVS, MDA5, pTBK1, RIG-I-CARD and pIRF3-5D were kindly provided by Prof. Katherine Fitzgerald, University of Massachusetts Medical School, USA. pNEMO was obtained from Prof. Karl-Klaus Conzelmann, MPI, Munich, Germany. All other plasmids were cloned from the empty vectors and inserts listed above and in table 2.10.

2.2 Methods

2.2.1 Molecular Biology Methods

Molecular biology provides techniques of RNA and DNA preparation and manipulation. Genes of interest can be cloned and modified by PCR, cut and pasted by enzymatic digestion and ligation, separated by electrophoresis, propagated as plasmids in bacteria, and inserted into expression vectors. Cells can be stimulated with artificially transcribed nucleic acids and mRNA expression levels monitored by qRT-PCR. All these tools are essential to study protein and cellular function.

Expression Cloning

Expression cloning is used to study the function of a protein. DNA coding for the protein is inserted into a circular expression vector using PCR or restriction enzymes. The expression vector can then be inserted and expressed, for example in a mammalian cell

Table 2.10: Plasmids

Plasmid	Insert	Vector	Tag
pcDNA5	none	pcDNA5-FRT/TO-FA	none
p5-mCherry	none	pcDNA5-FRT/TO-FA-mCherry	C-term. mCherry
p5-GFP	none	pcDNA5-FRT/TO-FA-GFP	C-term. GFP
p5-flag	none	pcDNA5-3xflag-FRT/TO-FA	N-term. flag
pCS2-myc	none	pCS2-MYC-FA	N-term. myc
p5-RIG-I	huRIG-I	pcDNA5-FRT/TO-FA	none
p5-RIG-I-mCherry	huRIG-I	pcDNA5-FRT/TO-FA-mCherry	C-term. mCherry
p5-RIG-I-GFP	huRIG-I	pcDNA5-FRT/TO-FA-GFP	C-term. GFP
p5-RIG-I-flag	huRIG-I	pcDNA5-3xflag-FRT/TO-FA	N-term. flag
p5-MAVS	huMAVS	pcDNA5-FRT/TO-FA	none
p5-MAVS-mCherry	huMAVS	pcDNA5-FRT/TO-FA-mCherry	C-term. mCherry
p5-MAVS-flag	huMAVS	pcDNA5-3xflag-FRT/TO-FA	N-term. flag
p5-MDA5	huMDA5	pcDNA5-FRT/TO-FA	none
pEGFP-CRIF1-C3	huCRIF1	pEGFP-C3	N-term. GFP
pCS2-CRIF1-myc	huCRIF1	pCS2-MYC-FA	N-term. myc
p5-CRIF1	huCRIF1	pcDNA5-FRT/TO-FA	none
p5-CRIF1-mCherry	huCRIF1	pcDNA5-FRT/TO-FA-mCherry	C-term. mCherry
p5-CRIF1-flag	huCRIF1	pcDNA5-3xflag-FRT/TO-FA	N-term. flag
p5-CRIF1-δMTS-mCherry	huCRIF1-δMTS	pcDNA5-FRT/TO-FA-mCherry	C-term. mCherry
p5-CRIF1-R26A-mCherry	huCRIF1 mut R26A	pcDNA5-FRT/TO-FA-mCherry	C-term. mCherry
pOTB7-RBM10	huRBM10	pOTB7	none
p5-RBM10	huRBM10	pcDNA5-FRT/TO-FA	none
p5-RBM10-GFP	huRBM10	pcDNA5-FRT/TO-FA-GFP	C-term. GFP
pTBK1	huTBK1	pcDNA3-flag	flag
pNEMO	huNEMO	pGCAGGS	N-term. flag
RIG-I-CARD	huRIG-I-CARD	pEF-Bos-flag	N-term. flag
pIRF3-5D	huIRF3-5D	pCMV-flag	flag

line. Restriction enzymes are bacterial enzymes that can degrade foreign, e.g. viral, DNA by recognizing and cutting specific palindromic sequences. As they do not degrade other parts of the DNA, a desired sequence can be cut precisely and pasted into a new vector using the enzyme T4 ligase. An expression vector requires an origin of replication and a selection gene such as an antibiotic resistance for selective amplification in bacteria, as well as a multiple cloning site to add a gene of interest. All vectors used here also contain a promotor for expression of the protein in mammalian cells. Inserts were cloned without a stop codon so n- or c-terminal tags as contained in the vector would be fused to the inserted protein when expressed.
To construct the expression vectors used here, the FseI-AscI (FA) system was used. With a restriction site for FseI at the 5'-end of the insert and AscI at the 3'end, inserts can be transferred easily into all vectors containing those same restriction sites as indicated by FA in their name.
Restriction sites for FA cloning of full-length CRIF1 and RBM10 as well as the mitochondrial targeting sequence (MTS) deletion mutant δMTS-CRIF1 were introduced via PCR. RIG-I, MDA5 and MAVS were already available in vectors containing FA restriction sites. To open restriction sites in the vector and insert for ligation, 1μg DNA was cut using 2U/50μL FseI, 10U/50μL AscI in 50μL in NEBuffer 4 (New England Biolabs) diluted with ddH_2O. The enzyme-DNA-mixture was incubated at 37 $^\circ$C for one hour before the enzymes were inactivated by heating them to 65 $^\circ$C for 20 minutes. To prevent religation of the vector, it was incubated with 1μL calf intestine alkaline phosphatase (CIAP) for another hour at room temperature (RT) to remove 5'-phosphate groups. Insert and linearized vector were each purified using agarose gel electrophoresis. Then the bands of interest were cut out, dissolved and extracted using JETQuick Spin Columns (GENOMED) according to the manufacturer's protocol.
For ligation, 0.5μL of the linearized and purified vector were incubated for one hour at RT with 16μL insert, 2μL ligase buffer and 1μL T4 ligase. Afterwards, 10μL of the ligation mixture were transformed into heat-competent DH5α.
After transformation, bacteria were plated on ampicillin selection plates and incubated at 37 $^\circ$C overnight. Colonies were picked the next day, amplified by culture in LB broth and plasmids were purified by Plasmid Miniprep (Thermo Fisher) according to the manufacturer's protocol. To ensure the correct insert, rotation and sequence, plasmids were tested via restriction digestion and sequencing (MWG value read tubes).

Polymerase Chain Reaction

Polymerase Chain Reaction (PCR) is an enzymatic reaction to amplify stretches of DNA and to modify desired sequences. It requires cycles of heating and cooling during which double-stranded DNA is melted and replicated with a heat-stable DNA polymerase. Primers with sequences complementary to the ends of the region of interest initiate the reaction and can be used to add changes to the sequence, like the addition of restriction sites. As newly produced DNA also serves as a template in following cycles, exponential amplification of the desired sequence is achieved.

PCR was utilized to retrieve inserts from their original vectors and to add the desired restriction sites for FseI and AscI at at the 5'- and 3'-end, respectively, using the primers listed in table 2.8.
For the reaction, 100ng of template DNA were mixed with 5μL Pfu buffer Mg^{2+} (Fermentas), 1μL deoxyribooligonucleotides (dNTPs), 1.25μL 5'- and 3'-primer each (10pmol/μL), 0.5μL Pfu polymerase (Fermentas) and dH_2O up to a total of 50μL. In a thermocycler, the reaction mix was heated to 95 $^\circ$C for two minutes and then underwent the following cycles 20-35 times: denaturing the double-stranded DNA by heating to 95 $^\circ$C for 45 seconds, annealing the primers by cooling down to at least 3 $^\circ$C below the melting temperature of each primer for 45 seconds, then elongating the sequence of interest during one minute per kilobase (kb) at 72 $^\circ$C. After the last cycle, all sequences were allowed a final extension time of ten minutes at 72 $^\circ$C before cooling them down for further processing.

Site-Directed Mutagenesis

Site-directed mutagenesis or Quick-change PCR inserts specific point mutations into a vector by amplifying the entire vector using primers that are complementary to it except for the desired mutation.
After amplification, parental DNA is degraded using the enzyme diplococcus pneumoniae restriction enzyme I (DpnI). DpnI only cleaves methylated DNA, so mutated DNA synthesized in vitro is left intact while parental DNA produced by E.coli is degraded.
The reaction mix was prepared using 5μL of 10x reaction buffer, 50ng of template vector, 1,25μL (125 ng) of each primer, 1 μL of dNTP mix and ddH_2O to a final volume of 50μL. After adding 1 μL of Pfu DNA polymerase (2.5 U/μL), the reaction was started by heating the mixture to 95 $^\circ$C for 30 seconds. This was followed by 18 cycles of heating to 95 $^\circ$C for 30 seconds to trigger strand separation, then cooling down to 55 $^\circ$C for one minute to allow annealing of the primers and heating to 68 $^\circ$C for one minute per kb of plasmid length to amplify the target vector.
After amplification, the mixture was cooled down to $\leq$ 37 $^\circ$C before 1μL DpnI was added to degrade the original, non-mutated DNA. The reaction mix was spun down and incubated at 37 $^\circ$C for one hour before transformation.
After transformation, bacteria were plated on selection plates and incubated at 37 $^\circ$C overnight. Colonies were picked the next day, amplified by culture in LB broth, purified by miniprep and sequenced (MWG value read tubes) to prove the desired mutation was present.

Agarose Gel Electrophoresis

Linearized DNA fragments were separated with, and isolated from, agarose gels. By applying an electric field to DNA in an agarose gel, the negatively charged molecules are pulled through the matrix and separated by size. DNA is made visible under ultraviolet (UV) light by adding ethidium bromide, which will fluoresce when intercalated into DNA. DNA bands made visible by ethidium bromide were cut and purified from the gel.

1.5% gels were cast using 3g agarose dissolved in 200mL tris-acetate EDTA (TAE) (40mM Tris acetate and 1mM EDTA) and 20μL ethidium bromide. 50μL of DNA sample was mixed with 10μL of loading dye and gels were run in TAE at 90V for 30-45 seconds. Afterwards, bands were visualized on a transilluminator (LKB) and cut out for further use or photographed for record on an AlphaImager (Alpha Innotech).
To reisolate DNA from bands cut out of agarose gels, JETQuick Spin Columns (GENOMED) were used according to the manufacturer's specifications.

Generation of Heat-Competent Bacteria and Transformation

Competence describes a bacterium's ability to take up extracellular DNA. Bacteria like DH5α can be made artificially competent by rubidium chloride treatment.
To achieve optimal competence, bacteria must be in exponential growth phase. For this, they were thawed, incubated overnight in 2mL LB-medium at 37 $^\circ$C, then incubated in 100mL LB-medium with 2mL 1M potassium chloride (KCl) and 2mL magnesium sulfate ($MgSO_4$) up to an OD_{600} of 0.4-0.55. The bacteria were then centrifuged 10' at 4000rpm, 4 $^\circ$C, and the supernatant was decanted. They were resuspended in 15mL TFB1 solution and incubated five minutes on ice. Afterwards, the bacterial suspension was centrifuged again, the supernatant was decanted, and the bacteria were resuspended in 4mL ice-cold TFB2. Aliquots of 100μL were frosted in liquid nitrogen and stored at -80 $^\circ$C.

Transformation, the uptake of extracellular DNA by bacteria, was achieved by incubating heat-competent bacteria with the plasmid on ice for ten minutes, then subjecting them to a heat shock of 42 $^\circ$C for one minute and placing them back on ice.

Quantitative Real Time Reverse Transcription PCR

In order to determine mRNA-expression levels, quantitative real time reverse transcription PCR (qRT-PCR) can be used.
First, RNA is isolated and transcribed to complementary DNA (cDNA) using the enzyme reverse transcriptase. In the case of mRNA, which has a poly-A-tail, an oligo-dT-primer can be used to initiate transcription.
Next, DNA is then detected and quantified simultaneously using real-time polymerase chain reactions. For this, fluorescently labeled DNA probes are combined with specific primers to detect a certain cDNA sequence. For this, a DNA probe marked with a fluorophore binds to the DNA sequence in question. A quencher molecule attached to the same probe hinders it from fluorescing due to its proximity. When the sequence is amplified, the exonuclease activity of the polymerase degrades the probe and separates fluorophore and quencher. Without close proximity of the quencher, fluorescence emmission of the fluorophore can be measured after excitation with UV light. As the target sequence is amplified exponentially by the polymerase, more and more fluorophores are set free and an exponential increase in fluorescence can be detected. From this increase, the amount of

original RNA relative to a constitutively expressed housekeeping gene can be calculated.

For reverse transcription, a volume of 10.5μL RNA (about 1μg) purified from cultured cells with an RNA extraction kit was annealed with 2μL oligo-dT-primer (10pmol/μL) at 70 °C for five minutes. 1μL reverse transcriptase, 4μL 5x reaction buffer, 2μL dNTPs (10mM ATP, CTP, GTP, and TTP in equal volumes), and 0.5μL RNAse inhibitor were added and the mixture was incubated at 37 °C for one hour before the enzyme was inactivated by heating it to 70 °C for ten minutes. The resulting cDNA mixture was diluted in 30μL H_2O. From this DNA mixture, 6μL were used per measurement together with 10μL 2x buffer (LightCycler 480 Probes Master), 0.4μL of each primer (10pM/μL), 0.2μL of a fluorescent probe from Roche Universal Probe Library and another 3μL of sterile water. Assays were designed using the Roche ProbeFinder Assay Design Software. The amount of target gene expression in the cDNA mixture was determined as copy numbers per copy of the housekeeping gene hypoxanthine-guanine phosphoribosyltransferase (HPRT).

In-Vitro Transcription

5'-triphosphate RNA was transcribed in vitro using T7 phage polymerase and the MEGAscript T7 Kit from Ambion.
First, transcription templates were generated from DNA oligonucleotide templates containing the 2.2s sequence TCAAACAGAGGTCGCATGCCTATAGTGAGTCGTA and a sequence complementary to the Ambion T7 promotor primer sequence TAATACGACTCACTATA at its 3' end. For this, 2μL DNA template 2.2s (100pmol/mL) was incubated with 2μL primer of the same concentration in 10μL DNA hybridization buffer. Double-stranded DNA was denatured at 70 °C and cooled down two hours to 4 °C. Incomplete 3' ends were filled with ExoKlenow® polymerase by adding 5μL RNAse-free water, 2μL ExoKlenow® buffer, 2μL dNTPs (2.5mM) and 2μL of the enzyme to the reaction mix and incubating at 37 °C for 30 minutes. Afterwards, the enzymes were denatured 5 minutes at 70 °C.
For the final in vitro transcription, the MEGAscript T7 Kit (Ambion) was used according to the manufacturer's specifications. RNA was extracted using phenol–chloroform extraction and measured photometrically by determining the absorption at 260nm.
The final sequence of 2.2s 5'-triphosphate RNA was GGCAUGCGACCUCUGUUUGA [78].
For stimulation, 5'-triphosphate 2.2 single-stranded RNA was annealed with 2.2 antisense OH-RNA to form double-stranded RNA.

2.2.2 Cell Biology Methods

Cell Culture

Cells were cultured at 37 °C, 5% CO_2 and 95% humidity. Every two to four days, they were split using 0.05% trypsin and medium was refreshed.

When not in use, cells were cryoconserved in FBS with 10% DMSO by reducing their temperature at 1K/minute in an isopropanol freezing container and storing them at -80 ° C.

Celltiter-Blue Viability Assay

The resazurin-based viability assay can be used to measure cell proliferation and viability. Resazurin is a blue redox dye that viable cells turn into a pink, fluorescent dye called resorufin. To measure cell viability with this assay, 20μL of the reagent are put into 500μL medium per well on a 24-well-plate and incubated for 20 to 30 minutes until there is a change in color. Fluorescence is measured with an excitation wavelength of 530 and an emission wavelength of 590nm with a Mithras Multiplate Reader.

SiRNA-Knockdown

For siRNA-knockdown in 1205Lu melanoma cells, 3x10^4 cells/well were plated in 0.5mL medium on a 24-well-plate and incubated overnight. The next day, 1μL 20μM siRNA and 0.9μL Lipofectamine™ RNAiMAX Transfection Reagent reagent were mixed with 50μL OptiMEM serum-free medium each and incubated at RT for five minutes. Then, the two reagents were combined and incubated at RT for 15 minutes. The mixture was added in small drops to the cells, which were then incubated at 37 ° C for 24 hours. The procedure was repeated after 24 or 48 hours.
For experiments, where 96-well-plates were used, the volumes were scaled down to 0.2μL Lipofectamine™ RNAiMAX and 0.2μL siRNA diluted in 25μL OptiMEM each, following the protocol described above.
For experiments in 6-well-plates, the volumes were scaled up to 5x10^5 cells in 3mL medium treated with 5μL Lipofectamine™ RNAiMAX and 5μL siRNA diluted in 150μL OptiMEM. siRNAs were designed using the online siDESIGN center (Dharmacon). All sequences were blasted against the National Center for Biotechnology Information (NCBI) human transcript database to avoid off-target effects.

Cell Stimulation with 5'-Triphosphate-RNA

5x10^3 cells/well were plated in 100μL DMEM into a 96-well-plate and stimulated with triphosphate RNA 24 hours after transfection of siRNA. For this, 0.2μL Lipofectamine™ RNAiMax and 200ng triphosphate-RNA were mixed with 25μL OptiMEM serum-free medium each and incubated for five minutes at RT. After combining the two ingredients and incubating them together for 15 minutes, the mixture was added to the cells one drop at a time. These were then incubated overnight, before cytokines were measured in the supernatant.

Plasmid Expression

3x10^4 cells were plated in one compartment of a 35mm 4-compartment cell culture dish with 500μL medium and incubated overnight. For transfection, 0.75μL GeneJuice Trans-

fection Reagent (EMD chemicals) were diluted in 20μL OptiMEM serum-free medium and incubated for five minutes, then mixed with 250ng plasmid and incubated for another five to fifteen minutes. The mixture was added to the cells one drop at a time and incubated at 37 $^\circ$C for 48 hours.

Flow Cytometry

Flow cytometry is a sensitive technique to detect different properties of cells or microscopic particles. A beam of laser light of a single wavelength is shot at a passing cell in a stream of fluid. Different light detectors analyze different characteristics of the passing cells: the forward scatter (FSC) contains information about the volume, the side scatter (SSC) contains information about the inner complexity of the cells. If the cell contains a fluorophore like GFP, light emitted from the excited molecule can be detected with a fluorescence detector.

Flow Cytometric Infection Assay

Using a mutant VSV that expresses free GFP within mammalian cells, it is possible to distinguish between infected and uninfected cells and to analyze infection rates in different populations. This technique was combined with siRNA knockdown experiments to obtain quantitative infection analyses.
For infection analyses, 3x10^4 1205Lu cells were plated in a 24-well-plate, then incubated overnight, and knockdowns were performed twice with a 24-hour incubation interval. Cells were then infected with a multiplicity of infection (MOI) of 0.1 of VSV M GFP in serum-free medium. The medium was changed to normal growth medium after one hour. Ten hours post infection, cells were harvested and analyzed.

Cell Cycle Analysis

Flow cytometry can be used to distinguish cells at different stages of the cell cycle. Cellular DNA is quantitatively stained with the fluorescent marker PI. As cells double their DNA content during S-phase, the relative amount of cells in G_0/G_1 (before S-phase) or G_2/M-phase (after S-phase) can be determined by measuring the fluorescence signal.
To analyze changes in cell cycle, 1205lu cells/well were plated into a six-well-plate and incubated overnight. Knockdowns were performed according to the experimental protocol described above. After the second knockdown, cells were trypsinized, washed with phosphate buffered saline (PBS), pelleted and fixated as well as permeabilized by resuspending them in 0.5mL 70% methanol and incubating them for one hour at RT. After two additional washes in PBS, the cells were resuspended in 250μL PBS. RNA that could interfere with the DNA stain was degraded by adding 1μL ribonuclease A (stock: 1mg/mL in aqua dest.) and incubating 20 to 30 minutes at 37 $^\circ$C. 5μL PI (stock: 1mg/mL in aqua dest.) were added and the solution was incubated on ice for at least 20 minutes.
PI fluorescence was measured on the FL3 channel on a FACSCalibur cytometer.

Plaque Assay

A plaque assay was used to measure the concentration of a cytolytic virus like VSV by infecting cells with different dilutions of the original virus solution and counting the cell-free spots called plaques that form on a cell layer.
Specifically, a layer of cells susceptible to the virus in question is grown to confluency and infected with a serial dilution of the virus. The virus has to be hindered from moving freely through the medium so newly produced virus will not infect all cells in the well. For this, cells are covered with an agarose lid. Underneath, the virus can only infect neighboring cells, so one infectious particle in the original solution will produce exactly one plaque. After a virus-specific incubation period, the agarose lid is removed and the cell layer is stained with crystal violet. After washing, plaques become visible and can be counted to calculate the original virus concentration.
To determine the concentration of VSV in the supernatant after an infection experiment, 10^6 BHK-21 cells were plated per well of a six-well-plate and grown to confluency. The viral supernatants were diluted ranging from 1:10^3 to 1:10^8 and the cells were infected for one hour in serum-free medium. To cover the cells, 1% agarose was dissolved in heated PBS, mixed with the same volume of medium, and allowed to cool down to less than 40 $^\circ$C so as to not harm the cells. Each well was covered with 2mL of the agarose solution. After a few minutes at RT, the agarose lid was hardened and the cells were incubated for 24 hours at 37 $^\circ$C. Next, the lid was removed and the cells stained with a few drops of crystal violet solution for three minutes before washing with tap water until plaques became visible. From the counted plaques in the wells of the dilution series, the original concentration was calculated as plaque forming unit (PFU)/mL.

Immunofluorescence Microscopy

In order to visualize and determine its intracellular localization, the target protein was either fused to a red or green fluorescent protein and overexpressed or marked with a fluorescently labeled antibody before being visualized with a confocal microscope.
For localization of tagged protein in living cells, 5x10^4 1205Lu cells were plated into one compartment of a 35mm 4-compartment glass bottom dish. After one night of incubation, 250ng of plasmid were transfected into the cells with GeneJuice Transfection Reagent (EMD chemicals) according to the manufacturer's protocol and the transfected cells were incubated for two days. Next, 20nM MitoTracker® Green FM and 0,2μg/mL Hoechst 33342 nucleic acid stain (both Invitrogen) were added to the culture medium to stain mitochondria and nuclei, respectively. After another 30 minutes of incubation, the cells were viewed with a confocal microscope.

To localize native protein in fixated cells, 5x10^4 1205Lu cells were plated on a round 12mm microscope cover slip. The prepared slip was put into one well of a 24-well-plate and incubated until the cells were 70-90% confluent. 30 minutes before fixation, the cells were stained with 100nM MitoTracker® Red CMXRos (Invitrogen). The medium was

removed and the cells were fixated in 100% methanol at -20 °C for ten minutes. After one hour of blocking in 10% FCS in PBS, they were stained with primary anti-CRIF1-antibody M-222 (Santa Cruz Biotechnology) for one hour at RT, rinsed twice with PBS, and stained for another hour with Alexa Fluor 488® chicken anti-rabbit antibody (Invitrogen), a green fluorescent secondary antibody. Next, they were rinsed twice with PBS again, stained with 4',6-diamidino-2-phenylindole (DAPI) (Sigma-Aldrich), a nuclear stain with a blue (461nm) emission, rinsed again and mounted on a microscope slide with hardset fluorescence mounting medium.

2.2.3 Biochemical Methods

SDS-PAGE and Western Blot

SDS-polyacrylamide gel electrophoresis (PAGE) separates proteins in an electric field according to their respective size and charge.

SDS, an anionic detergent, denatures proteins in the sample, linearizes them and provides them with a negative charge. The gel is made up of acrylamide and bisacrylamide polymerized by added ammonium persulfate and TEMED. It functions as a sieve that allows smaller proteins to pass quickly through the electric field while holding back larger proteins. However, the natural charge of a protein also influences its movement through the gel, hence the separation is not only dependent on size. The gel can be blotted onto a membrane to stain single proteins with a specific antibody. This process is called western blot.

For the experiments described here, 20μL laemmli buffer were mixed with 20μL protein lysate and heated to 95 °C for five minutes. For a 15% acrylamide gel, 2.4mL H_2O were mixed with 2.5mL 1.5M Tris-HCl, pH 8.8, with 10%SDS, 5mL Rotiphorese® Gel 30 acrylamide/bisacrylamide solution, 0.1mL APS (10%) and 0.004mL TEMED. A stacking gel of 4% was mixed using 2.26mL H_2O with 1mL 0.5M Tris-HCl, pH 6.8, with 10% SDS, 0.68mL acrylamide/bisacrylamide, 0.04mL APS and 0.004mL TEMED.

Protein marker and samples were filled into individual slots and the gel was run at 40mA in running buffer (Table 2.6) until sufficient separation of the marker bands was visible. Next, the gels were blotted onto a PVDF transfer membrane for 50 minutes at 360mA using a wet transfer system. To eliminate unspecific binding sites, the blot was blocked in blocking buffer for 30 minutes. After washing in TBST (TBS with 0.1% Tween 20), the blot was incubated for two hours with primary antibody diluted in 2% BSA in PBS according to the manufacturer's instructions. Unbound antibody was washed off with TBST before incubating the blot with the secondary, horseradish peroxidase (HRP)-conjugated antibody diluted 1:3000 in blocking buffer for another two hours. After another washing step, the blot was developed by mixing 500μL each of substrate reagent A and B (BD Biosciences) and adding the mixture to the membrane before taking chemiluminescence pictures with an AlphaImager HP (Alpha Innotech).

Enzyme Linked Immunosorbent Assay (ELISA) for IP-10 or IL-6

The levels of the cytokines interferon gamma induced protein 10 kDa (IP-10) and IL-6 in the supernatant of cells were detected using a sandwich enzyme linked immunosorbent assay (ELISA). This method uses antibodies to bind the substance to be measured and detect it by catalyzing a reaction that creates a measurable absorbance shift.
The coating antibody is bound to the surface of a plastic plate with a basic coating buffer, then the sample is added and the cytokine can bind to the antibody. In addition, a detecting antibody binds to a second epitope of the substance and is then bound by a secondary antibody. The secondary antibody is directed against the constant region of the detection antibody and carries the enzyme HRP. Superfluous sample or antibody is washed off after each step. Therefore, the substrate turnover is relative to the cytokine amount in the sample when a substrate for the enzyme is added.
To retrieve the supernatants with the secreted cytokines, 1205Lu melanoma cells were plated on a 24- or 96-well-plate and incubated at 37 °C. Transfection with siRNA was performed after 24 and 72 hours, respectively. 10 to 20 hours after the second siRNA transfection, cells were infected with VSV (MOI=3), 40U/mL SeV or stimulated with 200ng/well of triphosphate RNA. After 24 hours of stimulation, the plates were centrifuged at 400g for five minutes and 100-200 μL supernatants were acquired. The supernatants were diluted 1:2 or 1:4 in PBS to achieve concentrations within the test's range.
The assay was performed according to the manufacturer's specifications (BD Biosciences). Each time, an internal standard was included for all plates so that the absolute amount of IP-10 or IL-6 could be calculated from the measured absorbance at 450nm.

Protein Complex Immunoprecipitation (Co-IP)

Immunoprecipitation is a method to isolate a protein from a mixture or cell lysate using a specific antibody. For this procedure, the antibodies are bound to agarose beads that can be separated from the mixture via centrifugation. If the target protein is part of a larger complex, immunoprecipitation can be used to pull down interacting proteins together with the protein targeted by the antibody. Using this method, new interacting partners can be identified and verified.

For Co-IP, 2.5x10^4 HEK293 cells were plated in a 10cm dish and incubated overnight. Next, the cells were transfected with flag-tagged RIG-I plasmid or an empty control plasmid and either RBM10-GFP or CRIF1-myc plasmid, adding up to a total of 3μg DNA per dish. After another 24 hours of incubation, cells were infected with 0,1 MOI of VSV M in OptiMEM for one hour, then rinsed with PBS and incubated in full growth medium for another 16 hours. The infected cells were then washed in ice-cold PBS three times before being lysed in 400μL lysis buffer containing 0.2% NP40, 20mM Tris-HCl (pH 7.5), 150mM NaCl, 1.5mM $MgCl_2$, 10% Glycerol, and 0.5mM EDTA. 20mM beta-glycerophosphate, 1mM sodium orthovanadate, 1mM PMSF, and 10μg/μL LPC were added to the lysis buffer directly before use. For disruption of the cell membranes, cells were drawn into a

syringe five times. Membranes and cell detritus were pelleted by 30 minutes centrifugation at 4 °C and 10,000g and discarded, the supernatant was then incubated with 50μL anti-flag agarose beads for one hour. Afterwards, the bead-lysate mixture was centrifuged for one minute at 4 °C and 1000rpm and washed in lysis buffer three times before being loaded onto a Micro-BioSpin Chromatography Column and centrifuged again one minute at 1000rpm. To elute the proteins from the beads, the column was incubated with 30μL 3xflag-peptide (100μg/mL) in TBS for 15 minutes and then centrifuged three minutes at 1000rpm. Both the eluate and samples from centrifuged cell lysate and bead supernatant were analyzed by SDS-PAGE and western blot.

Luciferase Reporter Assay

Luciferase is an enzyme that can produce light by the oxidation of a luciferin. If it is expressed in a cell line under the control of a specific promotor, it can be used to quantify transcriptional activity.
For this study, stable HEK293 cell lines expressing a firefly luciferase under the control of an NF-κB dependent promotor were used. Additionally, one of the cell lines overexpressed TLR-7, the other TLR-9.
5x10^3 cells/well were plated in 100μL DMEM in a 96-well format and incubated overnight before they were stimulated with R848 for TLR-7 activation or untransfected cytosine phosphodiester guanine oligodeoxynucleotides (CpG ODNs) for TLR-9 activation. After 24 hours of stimulation, the supernatant was removed and cells were lysed with 50μL Passive Lysis Buffer (Promega) for 20 minutes at RT. A substrate stock was prepared from 20mM Tricine, 2.67mM $MgSO_4$.7H2O, 0.1mM EDTA pH8, 33.3mM DTT, 0.53mM ATP, 270μM Acetyl CoA, 5mM NaOH, 30mg luciferin, 0.265mM magnesium carbonate hydroxide and water to a final volume of 228ml. The substrate stock was aliquoted and stored at -20 °C. Of this stock, 20μL/well were placed in a luminescence reader plate and mixed with 20μL cell lysate. Luminescence was measured with a Mithras multiplate reader.

2.2.4 Statistical Analysis

For statistical analysis and graphs, GraphPad Prism 5 (GraphPad Inc.) was used. Two-tailed Student's t test was used to assess the significance of mean differences. Differences were deemed significant at a $p \leq 0.05$. Statistical significance is indicated by ns for $p \geq 0.05$, *$p \leq 0.05$, **$p \leq 0.01$, and ***$p \leq 0.001$. Data are shown as means ± standard error of means (SEM).

Chapter 3

Results

3.1 Depletion of CRIF1 Facilitates Viral Replication

The proteins CRIF1 and RBM10 were found by mass spectrometry to co-precipitate with RIG-I-FLAG in VSV-infected HEK293 cells. Neither of them have been previously reported in the literature to have a function in anti-viral immunity. However, some very preliminary experiments in our group had indicated they might play a role in RLH signaling.

Therefore, in order to further test the hypothesis that CRIF1 and RBM10 play a role in RIG-I-mediated antiviral immunity, loss-of-function experiments were performed in a human cell line using RNA interference to knock down the expression of CRIF1 and RBM10.

As an infection model, genetically modified VSV mutants that express GFP within infected cells were chosen. Infected cells are then easily identified by the expression of GFP and can be visualized by fluorescence microscopy or measured by flow cytometry.

VSV is an arthropod-born virus with a broad tissue tropism that is recognized by RIG-I. Its negative, single-stranded RNA genome encodes five proteins. Among them, the multifunctional matrix protein can disrupt cellular mRNA transcription and export from the nucleus [79]. Thus, the expression of anti-viral genes like IFN type I is inhibited. As wildtype (wt) VSV only induces small amounts of IFN-β in 1205lu cells, a well-described mutant strain was included in order to study IFN dependent anti-viral activity. This mutant strain had lost its ability to inhibit IFN production through a methionine to arginine mutation at position 51 of the matrix protein (M51R) [80].

As our cell culture model we used the human melanoma line 1205Lu that had been shown previously to have an intact RLH signaling pathway and had worked well in siRNA-mediated knockdown protocols before [71].

After optimization of infection time and MOI, we were able to establish an infection model using an MOI of 0.5 for the wildtype VSV and 5 MOI for the mutant VSV M that gave us similar intermediate infection rates after 8 hours in 1205Lu cells. Cells in this model responded well to external IFN type I with a decreased percentage of infected cells and reacted to inhibition of IFN-signaling with an increased percentage of infected cells. As VSV M induces more IFN type I, this virus is more susceptible to inhibition of IFN sig-

naling, while both viruses react equally to externally added IFN type I (see figure 3.1).

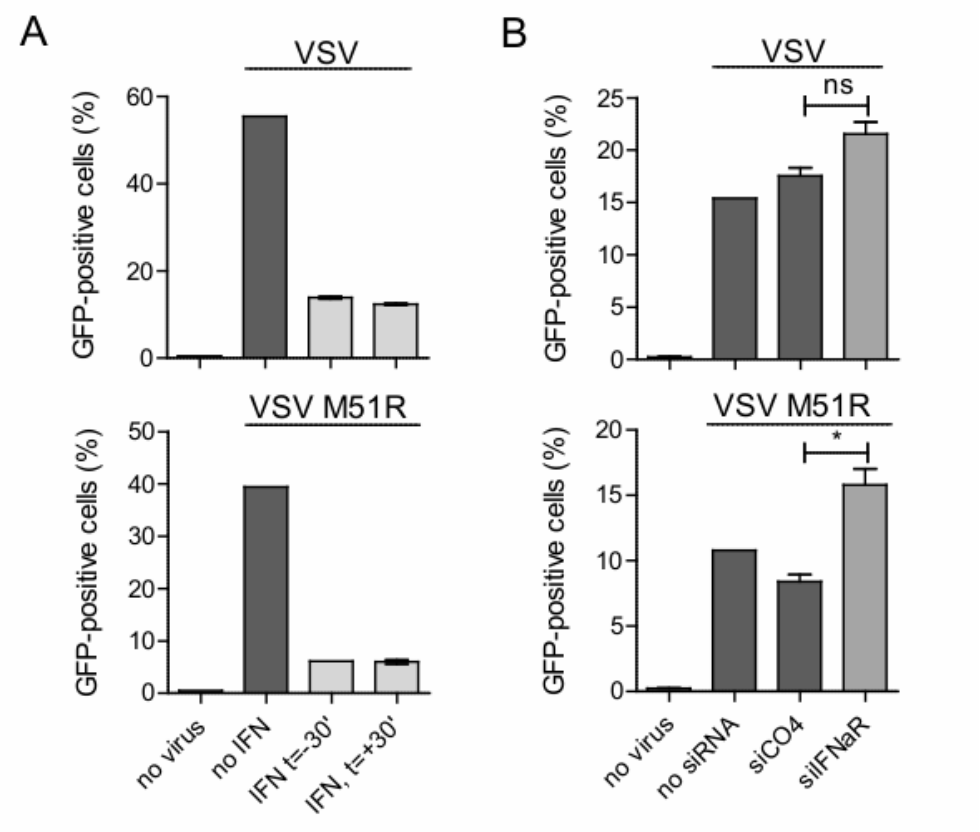

Figure 3.1: Infection Rates of 1205Lu Cells by VSV wt and VSV M51R are Sensitive to Both External Added IFN Type I and Blockade of IFN Receptor Signaling

A: 1205Lu cells were treated with IFN-β (2000U/ml) 30 minutes before or after infection with VSV GFP wt (MOI=0.5) or VSV GFP M51R (MOI=5). 8h later, the percentage of GFP-positive (=infected) cells was determined by flow cytometry. Data are shown as mean + SEM of n=3. B: 1205Lu cells were depleted of the IFN-α receptor using RNA interference. 48h after the first treatment with siRNA, the cells were infected with VSV GFP wt (MOI=0.5) or VSV GFP M51R (MOI=5). 8h later, the percentage of GFP-positive (=infected) cells was determined by flow cytometry. *p $\leq$ 0.05 indicates significance levels comparing cells treated with siRNA against IFNAR with cells treated with control siRNA.

This infection model was then used for loss-of-function assays depleting CRIF1 and RBM10 by siRNA.
An siRNA called CO4 without a mammalian target was used to control for unspecific effects. As positive controls, siRNAs targeting RIG-I or MAVS were used, as these molecules are both known to mediate innate immune responses to VSV.
Knockdown efficiencies were higher than 80% for all used siRNAs (see figure 3.3 and data not shown). As seen in figure 3.2, depletion of CRIF1 leads to a significantly increased number of VSV-infected cells. This effect is as strong as or even stronger than knocking down the known antiviral proteins RIG-I or MAVS. In addition, measuring the virus titer via plaque-assay in the supernatant of VSV-infected cells depleted of CRIF1 also showed

an increase in virus titer, confirming the notion that loss of CRIF1 leads to an advantage for the virus. Loss of RBM10, in contrast to CRIF1, showed no consistently significant effect on the number of virus-infected cells or the virus titer in the supernatant.

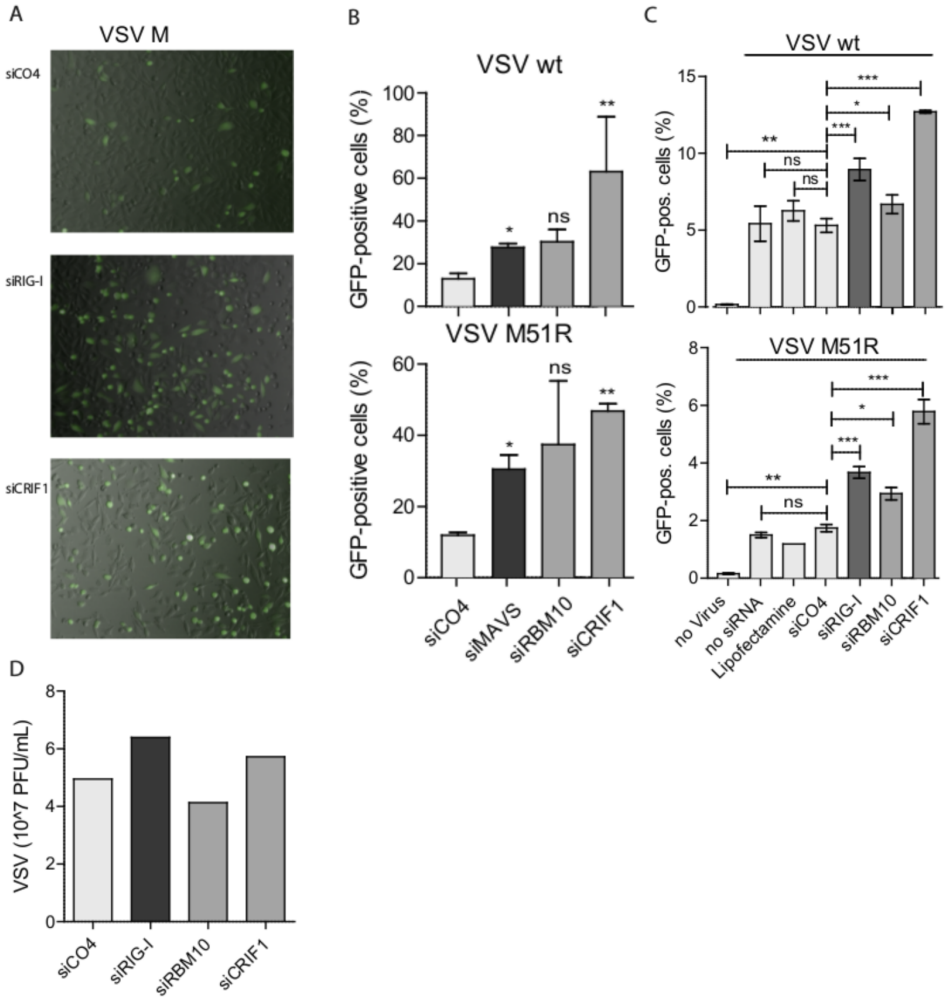

Figure 3.2: Depletion of CRIF1 Facilitates Viral Replication

1205Lu cells were depleted of the indicated proteins using RNA interference. Cells were treated twice (24h apart) with siRNA or the non-targeting control CO4. 48h after the first treatment, cells were infected with VSV GFP wt (MOI=0.5) or VSV GFP M51R (MOI=5). 12h later, the percentage of GFP-positive (=infected) cells was determined by microscopy or flow cytometry and the titer of infective particles was determined in the supernatant by plaque assays. A: Representative microscopic pictures of one experiment are shown. B: The percentage of GFP-positive cells was microscopically counted in 4 representative visual fields and is given as means + SEM of n=4 independent experiments. C: The percentage of GFP-positive cells was determined by flow cytometry and is given as means + SEM of n=5. D: The titer of infective VSV particles was determined in the supernatant by plaque assays. One representative experiment out of three is shown. *p $\leq$ 0.05, **p $\leq$ 0.01.,***p $\leq$ 0.001 indicate significance levels comparing CO4-treated cells and cells treated with targeting siRNAs.

3.2 Depletion of CRIF1 or RBM10 Leads to Reduced Cytokine Production after Infection with RNA Viruses or Stimulation with RLH Ligands

Depletion of CRIF1 was found to increase the viral replication rate by a mechanism that was left to be explained. As seen in Figure 3.1, the replication assay used is very sensitive to changes in interferon signaling. We therefore investigated if knockdown of CRIF1 or RBM10 influences the induction of interferon or the production of interferon-inducible genes. To that end the transcription of IFN-β and production of interferon gamma induced protein 10 kDa IP-10 were measured in cells stimulated with the known RIG-I-triggering stimuli triphosphate RNA, VSV or SeV (Figure 3.3)

While 1205lu cells did not produce detectable levels of IP-10 without a stimulus (not shown), RIG-I stimulation resulted in the secretion of 100-400pg/mL IP-10 in the supernatants of wild-type cells (not shown) or cells treated with a non-targeting control siRNA (Figure 3.3 A). Interestingly, depletion of both CRIF1 and RBM10 via siRNAs effectively diminished IP-10 induction and IFN-β production induced by stimulants of RIG-I signaling to a similar extent as the siRNA-mediated depletion of RIG-I and MAVS used as positive controls (figure 3.3). These results suggest depletion of CRIF1 or RBM10 impairs signaling via the RIG-I-IFN pathway.

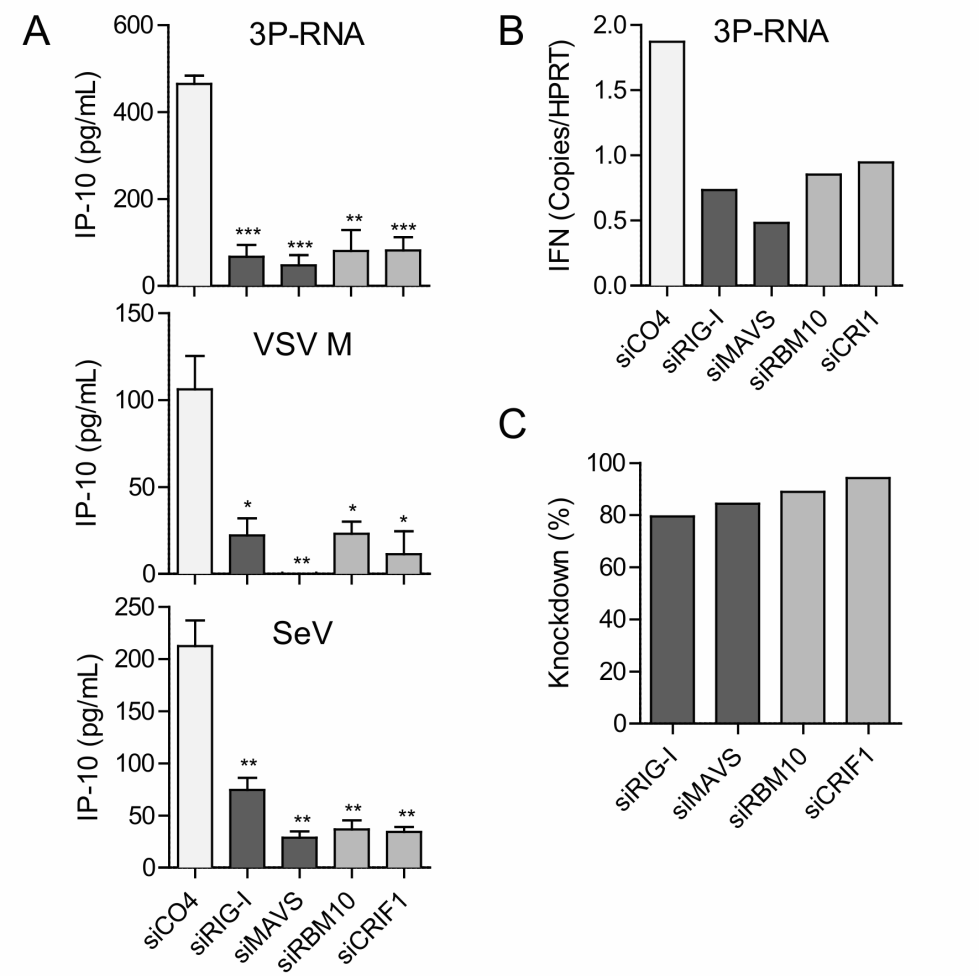

Figure 3.3: Depletion of CRIF1 or RBM10 leads to reduced IP-10 and IFN-β production in response to RIG-I stimulation

5x10^3 1205lu melanoma cells per well were plated on a 96-well plate and treated twice, 24h apart, with the indicated siRNAs. 48h after the first treatment, cells were stimulated with the indicated stimuli. 24h later supernatants were harvested and IP-10 was measured by ELISA and the cellular expression of IFN-β was determined on RNA level by qRT-PCR analysis.
A: IP-10 production after stimulation with transfected triphosphate RNA (50ng/well), VSV M51R (MOI=10), Sendai virus (1:100). Data are shown as mean + SEM of n=3. B: qRT-PCR for IFN-β after stimulation with triphosphate RNA (50ng/well). One representative experiment of three is shown. C: qRT-PCR to calculate knockdown efficiency for the siRNAs used in A-B. Knockdown efficiency was calculated as 1-(mRNA levels with specific siRNA/mRNA levels with control siRNA)x100%. One representative experiment of three is shown. *p $\leq$ 0.05, **p $\leq$ 0.01, ***p $\leq$ 0.001 indicate significance levels comparing CO4-treated cells and cells treated with targeting siRNA.

To rule out off-target effects of the used siRNAs, siRNAs with different binding sites within the CRIF1 and RBM10 mRNAs were designed. To validate the control siRNA CO4 used as the non-targeting negative control, a second control siRNA was produced that targets firefly luciferase (GL2). Mammalian cells like 1205lu do not naturally express luciferase,

but an overexpressed luciferase construct could effectively be silenced by it (not shown), indicating it is a functional siRNA and valid control. Cells treated with this second set of siRNAs however showed the same results as the first set of siRNAs after stimulation with triphosphate RNA using IP-10 in the supernatant as readout (Figure 3.4 A, upper panel). As a supposedly nuclear protein, CRIF1 might interfere with IP-10-induction on the promotor level. Then it would be interesting to test if the observed effect is specific for IP-10 or also influences the induction of other cytokines triggered by RIG-I activation, such as IL-6. However, if the observed phenotype is due to a specific interaction with RIG-I as the initial pull-down assay suggested, it should influence all effector proteins of RIG-I signaling, but not the signaling downstream of other PRR like, e.g., MDA5 or the Toll-like receptors. Therefore, IP-10 and IL-6 induction triggered via MDA5-mediated recognition of poly(I:C) was also tested in loss-of-function experiments with CRIF1 and RBM10 siRNA (Figure 3.4 B) and compared with cytokine production triggered by triphosphate RNA via RIG-I. In the case of poly(I:C) stimulation, siRNA against RIG-I functions as a negative control as RIG-I is not involved in the recognition of poly(I:C), while MAVS, the positive control, acts as the downstream adaptor of both RIG-I and MDA5.

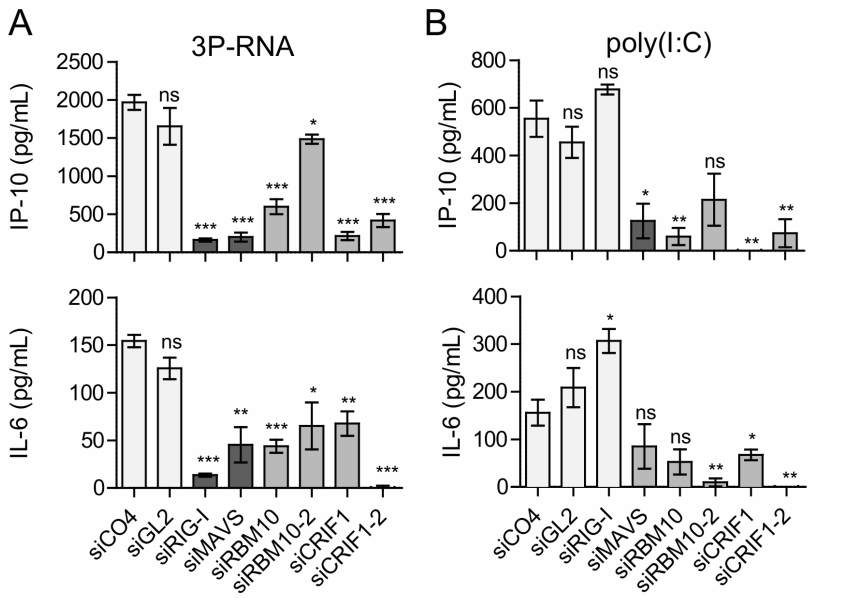

Figure 3.4: Depletion of CRIF1 by siRNAs with Different Binding Sites Leads to Reduced IP-10 and IL-6 Production in Response to RIG-I- and MDA5-Stimulation

5x10^3 1205lu melanoma cells per well were plated on a 96-well plate and treated twice, 24h apart, with the indicated siRNAs. 48h after the first treatment, cells were stimulated with the indicated stimuli. 24h later supernatants were harvested and IP-10 and IL-6 levels were measured by ELISA. A: IP-10 and IL-6 production after stimulation with transfected triphosphate RNA (100ng/well). Data are shown as means + SEM of n=3. B: IP-10 and IL-6 production after stimulation with transfected poly(I:C) (100ng/well). Data are shown as means + SEM of n=3. *p $\leq$ 0.05, **p $\leq$ 0.01.,***p $\leq$ 0.001 indicate significance levels comparing CO4-treated cells and cells treated with targeting siRNA.

Both triphosphate RNA and poly(I:C) induce IL-6 as well as IP-10. Stimulation after treatment with the non-targeting controls siCO4 and siGL2 produced similar levels of IP-10 and IL-6. Depleting RIG-I by siRNAs significantly lowered IP-10 and IL-6 induction in triphosphate RNA-stimulated cells, but showed no effect on poly(I:C)-stimulated induction. Depletion of MAVS lowered cytokine induction by RIG-I and MDA5 dependent stimuli. Depletion of CRIF1 by siRNAs again strongly diminished both IP-10 and IL-6 production after stimulation with either triphosphate RNA or poly(I:C).

This shows that depletion of CRIF1 does not exclusively influence RIG-I signaling, but also influences MDA5 signaling and not only influences the induction of IFN, but also the induction of inflammatory cytokines like IL-6.

3.3 CRIF1-Depleted Cells Are Viable and Do Not Show Cell Cycle Arrest

Deficiency of CRIF1 was found to increase viral replication and to decrease cytokine production by a so far unknown mechanism. As CRIF1 knockout mice die at an early stage in embryonic development [67], cell death has to be ruled out as an explanation of the observed anti-viral phenotype.

To test the influence of CRIF1-knockdown on cell viability, viability assays were performed using the commercially available CellTiter-Blue Cell Viability Assay (Figure 3.5 A).

While viability was reduced to about 60% in all cells treated with lipofectamine and siRNA, no significant difference could be detected among cells treated with control siRNA or siRNAs depleting RIG-I, MAVS or CRIF1.

Transfection of siRNA is toxic to cells [81]. However, as control siRNA and CRIF1 siRNA were equally toxic, cell death cannot explain the differences in viral replication and cytokine induction seen before (Figure 3.2-3.4).

Deficiency of RBM10 showed a small reduction in cell viability. Possibly, some part of the loss of cytokine release in knockdown cells can be attributed to this loss of viability, but it cannot be said for certain if it explains the whole effect.

Apart from cell death, a role for CRIF1 in cell cycle modulation has also been described in the literature [61]. As the single experiment underlining this claim shows an unusual cell cycle status in the negative control, it was important for this study to see if this finding could be replicated in the CRIF1-knockdown system and possibly explain the observed effect.

Untreated 1205lu cells showed a ratio of about 60% of cells in G1 stage, 20% in S/G2 and 10% in the M phase. Neither cells depleted of CRIF1 nor cells depleted of RBM10 differed more than 5 percentage points from this ratio.

All cells showed a ratio typical for asynchronous cells, so no cell cycle block as described in [61] was found by depletion of CRIF1 in our setting.

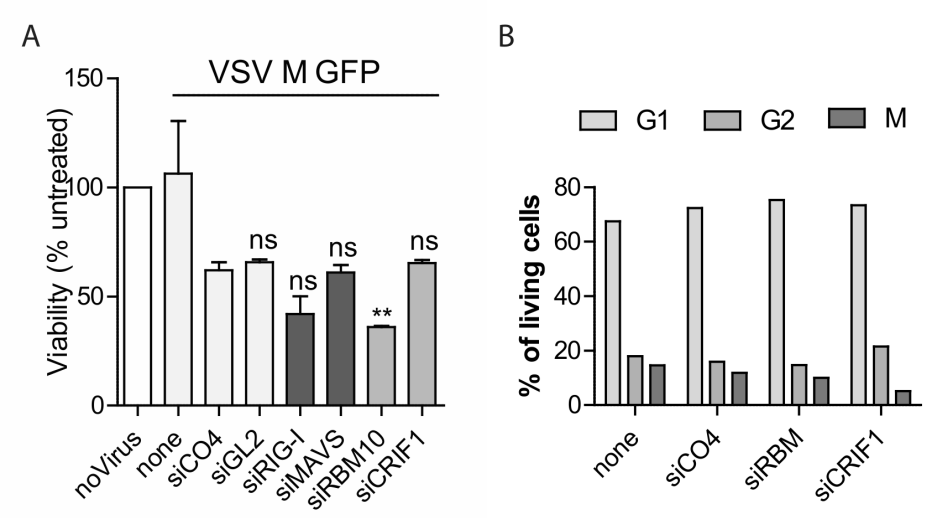

Figure 3.5: Viability and Cell Cycle Analysis of CRIF1 or RBM10 Depleted Cells

5x10^3 1205lu melanoma cells per well were plated on a 96-well plate and treated twice, 24h apart, with the indicated siRNAs. A: 48h after the first treatment, cells were infected with VSV GFP M (MOI=10) and cell viability was measured 24h later with CellTiter-Blue Cell Viability Assay (Promega). Error bars indicate SEM (n=3), **p $\leq$ 0.01 indicate significance levels comparing CO4-treated cells and cells treated with targeting siRNA. B: 24h after the second knockdown, cells were stained with the DNA marker PI and DNA content was measured by flow cytometry to distinguish cell populations in the different cell cycle stages. One representative experiment out of n=3 is shown.

3.4 CRIF1 Shows no Significant Effect on Infection Rates with the Model DNA Virus MVA

Having observed a role for CRIF1 in RLH-mediated antiviral immunity, a further question was whether this influence on the cellular defense status is specific for immunity against RNA viruses or whether this is also observed in other viral infections. To test this, the Modified vaccinia Ankara (MVA) virus was chosen as the model agent for infection assays. MVA is a highly attenuated, replication-deficient and well established model DNA virus and a genetically modified variant expressing GFP existed [70].

To find out whether the defect in antiviral immunity in CRIF1-knockdown cells extends to DNA viruses, infection rates of MVA virus expressing GFP were monitored by flow cytometry. Two types of assay were tested, an infection of 24h (Figure 3.6 A) or two subsequent infections of 12h each to imitate a replication cycle of the non-reproductive MVA virus (Figure 3.6 B). HEK293 cells which do not express functional RIG-I were used in this assay to search for an RLH-independent effect of CRIF1 depletion. An siRNA against IRF3 was chosen as a positive control.

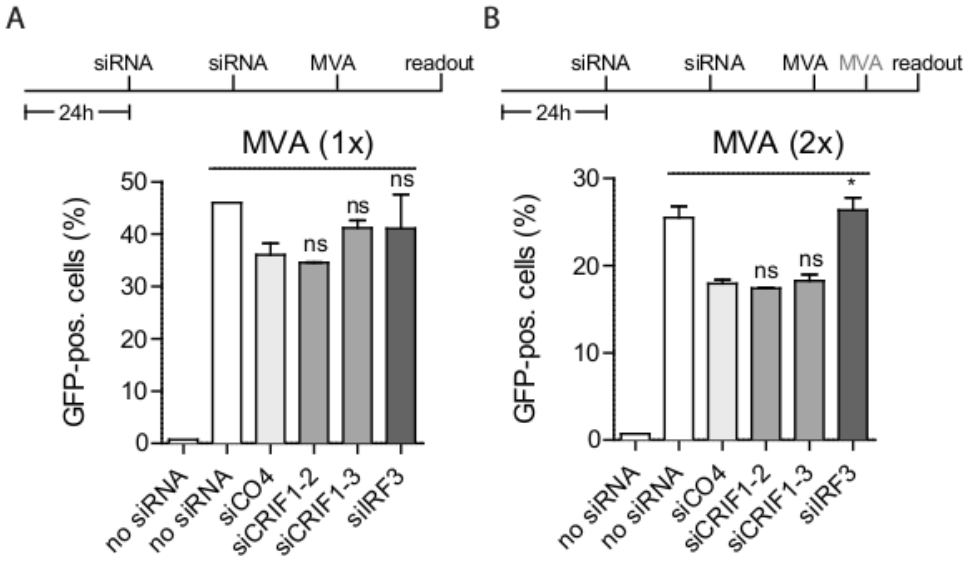

Figure 3.6: Depletion of CRIF1 does not Influence Infection Rates with MVA after Single or Double Infection

HEK293 cells were depleted of the indicated proteins using RNA interference. Cells were treated twice (24h apart) with siRNA or the non-targeting control CO4. The timeline of the experiments is indicated above the panels. A: 48h after the first siRNA treatment, cells were infected with a GFP-expressing MVA (MOI=3) for 24h. GFP-positive (=infected) cells were determined by flow cytometry. Data are shown as mean + SEM of n=3. B: 48h after the first siRNA treatment, cells were infected twice with MVA (MOI=1) for 12h each. GFP-positive (=infected) cells were determined by flow cytometry. Data are shown as mean + SEM of n=3. *p $\leq$ 0.05, **p $\leq$ 0.01.,***p $\leq$ 0.001 indicate significance levels comparing CO4-treated cells and cells treated with targeting siRNA.

Primary infection rates of the non-replicative MVA virus do not seem to change upon inhibition of IFN signaling (Figure 3.6 A). When mimicking replication with a second infection, IRF3-knockdown cells showed an increased infection rate. CRIF1-knockdown, however, had no such effect, indicating that facilitated viral replication after CRIF1-knockdown does not occur after infection with DNA viruses like MVA.

3.5 Depletion of CRIF1 Leads to Enhanced TLR7 and TLR9 Activation of NF-κB while Inhibiting RLH-mediated Activation of ISGs

TLRs play an important role in the recognition of a great number of viruses, bacteria, parasites and funghi. As CRIF1 was found to influence RLH signaling, it was tested if CRIF1 also plays a role in the signaling pathways of other pattern recognition receptors. For this, 1205lu cells depleted or not of CRIF1 by siRNAs were stimulated for 24h with untransfected poly(I:C) for TLR3 stimulation, R848 for TLR7/8 stimulation, CpG ODN

for TLR9 stimulation, lipopolysaccharid (LPS) for TLR4 stimulation, D-glutamyl-meso-diaminopimelic acid (iE-DAP) for nucleotide-binding oligomerization domain-containing protein 1 (NOD1) stimulation and transfected triphosphate RNA and poly(I:C) for RIG-I and MDA5 stimulation, respectively. IP-10 in the supernatant was used as the readout (Figure 3.7).

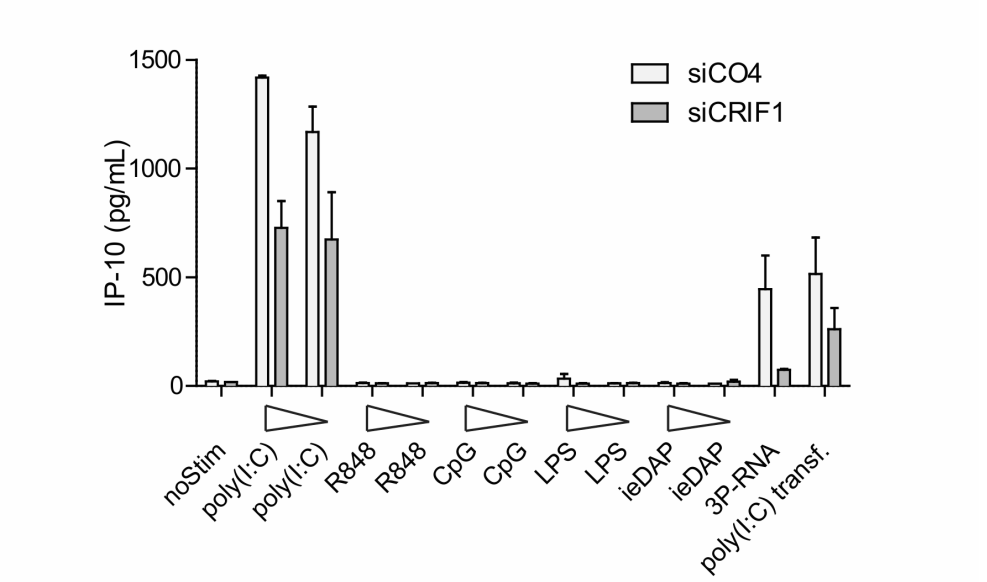

Figure 3.7: Depletion of CRIF1 Leads to Reduced IP-10 Production in Response to RIG-I-, MDA5- and Possibly TLR3-Stimulation

5x10^3 1205lu melanoma cells per well were plated on a 96-well plate and treated twice, 24h hours apart, with CRIF1-depleting siRNA or the non-targeting control CO4. 48h after the first treatment, cells were stimulated with high and low concentrations of the following stimuli: untransfected poly(I:C) (200 and 100μg/mL), R848 (10 and 5μg/mL), CpG (3 and 1.5μg/mL), LPS (1 and 0.5μg/mL), iE-DAP (1:1000 and 1:2000), transfected triphosphate RNA and transfected poly(I:C) (each 200ng/well). After 24h, supernatants were harvested and IP-10 levels were measured by ELISA. Data are shown as mean + SEM of n=3.

This experiment showed that 1205lu cells do not induce IP-10 in response to TLR4, TLR7/8, TLR9 or NOD1 stimulation, indicating that these cells are either not expressing those receptors or are missing relevant signaling modules for those receptors. Therefore, the same assay used to show the effect of CRIF1 on RLH signaling cannot be used to rule out an influence on these signaling systems.
RIG-I, MDA5 and most likely TLR3-stimulation, however, produced a response which was diminished strongly in the case of RIG-I activation and less for MDA5 and TLR3. As TLR3 is activated by endosomal poly(I:C), whereas MDA5 is activated by cytoplasmic poly(I:C), a cross-reaction cannot be ruled out completely. High amounts of uncomplexed polyI:C are required to stimulate endosomal TLR3 and considering the effect of CRIF1 knockdown is less for uncomplexed than for complexed poly(I:C), it cannot be excluded that uncomplexed poly(I:C) also to a certain extend activates MDA5 and the effect of

CRIF1 depletion is only mediated via its effect on the MDA5 pathway.

Because of the limitations to evaluate the role of CRIF1 in TLR-signaling in our 1205Lu cell model, a reporter assay using overexpressed TLR7 and 9 in HEK293 cells was used to examine this question further.
For this, HEK293 cells stably overexpressing TLR7 or TLR9 and a luciferase reporter controlled by the NF-κB promotor were assessed with or without prior depletion of CRIF1 for the activation of NF-κB after stimulation with CpG ODNs or R848, respectively (Figure 3.8).

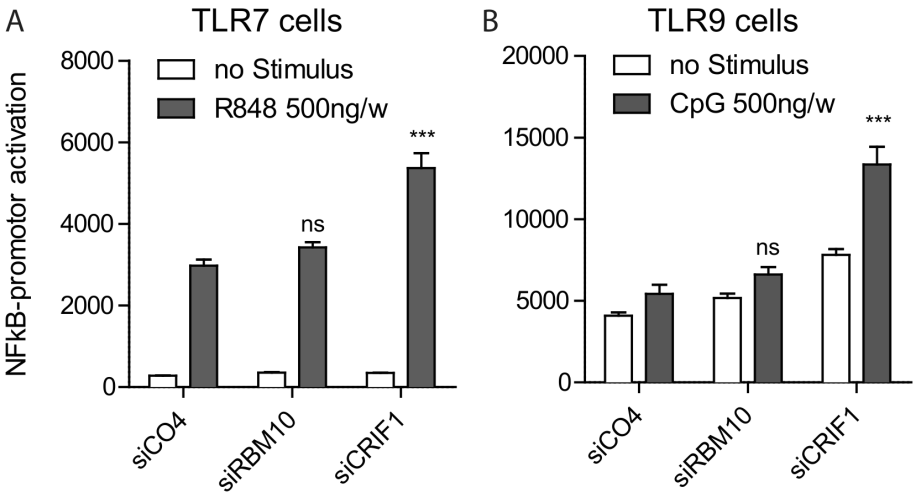

Figure 3.8: Depletion of CRIF1 Increases NF-κB Promotor Activation in Response to TLR7- and TLR9-Stimulation

1x10^4 HEK293 cells per well stably overexpressing TLR7 or TLR9 as well as a luciferase reporter controlled by the NF-κB promotor were plated on 96-well plate and treated twice, 24h apart, with the indicated siRNAs. 48h after the first treatment, cells were stimulated with A: 500ng R848 per well or B: 500ng CpG per well. 24 hours later the NF-κB-dependent luciferase activity was determined in a luminescence reader. Data present the unnormalized light counts per second as mean + SEM of n=3. ***p $\leq$ 0.001 indicate significance levels comparing CO4-treated cells and cells treated with targeting siRNA.

The HEK cell line expressing TLR7 showed a low baseline activation of the NF-κB promotor that was strongly induced upon stimulation with R848. Cells treated with RBM10-targeting siRNA showed the same level of activation as those treated with control siRNA, while cells treated with the siRNA against CRIF1 showed an increased activation of NF-κB (Figure 3.8 A).
Similarly, in the cell line expressing TLR9, cells treated with siRNA depleting CRIF1 showed a stronger inductione of NF-κB than those treated with control siRNA or siRNA targeting RBM10 (Figure 3.8 B) In the TLR9-expressing cell line, a higher baseline activation of the NF-κB promotor and a weaker induction by the corresponding TLR9-stimulus CpG could be seen (Figure 3.8 B).

These results suggest that CRIF1 might not only play a role in RLH-signaling but also influence TLR-signaling. However, it seems to play a different role here than in RLH-signaling, as the effect is inverted and depletion of CRIF1 enhances the TLR-dependent activation of NF-κB.

3.6 CRIF1 Exerts its Influence in RLH Signaling Upstream of TBK1 and Independent of the IFNAR-dependent Feedback-loop

Loss-of-function assays have implicated a role of CRIF1 in RLH-dependent anti-viral immunity, but it remains unclear how and on what level of the signaling cascade CRIF1 influences the RLH pathway. As CRIF1 has been described to be a nuclear protein and transcription factor cofactor [67], it might not exert its effect in the RNA recognition cascade initiated by RIG-I as our initial pull-down screening suggested. Instead, it could also influence IFN effector function as a cofactor downstream of the IFN feedback loop. To determine where the inhibition occurs, the IFN feedback loop was blocked with siRNA against IFNAR. Any protein whose knockdown would then still influence IP-10 induction should be involved in signaling upstream of the loop.

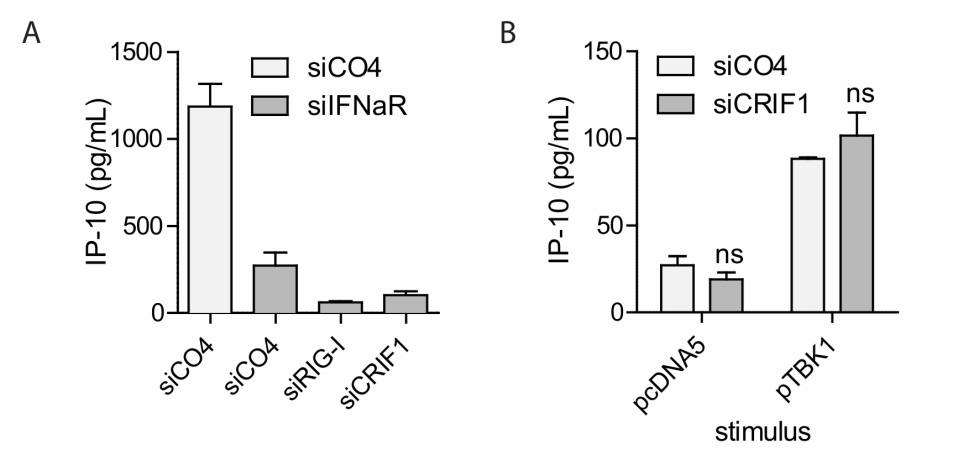

Figure 3.9: Depletion of CRIF1 Leads to Reduced IP-10 Production in Response to RIG-I Stimulation after Blockade of the IFN Feedback Loop but not in Response to Overexpression of TBK1

A: 5x10^3 1205lu melanoma cells per well were plated on a 96-well plate and transfected twice, 24h apart, with equal amounts of siRNA targeting IFNAR or the non-targeting control CO4 together with siRNA targeting either RIG-I or CRIF1 or control CO4. 48h after the first treatment, cells were stimulated with triphosphate RNA (200ng/well). 24h later supernatants were harvested and IP-10 levels were measured by ELISA. Data are shown as mean + SEM of two independent experiments. B: 5x10^3 1205lu melanoma cells per well were plated on a 96-well plate and transfected with 50ng/well of an empty pcDNA5 plasmid or a plasmid expressing TBK1 within the cells. After 12h, cells were treated twice, 24h apart, with siRNA. 48h after the first siRNA treatment, supernatants were harvested and IP-10 levels measured by ELISA. Data are shown as mean + SEM of n=2.

As can be seen in Figure 3.9 A, blockade of the IFN feedback loop with an siRNA targeting IFNAR substantially diminished IP-10 production upon triphosphate RNA stimulation. However, IP-10 levels were still reduced further by both siRNAs targeting RIG-I and CRIF1. This indicates that CRIF1, like RIG-I, plays a role upstream of the IFN feedback system.

As initially, CRIF1 was believed to be a nuclear protein, it was hypothesized to influence IFN production at a promotor level downstream of TBK1, the kinase responsible for phosphorylation of IRF3 downstream of MAVS in the RLH signaling pathway.

To test this hypothesis, TBK1 was overexpressed in 1205Lu cells with CRIF1 either depleted or not, thereby triggering the signaling pathway downstream of TBK1, and IP-10 levels were measured as the readout.

As seen in Figure 3.9 B, overexpression of TBK1 was sufficient to induce IP-10. However, this induction was not influenced by depletion of CRIF1.

This assay indicates CRIF1 exerts its influence in the signaling pathway upstream of TBK1.

3.7 CRIF1 Exerts its Influence Independently of Previously Described Interacting Proteins

In a different approach to identify the mechanism of the observed phenotype of increased RNA virus replication in CRIF1-depleted cells, the effect of depleting proteins previously reported to interact with CRIF1 was tested to see if they might influence cytokine induction by RIG-I ligands like CRIF1 does. siRNAs were designed against the three proteins STAT3, casein kinase II (CKII) and growth-arrest and DNA-damage inducible protein gamma (GADD45γ), for which an interaction with CRIF1 has been described previously [61, 62, 67].

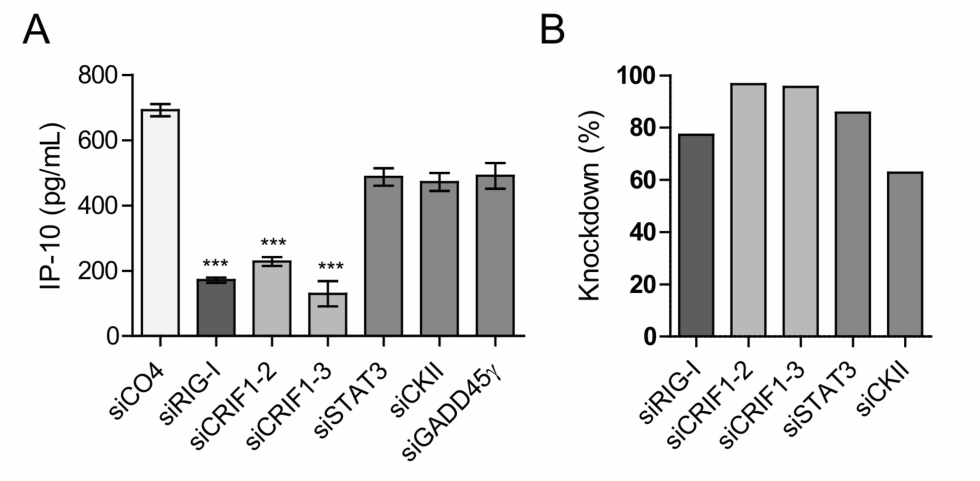

Figure 3.10: Depletion of CRIF1 Interacting Proteins does not Lead to Reduced IP-10 Production in Response to RIG-I Stimulation to the Same Extent that Depletion of CRIF1 does

1205Lu cells were depleted of the indicated proteins using RNA interference. Cells were treated twice (24h apart) with siRNA or the non-targeting control CO4. 48h after the first treatment, cells were stimulated with triphosphate RNA (200ng/well). 24h later supernatants and cells were harvested. A: IP-10 levels in the supernatant were measured by ELISA. Data are shown as mean + SEM of n=3. B: qRT-PCR of the cells was used to determine the knockdown efficiency for the siRNAs used in A. Knockdown efficiency was calculated as 1-(mRNA levels with specific siRNA/mRNA levels with control siRNA)x100%. ***p $\leq$ 0.001 indicate significance levels comparing CO4-treated cells and cells treated with targeting siRNA..

Neither knockdown of STAT3, CKII nor GADD45γ, however, inhibited cytokine induction to the extend knockdown of RIG-I or CRIF1 did (Figure 3.10 A). Knockdown efficiencies for the tested siRNAs were between 60 and 90% (Figure 3.10 B). For GADD45γ, no mRNA could be detected in 1205Lu cells, so it is unlikely to be involved in the CRIF1 phenotype observed in these cells.

These results suggest that CRIF1 exerts its influence through a mechanism independent of previously reported CRIF1-interacting proteins.

3.8 CRIF1 and RBM10 Expression does not seem to be Significantly Induced upon Viral Infection

Many anti-viral genes are strongly upregulated during viral infection. Indeed, many anti-viral proteins were identified because they were strongly induced by IFN in the course of viral infection.

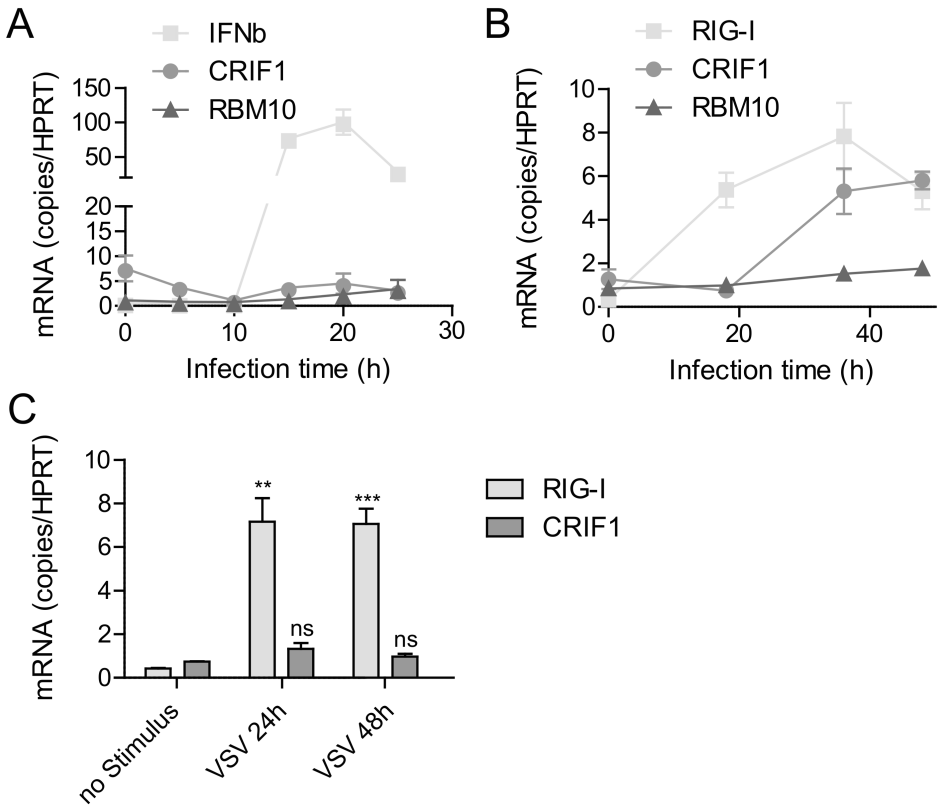

Figure 3.11: CRIF1 is Weakly Induced on mRNA Level After 36 Hours of VSV Infection

A: 1x10^5 HEK293 cells per well were plated on a 24-well plate and infected with VSV M51R at an MOI=2. After the indicated time, cells were harvested and levels of the indicated mRNAs were measured by qRT-PCR. Data are shown as mean + SEM of two independent experiments. B: 5x10^4 HEK293 cells per well were plated on a 24-well plate and infected with VSV M51R at an MOI=3. After the indicated time, cells were harvested and levels of the indicated mRNAs were measured by qRT-PCR. Data are shown as mean + SEM of two independent experiments. C: 1x10^5 PBMCs per well were plated on a 24-well plate and infected with VSV M51R at an MOI=5. After the indicated time, cells were harvested and levels of the indicated mRNAs were measured by qRT-PCR. Data are shown as mean + SEM of three independent experiments. **p $\leq$ 0.01.,***p $\leq$ 0.001 indicate significance levels comparing cells before and after stimulation.

To find out whether CRIF1 or RBM10 are induced upon viral infection, HEK293 cells were infected with VSV and mRNA levels were measured over the following 48 hours. To analyze possible differences between cell lines and primary cells, CRIF1 mRNA levels were

also measured in PBMCs after stimulation with VSV.

While IFN-β and the known IFN-inducible gene RIG-I were strongly induced in HEK293 cells, no specific induction could be detected for RBM10 or CRIF1 mRNA within the first 24 hours (see Figure 3.11 A).

However, 36 and 48 hours after infection with VSV, an up to six-fold induction of CRIF1 could be observed in HEK293 cells on mRNA level (Figure 3.11 B).

In PBMCs, such an increase in mRNA levels could not be observed (Figure 3.11 C), indicating that this response is either limited to cell lines in contrast to primary cells or to tissue cells in contrast to immune cells.

For RBM10, levels do not seem to react to viral infection.

3.9 Overexpression of CRIF1 Does Not Enhance RLH Signaling

Since loss of CRIF1 function diminishes cellular cytokine response to RLH stimulation, it was tested if gain of function by overexpression of CRIF1 might in turn have an opposite effect.

To do so, an untagged CRIF1 was overexpressed in 1205lu cells and cytokine response was measured in cells stimulated or not with triphosphate RNA or poly(I:C). Overexpression of untagged RIG-I, MAVS or MDA5 were used as positive controls, empty pcDNA5 vector as negative control.

None of the transfected plasmids resulted in a significant stimulation of the cells without an additional stimulus (data not shown). Both triphosphate RNA and poly(I:C) treatment resulted in a strong induction of IP-10 and IL-6 which was significantly increased in cells overexpressing MAVS or the corresponding RLH, but not in cells overexpressing CRIF1 or RBM10 (figure 3.12).

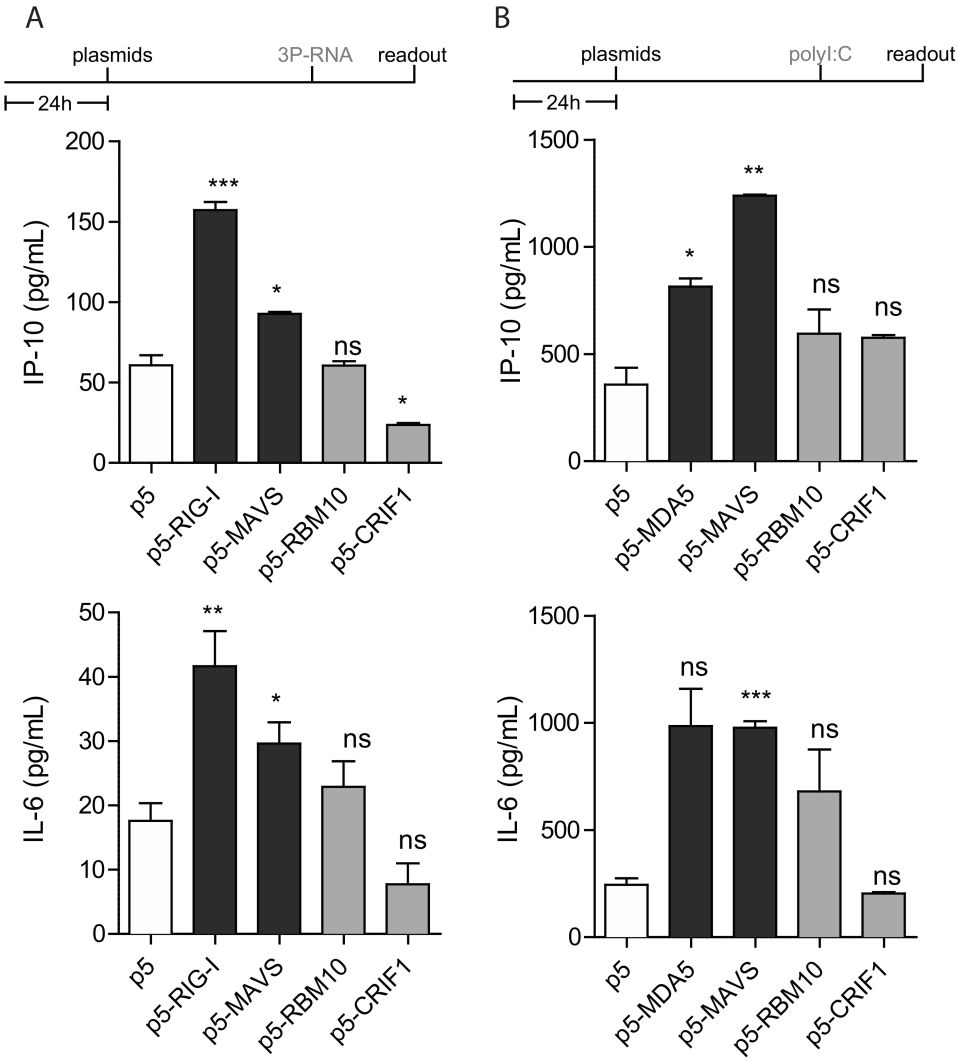

Figure 3.12: Overexpression of CRIF1 or RBM10 does not Enhance RLH-Mediated Cytokine Induction

$2x10^3$ 1205lu melanoma cells per well were plated on a 96-well plate and transfected with empty pcDNA5 vector or pcDNA5 vector expressing untagged RIG-I, MAVS, MDA5, RBM10 or CRIF1 within the cells. After 48h, cells were stimulated with A: triphosphate RNA (25ng/well) or B: poly(I:C) (100ng/well). After 24h supernatants were harvested and levels of IP-10 and IL-6 were measured by ELISA. The timeline of the experiment is indicated above the panels. Data are shown as mean + SEM of n=3. *p $\leq$ 0.05, **p $\leq$ 0.01.,***p $\leq$ 0.001 indicate significance levels comparing cells treated with the empty control vector to cells transfected with the indicated expression vector.

In the case of CRIF1, overexpression does not show the opposite phenotype of the loss-of-function assays desribed before. This negative result does not allow any firm conclusions, but is compatible with the interpretation that the endogenous expression of CRIF1 in 1205Lu does not seem limiting for RIG-I signaling.

3.10 CRIF1 and RBM10 Co-immunoprecipitate with Anti-flag Agarose Beads Independently of RIG-I

As CRIF1 and RBM10 were originally found by mass spectrometry in a screening assay searching for RIG-I-interacting proteins in cells stimulated with VSV, co-immunoprecipitation was repeated to confirm the specific interaction of CRIF1 with RIG-I by western blot.
For immunoprecipitation, HEK293 cells were used just as in the original screening assay. These cells were transfected with either flag-tagged RIG-I or the empty control vector and either RBM10 or myc-tagged CRIF1. After infection with VSV for 18h, immunoprecipitation was performed and the eluate was compared to the lysate used as input and the supernatant by western blot (Figure 3.13).

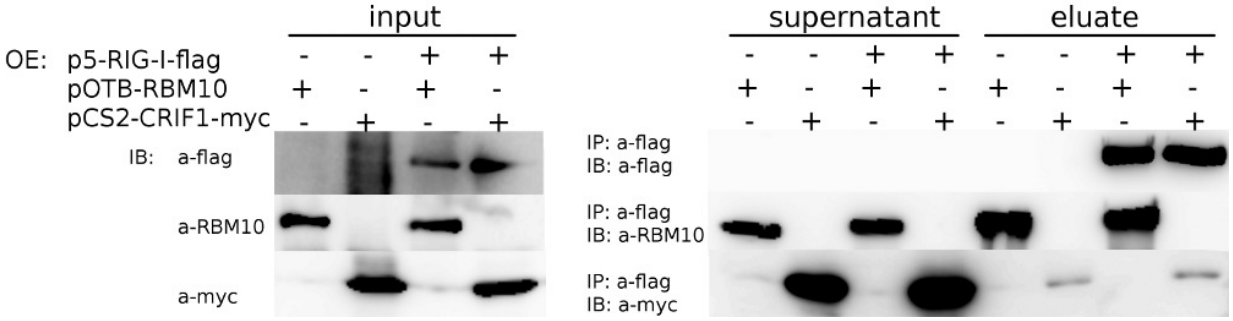

Figure 3.13: Both CRIF1 and RBM10 Co-Immunoprecipitate with Anti-Flag Agarose Beads Independently of RIG-I

2.5x10^6 HEK293 cells per condition were plated in a 10cm-dish and subsequently transfected with plasmids expressing flag-tagged RIG-I, RBM10 together with myc-tagged CRIF1 or an empty control vector to a total of 6μg DNA. After 24h, cells were infected with VSV at an MOI of 0.1. 18h later cells were lysed on ice and the lysate was used as input for immunoprecipitation using anti-flag agarose beads. Lysate, supernatant and eluate were immunostained by western blot using anti-flag antibody to stain RIG-I, anti-myc antibody to stain CRIF1 and anti-RBM10 antibody respectively. The depicted results are representative for three independent experiments.

As seen in Figure 3.13, RIG-I-flag was found in the lysate and eluate, but not in the supernatant. RBM10 and CRIF1-myc could be seen in the lysate and supernatant of transfected cells. Both were also found in the eluate of both RIG-I-flag expressing and non-expressing cells.
The immunoprecipitation worked as all overexpressed RIG-I was pulled from the lysate into the eluate, depleting the supernatant completely. However, although both RBM10 and CRIF1 could be found in the immunoprecipitate eluted from anti-flag-antibodies in cells overexpressing RIG-I-flag, surprisingly they could also be found in the immunoprecipitate of cells not expressing RIG-I-flag (Figure 3.13). These results show that CRIF1 and RBM10 do not interact specifically with RIG-I, but in fact interact RIG-I-independently with anti-flag-beads. They were not found in immunoprecipitation carried out with control IgG beads (not shown), but seem to solely interact with anti-flag beads.

3.11 CRIF1 is a Mitochondrial Protein That is Targeted to Mitochondria by a Mitochondrial Targeting Sequence at the N-terminus

In the literature, CRIF1 has been described as a nuclear protein [61, 63, 67] based on observations using overexpressed tagged proteins. In our setting, we did not find functional clues to support a nuclear localization. As the localization of a protein within the cell is important for its function, we chose to examine the localization of CRIF1 using fluorescently tagged constructs.

A plasmid containing CRIF1 fused to N-terminal GFP [77] and a plasmid containing CRIF1 fused to C-terminal mCherry, a red fluorescent protein, were used to visualize CRIF1 in transfected 1205lu cells.

Both constructs were expressed by the cells and could be seen in live cell imaging. However, the two differently tagged proteins localized differently: While n-terminally tagged GFP-CRIF1 co-localized with the nuclear dye, c-terminally tagged CRIF1-mCherry was found outside the nucleus (Figure 3.14 A), co-localizing with a mitochondrial dye (Figure 3.14 B).

These images show CRIF1 is localized differently depending on tagging. A construct tagged at the N-terminus is transported to the nucleus, a C-terminally tagged one resides in the mitochondria.

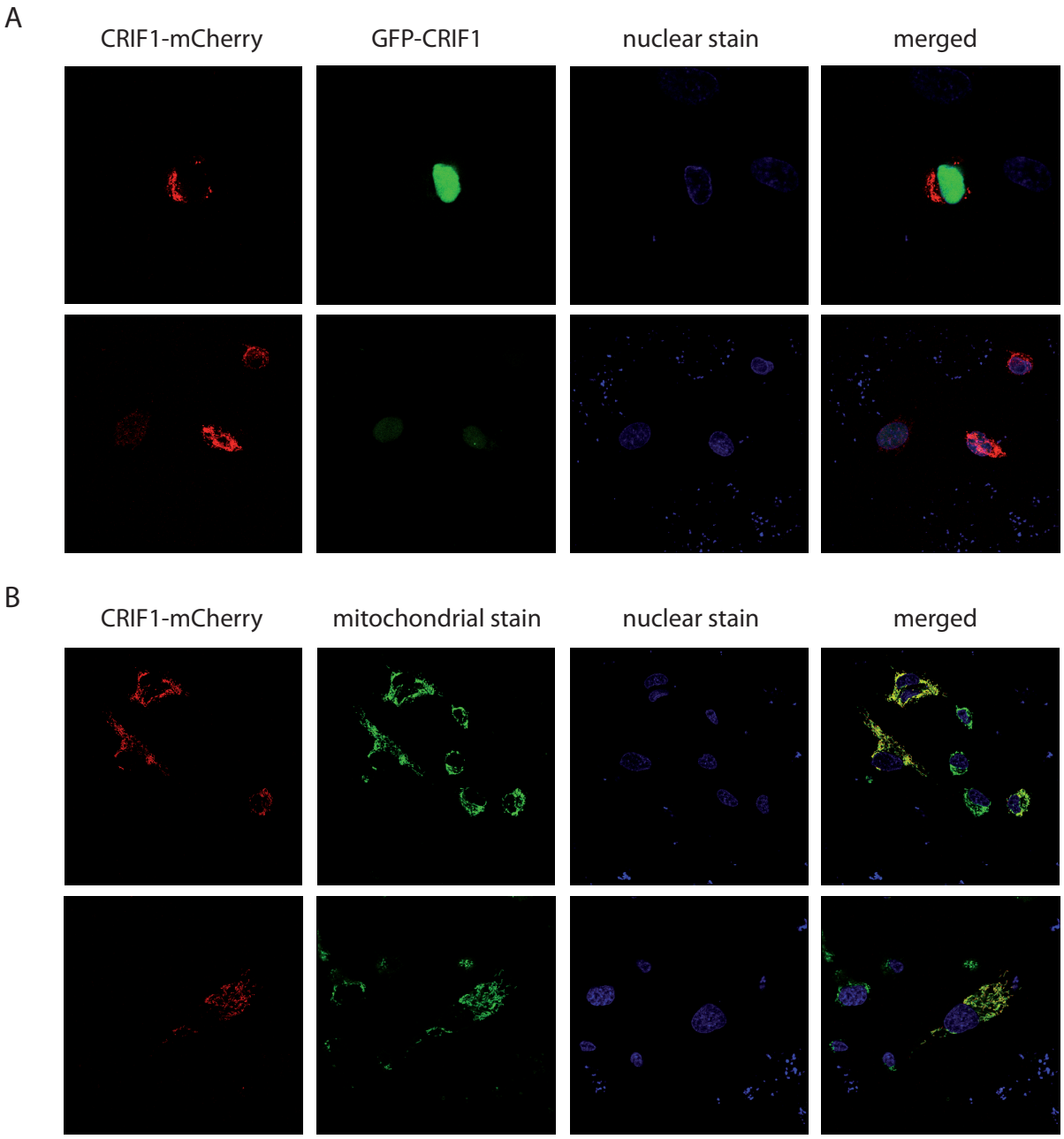

Figure 3.14: Overexpressed CRIF1 is Localized in the Nucleus or Mitochondria Depending on Tag Localization

3x10^4 1205lu cells were plated onto a glass bottom dish, transfected with 250ng p5-CRIF1-mCherry alone or together with pEGFP-CRIF1-C3 for 48h and stained with Hoechst nuclear dye alone or together with the mitochondrial stain MitoTracker® Green FM (Invitrogen) before live cell confocal microscopy. A: Confocal images of the intracellular localization of N-terminally tagged GFP-CRIF1 in relation to CRIF1-mCherry and nuclear stain Hoechst. B: Confocal images of the intracellular localization of C-terminally tagged CRIF1-mCherry compared to mitochondrial stain MitoTracker® Green FM (Invitrogen) and nuclear stain Hoechst.

Given that CRIF1 has two different localizations depending on tagging which seemed to be mutually exclusive, the question was where native protein localizes within the cell.
To address this question, CRIF1 was visualized in untransfected cells using immunofluorescence.

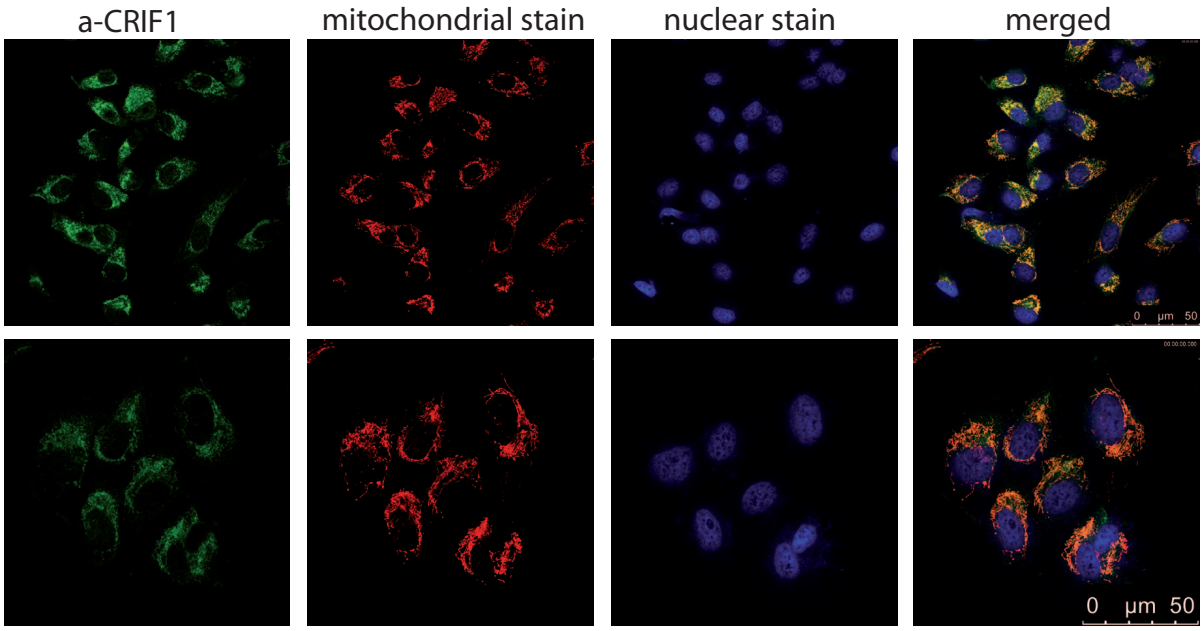

Figure 3.15: Native CRIF1 is Localized at the Mitochondria

5x10^4 1205Lu cells were plated on a microscope cover slip and subsequently stained with 100nM MitoTracker® Red CMXRos (Invitrogen). After methanol fixation, cells were stained with anti-CRIF1-antibody and a green fluorescent secondary antibody before being stained with DAPI nuclear stain and visualized by fluorescence microscopy.

As seen in Figure 3.15, immunofluorescently labeled endogenous CRIF1 shows a clear co-localization with mitochondrial stains, not with the nuclear stain, leading to the conclusion that native CRIF1 is localized mainly or exclusively in mitochondria.
As a mitochondrial localization was observed with both overexpressed and native protein, the CRIF1 protein sequence was analyzed using the MitoProt algorithm [82] offered by the Helmholtz Center Munich and a mitochondrial targeting sequence (MTS) was predicted at amino acids 1-35 of the protein.
To test whether this N-terminal MTS was necessary for its mitochondrial localization, a deletion mutant was created missing the first 34 amino acids after the methionine and containing a fluorescent tag at the C-terminus.
Mitochondrial targeting signals are typically hydrophilic and positively charged sequences contained in amino-terminal prepeptides [82]. If these properties in the MTS are necessary, a point mutation changing a positively charged amino acid into a neutral one might impair the mitochondrial localization. By switching the arginine (R) residue in position 26 to an alanine (A), the localization of the protein could be studied with a reduced positive charge

of the MTS.

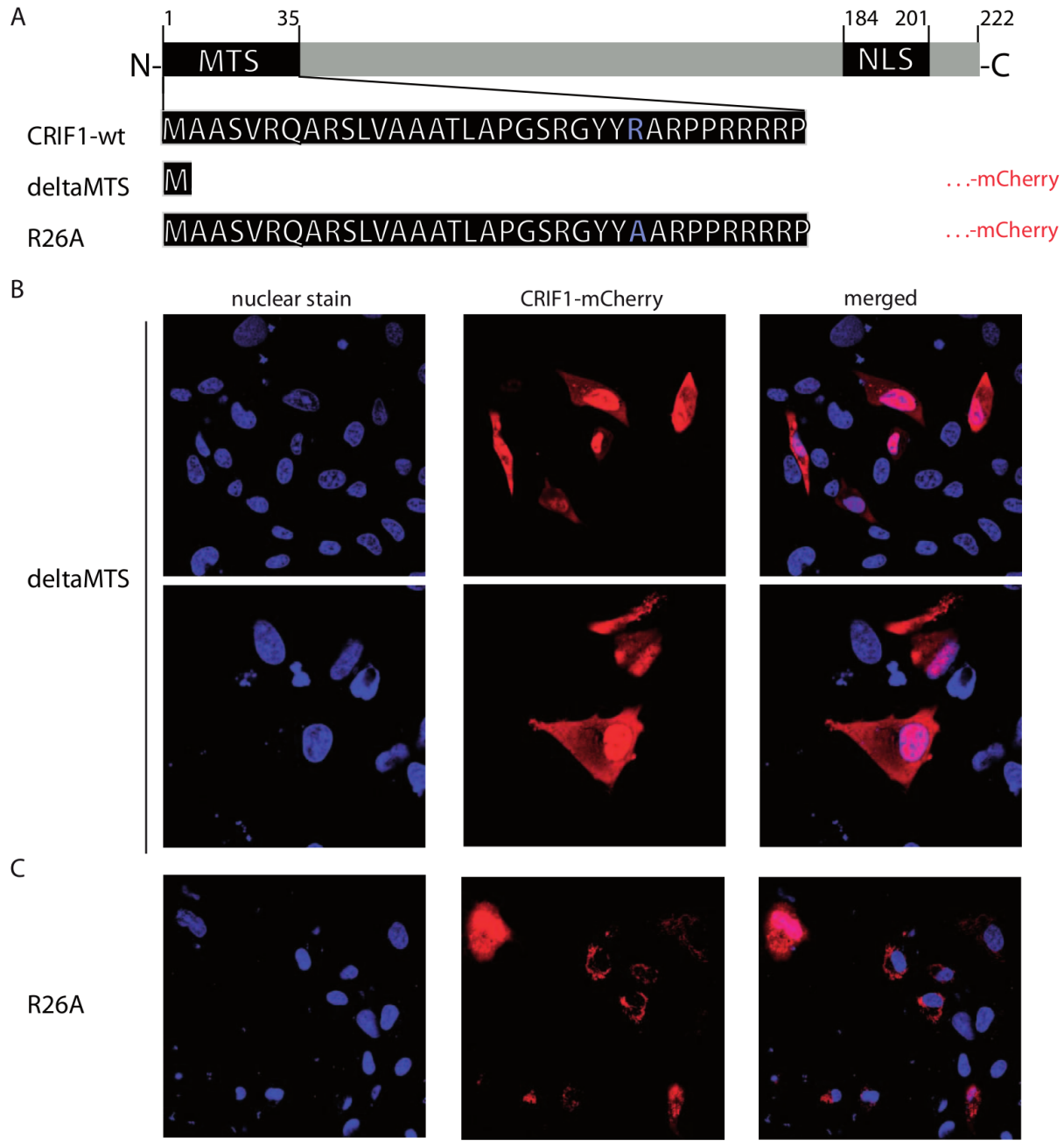

Figure 3.16: A Missing or Mutated MTS Mislocalizes CRIF1 to the Nucleus or Cytoplasm

A: Schematic representation showing the proposed mitochondrial (MTS) and nuclear (NLS) localization sequences of wildtype CRIF1 and the sequence changes in the δMTS and R26A mutant. B: 1205lu cells were transfected with the MTS deletion mutant p5-CRIF1-δMTS-mCherry for 24h, then treated with Hoechst nuclear stain and viewed live under a confocal microscope. B: 1205lu cells were transfected with the MTS point mutant p5-CRIF1-R26A-mCherry for 24h, then treated with Hoechst nuclear stain and viewed live under a confocal microscope.

Plasmids expressing the MTS deletion mutant δMTS or the point mutation R26A fused to a c-terminal red fluorescent tag were expressed in 1205lu cells and analyzed by live cell fluorescence microscopy.
As seen in Figure 3.16 A, the overexpressed MTS deletion mutant was localized in the nucleus and in the cytoplasm of all transfected cells. CRIF1 with the R26A mutation was partly imported into mitochondria and partly expressed in the cytoplasm and nucleus (Figure 3.16 B).
This shows that deletion of the putative MTS results in a complete loss of the mitochondrial localization phenotype and a single amino acid change is enough to disrupt mitochondrial localization in some cells. These observations indicate that the MTS is responsible for targeting CRIF1 into mitochondria and positive charge is necessary for efficient translocation.

Chapter 4

Discussion

4.1 Overview of the Experimental Results

CRIF1 and RBM10 were previously identified in a mass spectrometry-based screen searching for proteins interacting with the innate pattern recognition receptor and sensor for viral RNA RIG-I. The present study further examined a potential role for CRIF1 and RBM10 in antiviral signaling. The main findings were the following:

- In a cell culture model, depletion of CRIF1 by RNA interference resulted in an increased infection and replication rate of RNA viruses (VSV, Sendai Virus). No such effect could be observed upon infection with a DNA virus (MVA)

- Depletion of CRIF1 led to a decrease in RLH-dependent IFN-, IP-10- and IL-6-induction, both upon activation of RIG-I and MDA5. Conversely, TLR-dependent NF-κB activation did not show a reduction upon depletion of CRIF1, instead, a slight increase could be seen.

- The decrease in RLH-induced cytokine-production after depletion of CRIF1 was only observable when the stimulation occurred upstream of TBK1, and occurred independently of the positive-feedback loop active in interferon signaling.

- Overexpression of CRIF1 did not influence cytokine induction upon RLH stimulation, or viral infection rates (not shown).

- CRIF1 does not directly interact with RIG-I but unspecifically binds to anti-FLAG agarose beads

- Endogenous CRIF1 is localized to mitochondria via its N-terminal MTS. Truncation, loss of charge or blockade of this MTS by mutation or N-terminal tagging result in mislocalization to the cytoplasm or the nucleus.

4.2 Methodological Aspects of the Observed CRIF1 Function

CRIF1 knockdown cells showed a highly increased viral replication rate in different types of assays, e.g., flow cytometry or plaque assay. Cytokine response to different stimuli triggering RIG-I or MDA5 activation was diminished. Can these results be trusted considering they rely solely on RNA interference experiments?

siRNA-based loss of function assays present two types of problems that can contest their validity: sequence dependent off target effects and immune activation by recognition of the introduced foreign RNA. Both can never be completely excluded, but can be minimized and controlled for by strategies employed in this study.

Sequence-dependent off-target effects occur when an siRNA binds to and induces the cleavage of other mRNA than the one it was designed for. To reduce this risk, all siRNA sequences were blasted against the NCBI human transcript database before they were used to ensure they only had one single expected target. Also, several siRNAs with different, non-overlapping sequences were designed for each target. These different sequences are likely to differ in their off-target effects, so if the same effect is seen with different siRNAs against the same mRNA, an off-target effect as explanation becomes less likely. All three different CRIF1 siRNAs showed the same phenotype alongside a robust knockdown of CRIF1 on mRNA level. This indicates the observed effect is most likely target-specific.

In addition to unwanted targeting of other mRNAs, siRNAs, like all dsRNAs, have the capability to potently activate the innate immune system through PRRs and produce numerous unwanted effects. PRRs capable of recognizing and responding to foreign RNA include TLR3, 7 and 8 as well as the cytoplasmic sensors PKR, MDA5 and RIG-I [83]. Epithelial cells like 1205lu used in this work do not routinely express TLR7 and 8, as could also be seen in the screening assay presented in figure 3.7. PKR is expressed in most mammalian cells, but responds to longer strands of RNA than siRNA. TLR3 can be expressed on the cell surface and endosome of epithelial cells, where it should theoretically not come into contact with siRNA transfected into the cytoplasm. Cytosolic RIG-I recognizes uncapped triphosphate RNA and blunt RNA, so 5' monophosphate siRNA with a 3' dTdT overhang was used to avoid RIG-I stimulation. To control for stimulation of TLR3 or RIG-I that might have occurred, cytokine levels of unstimulated siRNA treated cells were also monitored, and no induction of IP-10 or IL-6 by the siRNAs used in this work could be detected.

Another drawback of the available methods was the lack of a reliable system to test the influence of CRIF1 on TLR-signaling, as the readout in this system was NF-κB activation, whereas for RLH signaling, it was IRF-mediated IP-10 induction. The difference observed upon stimulation of RLH-and TLR-signaling after depletion of CRIF1 could therefore be

due to an impact on IRF versus NF-κB signaling. However, RLH-mediated induction of IL-6, which is mostly NF-κB-dependent, showed a similar reduction in response to CRIF1 depletion as induction of IP-10 did. Therefore, it is likely that it is an influence on RLH- in contrast to TLR-signaling that mediates the different phenotypes upon CRIF1 depletion observed in our assays.

In conclusion, appropriate measures were taken to avoid siRNA-related artefacts since no better system to study CRIF1 function was available. Assays controlled in this way showed loss of CRIF1 function has an impact on viral replication and cytokine response in human epithelial cells.

Later experiments by Simon Hirschberger, another member of this working group, strengthened the validity of these findings: using an inducible murine knockout system [84], he also observed a repression of anti-viral signaling in CRIF1$^{-/-}$ mouse embryonic fibroblasts (MEFs).

4.3 CRIF1 Function in Antiviral Immunity: the Role of Mitochondria

Open questions remain concerning the exact mechanism of this anti-viral function of CRIF1. Evidence suggests that there is a direct effect on the cytosolic part of the signaling cascade activated by RLHs, not on the antiviral response initiated by interferon after binding to IFNAR. Taken together with our findings regarding the strict mitochondrial localization of native CRIF1, it seems likely that CRIF1 influences RLH signaling on the level of mitochondria.

The essential role of mitochondria for antiviral immunity is currently being discovered and many mitochondrial functions and characteristics have been shown to influence RLH-dependent signaling. The first link to be described was MAVS, the central adapter protein located on the outer mitochondrial membrane. A direct interaction between CRIF1 and MAVS might be possible, although the MTS classifies CRIF1 as probably being a matrix protein, thus not in contact with the outer membrane. Subfractioning studies done by our group (data not shown) support this localization.

Other mitochondrial features influencing antiviral signaling include a stable membrane potential [37], intact mitochondrial fusion [55] and the production of ROS [58, 59]. Exactly how these factors exert their influence and how they might be regulated by the cell to modulate antiviral signaling is not described well yet. The influence of CRIF1 on antiviral signaling could be mediated by any or several of these mechanisms.

Further research will be needed to examine this effect and to determine whether it is a specific antiviral function mediated by CRIF1 or a general mitochondrial defect that produces the effect.

4.4 RBM10 and Anti-viral Immunity

RBM10 was found alongside CRIF1 and, as an RNA binding protein, seemed a promising candidate in RNA-induced anti-viral signaling. However, loss of function assays did not show a reproducibly convincing influence on viral infection rate. Cytokine induction was repressed in knockdown cells, although RBM10 siRNA 1 and 2 differed in the extent of repression while knockdown efficiency was similar.
Similar to CRIF1, RBM10 was shown to interact with anti-flag beads instead of interacting specifically with RIG-I.

Taken together, there is some evidence from this study that RBM10 might play a role in RLH-mediated antiviral signaling. These results, however, were not always consistent in different types of assays and suffer from the limited validity of siRNA-based knockdown experiments. As no other system was available to us to study RBM10 function, the project was discontinued and efforts were focused on CRIF1 as the more promising candidate.

4.5 Interpretation of the Experimental Results with Regard to Current Literature

4.5.1 Described Functions of Nuclear CRIF1

Reports on CRIF1 function so far have been highly controversial.
Chung et al. first described CRIF1 as an interactor of the cell cycle modulator GADD45γ, which is also known as CR6, and hence named it cytokine-responsive protein CR6-interacting factor 1 [61]. This interaction was discovered by yeast two-hybrid screens and confirmed by immunoprecipitation of in-vitro translated CRIF1 using GADD45 proteins as bait as well as immunoprecipitation of myc-CRIF1 in mammalian cells. Hypothesizing a function in cell cycle regulation, they show that recombinant CRIF1 inhibits kinase activity of immunoprecipitated Cdc2-cyclin B1 and Cdk2-cyclin E, two cyclin-dependent kinases involved in cell cycle regulation. They also see a block of G1 to S phase progression in NIH 3T3 mouse embryo fibroblast cells upon overexpression of flag-CRIF1, which also decreases Rb phosphorylation in a manner reversible by CRIF1 siRNA.
Two years later, the same group described a functional interaction between CRIF1 and NUR77, a transcription factor involved in regulation of the hypothalamic-pituitary-adrenal axis [63]. This interaction was also discovered by yeast two-hybrid assay and confirmed by GST pulldown and immunoprecipitation of overexpressed GFP-CRIF1. In their assays, overexpressed flag-CRIF1 inhibits NUR77 transactivation and transcriptional activity in a manner partially reversible by siRNA. HEK293 cells overexpressing GFP-CRIF1 show a mild increase of cells in G1 phase and an inhibition of NUR77 dependent cell cycle progression.
After another two years, the same group published an interaction between CRIF1 and cell cycle regulator CKII seen by yeast two-hybrid assays, in-vitro Ni-pulldown assays and

immunoprecipitation of overexpressed myc-CRIF1 in HeLa cells [62]. They show CRIF1 is phosphorylated by CKII in vitro at serine residue 221. Upon overexpression of flag-CRIF1, COS7 monkey fibroblast cells show no change in cell proliferation, while overexpressing flag-CRIF1 with a mutation of serine 221 to glutamic acid, which is supposed to mimic a phosphorylated serine, leads to an increased proliferation rate. This contradiction to previous reports stating CRIF1 inhibits cell cycle progression and cell proliferation was explained as being due to different cell lines.
In the subsequent year, Suh et al. described how "CRIF1 represses the transactivation of androgen receptor by direct interaction" [64]. Again, their results are mainly obtained by overexpression of flag-CRIF1.

All these publications rely on overexpression of N-terminally tagged CRIF1 to describe interactions or functional characteristics. Considering the localization in different cellular compartments of native and N-terminally tagged CRIF1 as seen in this work, it is questionable how many of these described interactions have functional implications in vivo.

In 2008, Kwon et al. published CRIF1 to be a transcriptional co-activator of STAT3 [67]. In their assays, overexpression of HA-CRIF1 increases the transcriptional activity of overexpressed STAT3. This publication is the first to describe CRIF1 knockout mice, which show defective proliferation and massive apoptosis and die around embryonic day E6.5. The authors trace the onset of this phenotype to the degradation of residual maternal CRIF1 mRNA during blastocyst stage. Investigating cultured CRIF1 blastocyst cells, they find decreased expression of STAT3 target genes shortly before they die in culture. Conditional knockout of CRIF1 induced by infection with a Cre-bearing viral MSCV vector showed a reduced induction of STAT3 target genes by oncostatin stimulation and abolished activity of constitutively active STAT3-c in CRIF1 knockout MEFs. Being observed in knockout cells, these results are more reliable than overexpression of a tagged and possibly mislocalized protein. However, these cells die soon after the measurements are taken, so a decreased transcription might also be due to impending cell death.

In a different publication, Kwon et al. find intestinal epithelium-specific CRIF1 knockout results in perinatal lethality displaying alterations of tissue architecture in the small intestine and abnormal differentiation of absorptive enterocytes [66]. They attribute this phenotype to a defect in Elf3-mediated differentiation of intestinal epithelium, but instead of using their knockout system to reinforce that claim, overexpressed HA-tagged CRIF1 is used for interaction and functional studies.

Similarly, Kang et al. use flag-tagged CRIF1 to show that oxidative stress response protein NRF2 levels are decreased upon overexpression of CRIF1 [65]. They use flag-NRF2 as bait in an anti-flag immunoprecipitation controlled with IgG beads and find CRIF1 in the eluate. As the work presented here shows CRIF1 can bind to anti-flag-beads independently of the bait, it is not sure whether there is a direct interaction between CRIF1 and NRF2 in vivo.

4.5.2 Localization of CRIF1

Alongside different functions of CRIF1, different localizations were hypothesized and evidence was found for each of them.
A nuclear localization of the protein was claimed [61, 63, 67, 62] as it was seen in this study by overexpression of the N-terminally tagged protein.

In contrast, using immunohistochemistry with rabbit CRIF1 antiserum, Chung et al. see CRIF1 expression in the nucleus and cytoplasm of adrenal cortex and thyroid epithelial cells [61]. Due to low magnification and resolution, it cannot be deduced whether these images show a cytoplasmic or mitochondrial localization. Similar results are obtained by Kang et al., who use a monoclonal CRIF1 antibody and see both a nuclear and cytoplasmic localization [65]. Interestingly, their stain is not homogenous, as the stain of cytoplasmic proteins tends to be, but is instead freckled and forms networks compatible with a mitochondrial localization. The nucleus shows less staining in their images, but is not excluded completely as we see it in our settings.

During the course of the experimental work presented here, a new publication dealt with the subject of different localizations extensively [84]. Kim et al. show a nuclear localization of N-terminally tagged CRIF1 in contrast to C-terminally tagged CRIF1 which is localized predominantly in the mitochondria. Some cells in their setting also contain C-terminally tagged CRIF1 in the nucleus, a localization we also saw when overexpression levels were very high (data not shown). To resolve this conflict and examine the localization of native protein, they use immunohistochemistry. Interestingly, they describe their findings as localized to the "cytoplasm in all cells, with approximately 10% of cells also showing staining in both the mitochondria and the nucleus" [84], while their figure shows a clear and exclusive mitochondrial stain in all cells. This and the following subcellular fractioning confirms our finding of CRIF1 as a mitochondrial protein.

The same publication also describes a 35aa sequence at the N-terminus which, if deleted, results in a nuclear localization. If this sequence is added at the N-terminus of an N-terminal GFP-tag, the resulting protein is localized exclusively to mitochondria. Thus, our finding that an N-terminal MTS is responsible for the mitochondrial localization of CRIF1 is confirmed by this publication.

So is the answer simply that CRIF1 is a mitochondrial protein, and all nuclear observations were based on artefacts? Our results using rabbit anti-CRIF1 antibody in 1205lu cells and Kim et al. using goat anti-CRIF1 antibody in HeLa cells certainly suggest the same, and offer an explanation for earlier observations using tagged and overexpressed CRIF1. But why is there a nuclear localization signal (NLS) conserved near the C-terminus and functional the moment mitochondrial localization is blocked?

Dual targeting of mitochondrial proteins is not an uncommon phenomenon [85]. Competition between two targeting signals can occur, and inaccessibility of a signal by folding, protein binding or post-translational modification of the distributed polypeptide can direct a protein to one location or the other. An incomplete import or retrograde translocation by membrane leakage or protein export from organelles can also occur [86]. Thus, one could speculate on a differential localization of CRIF1 in the cell depending on stimulation, e.g. during apoptosis when mitochondria become leaky, to perform different functions in mitochondria or nuclei.
Chung et al. see a nuclear location of CRIF1 in primary tissue using anti-CRIF1 antiserum [87]. Is staining of CRIF1 dependent on the cell or tissue type, or on the antibody used? Many questions about the location of this essential yet elusive protein remain to be answered.

4.5.3 Functions of Mitochondrial CRIF1

In their recent paper, Kim et al. not only show a mitochondrial localization of CRIF1, but examine its function elaborately using CRIF1 knockout MEFs and brain-specific knockout mice [84].

These knockout animals exhibited reduced lifespans as well as locomotion disabilities due to neurodegeneration in the hippocampus and cerebral cortex. Mitochondria in these areas displayed morphological abnormalities including loss of electron-dense material from the matrix and distorted or reduced number of christae. Tracing this degeneration to protein levels, CRIF1 knockout mice showed reduced levels of oxidative phosphorylation (OXPHOS) complexes I and IV.

To study a mitochondrial function of CRIF1, CRIF1$^{-/flox}$ MEFs were infected with a retrovirus expressing Cre-recombinase to obtain CRIF1 knockout MEFs. Oxygen consumption rates in these knockout MEFs were drastically decreased compared to wildtype MEFs and did not respond to treatment with chemical inhibitors of mitochondrial respiratory chains. Mitochondrial membrane potential measured with JC-1 was reduced and superoxide levels were elevated. This suggests mitochondria lacking CRIF1 are depolarized and dysfunctional.
ATP levels in CRIF1 knockout cells were normal in high-glucose medium, but decreased when grown in glucose-free medium compared to wildtype cells, indicating these cells rely on glycolysis for ATP production. Enzyme activity of OXPHOS complexes I, III, IV and V was markedly reduced in CRIF1 knockout MEFs, and their mitochondria showed structural abnormalities consistent with impaired OXPHOS complexes. Isolated mitochondria showed lower levels of OXPHOS subunits of complexes I, III and IV originating from both mitochondrial and nuclear genomes while transcripts of these proteins were at a similar level as in wildtype cells. As the formation of respiratory complexes and supercomplexes was also impaired in CRIF1 knockout cells, the authors concluded CRIF1 functions in the

posttranslational biogenesis of OXPHOS complexes.

To pin down the role of CRIF1 in the mitoribosomal biogenesis of OXPHOS complexes, gradient sedimentation analysis was performed and CRIF1 was found to co-migrate with assembled 55S mitoribosomes and with the 39S large ribosomal subunits. As CRIF1 knockout MEFs showed a decrease in assembled 55S mitoribosomes while both subunits by themselves were assembled similarly to wildtype cells, it was hypothesized that CRIF1 is necessary for intersubunit assembly.
Pulse-chase assays showed a reduced protein synthesis in CRIF1 knockout cells and organelle translation assays revealed CRIF1 knockout mitochondria produced reduced amounts and aberrant patterns of nascent translation products. In addition to these impaired synthetic activities, CRIF1 knockout mitochondria also showed significantly less membrane embedded and more soluble, extractable proteins compared to mitochondria expressing CRIF1, suggesting that the integration of translation products into the inner mitochondrial membrane also depends on CRIF1.
Using immunoprecipitation, native CRIF1 was found to interact with large mitoribosomal subunits and molecular chaperones as well as several nascent OXPHOS polypeptides.

The authors conclude CRIF1 is essential for the synthesis and insertion of nascent OXPHOS polypeptides into the inner mitochondrial membrane. Indeed, the reduced levels of OXPHOS subunits could be rescued by expressing CRIF1-HA within the knockout cells. HA-CRIF1, which localizes to the nucleus, did not alter expression of OXPHOS subunits in CRIF1 knockout cells, verifying it is mitochondrial CRIF1 that produces the observed knockout phenotype.

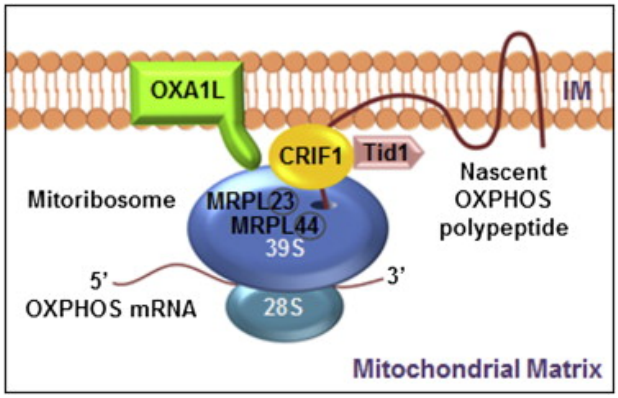

Figure 4.1: CRIF1 in Mitoribosomal Synthesis of OXPHOS Polypeptides

Schematic representation of CRIF1 function in mitoribosomal synthesis of OXPHOS polypeptides (from [84]).

Figure 4.1 summarizes how Kim et al. hypothesize CRIF1 to be involved in the synthesis and insertion of nascent OXPHOS polypeptides into the inner mitochondrial membrane.

Based on their findings on the mitochondrial function of CRIF1, the same group studied the mitochondrial defects produced by CRIF1 insufficiency in adipose tissue and cardiomyocytes.
Using CRIF1 haploinsufficient adipocytes, they find increased ROS production and a chemokine dysregulation [87]. Interestingly, they report an increase in IP-10 levels in response to CRIF1 siRNA treatment in otherwise unstimulated cells. It remains to be seen if this contrast to our findings is due to different cell lines or possibly a stimulatory effect of the siRNA. Their findings based on CRIF1 knockout cells, however, have to be viewed critically with regard to immune signaling as there is a genomic overlap between CRIF1 and the untranslated region of UV excision repair protein RAD23, which has been shown to negatively regulate antiviral signaling [88]. In our studies, we find a decreased expression of RAD23 in CRIF1$^{f/f}$ cells, possibly explaining a difference in immune activation in these cells.
Using the same conditional knockout system of CRIF1 in cardiomyocytes, Shin et al. show a fragmented mitochondrial network with a lack of christae and an increased mitochondrial membrane potential followed by a loss of membrane potential after several days [89].

In conclusion, CRIF1 seems to influence mitochondrial ROS production, dynamics and membrane potential.
In later experiments, our group could also show that CRIF1 knockout MEFs had a decreased mitochondrial membrane potential which has been shown to be critical for MAVS activation and signaling [37]. A decreased mitochondrial membrane potential in CRIF1-depleted cells could thus explain the decrease in RLH-dependent signaling we observed.
In contrast, ROS production has been linked to increased TLR signaling [90, 91] and NF-κB activation [92]. Hence, the increase in NF-κB activation we see upon TLR stimulation in CRIF1-depleted cells could be due to an increased ROS production, whereas mitochondrial membrane potential is not essential here.
Figure 4.2 summarizes the putative role of CRIF1 in anti-viral signaling.

4.5.4 CRIF1 in Health and Disease

Based on this work, CRIF1 can be used to modify and study the role of early mitochondrial damage in the context of antiviral signaling, but its application is not limited to this.
Recently, mitochondrial dysfunction has been shown to be essential in the development of various diseases such as diabetes [93], atherosclerosis [94] and ischemia reperfusion injury [95], cancer [96] and ageing [97], as well as various neurodegenerative diseases like Parkinson's, Huntington's, Alzheimer's disease, epilepsy and Friedreich ataxia [98], often in conjunction with innate immune signaling, as in liver cirrhosis [90].
Here, conditional CRIF1 knockout cells might provide a model to study pathogenetic and therapeutic aspects, as it was done with cardiomyopathy [89].

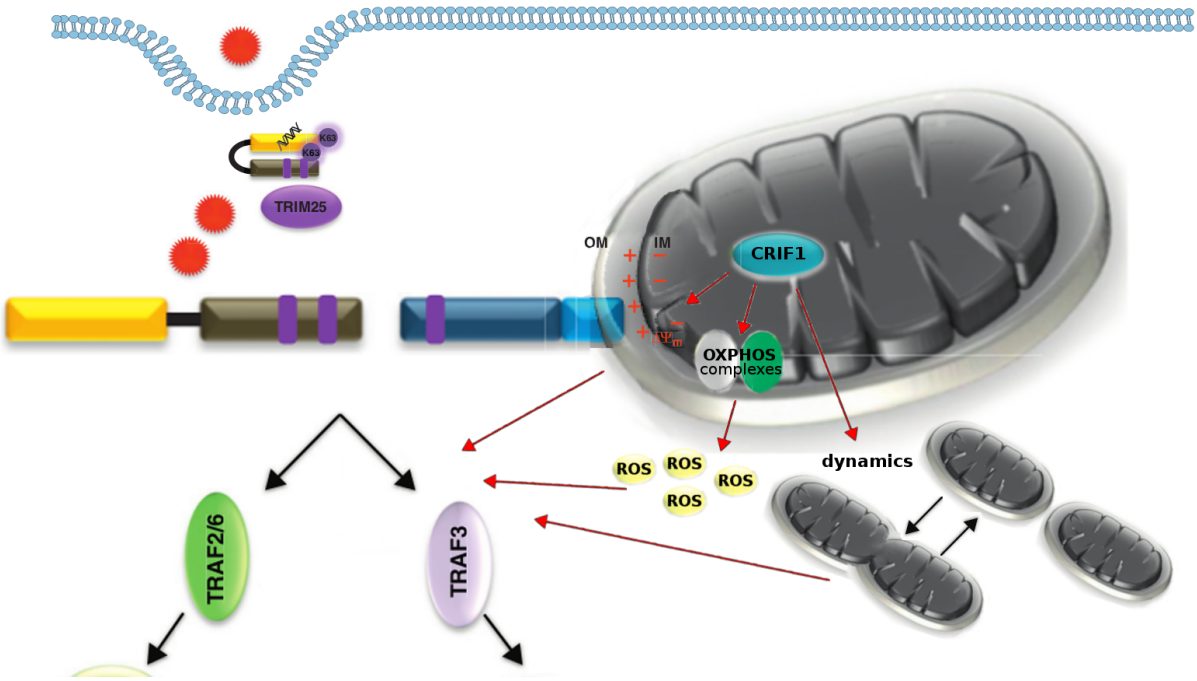

Figure 4.2: Putative Influence of CRIF1 in Antiviral Signaling

CRIF1 localized in the mitochondria and involved in the production and membrane-insertion of proteins translated in the mitochondria including the oxphos-complexes of the respiratory chain might influence RLH signaling directly via MAVS, by influencing mitochondrial membrane potential, dynamics or ROS production or through an as yet unknown mechanism (adapted from [38]).

Summary

RIG-I-like helicases are ubiquitously expressed pattern recognition receptors of the innate immune system that are indispensable for sensing the presence of replicating viruses. They are activated by viral RNA to induce a precisely modulated signaling cascade inducing an antiviral gene program that helps the infected cell to resist viral replication and dissemination.
In an effort to identify new regulators of the RIG-I pathway, proteins that co-immunoprecipitated with overexpressed RIG-I-FLAG in VSV-infected cells were identified by mass spectrometry. In these screening experiments CRIF1 and RBM10 were identified as potential RIG-I interacting proteins. The aim of the present study was to investigate if CRIF1 or RBM10 indeed had a function in antiviral immunity and if so, by what mechanism.
In a cell culture model depletion of CRIF1 using RNA interference resulted in an increased infection and replication rate by RNA viruses (VSV, Sendai Virus). No such effect could be observed upon infection with a DNA virus (MVA). Mechanistically, RIG-I- and MDA5-dependent IFN-, IP-10- and IL-6-induction was diminished upon depletion of CRIF1, while a mild increase in TLR-dependent NF-κB activation could be observed. The interaction of CRIF1 with the RLH-dependent antiviral signaling cascade seemed to occur upstream of TBK1, but downstream of RIG-I, as a direct interaction between CRIF1 and RIG-I could not be established. Our experiments suggest CRIF1 influences antiviral signaling on the level of MAVS, the common adapter of RLH located in the outer mitochondrial membrane.
Previous reports described CRIF1 as a nuclear protein. In contrast, this study found CRIF1 to be localized exclusively to the mitochondria by an N-terminal mitochondrial targeting sequence, whereas nuclear localization occurred only as an artefact upon overexpression or N-terminal tagging of the protein.
Mitochondria play an essential role in antiviral signaling via the central adaptor protein MAVS and mitochondria-derived reactive oxygen species, mitochondrial membrane potential and dynamics have all been described to influence RLH signaling.

Our data suggests CRIF1 influences RLH signaling at the level of mitochondria. Further research will be needed to determine the exact mechanisms how CRIF1-induced changes in mitochondrial function lead to the observed effects on antiviral signaling.

Zusammenfassung

RIG-I-*like* Helikasen sind ubiquitäre Rezeptoren, die für die Erkennung sich vermehrender Viren unabdingbar sind. Nach ihrer Aktivierung durch virale RNA induzieren sie eine genau modulierte Signalkaskade, welche ein genetisches Programm aktiviert, das der infizierten Zelle hilft, Replikation und Ausbreitung des Virus zu verhindern.

Um neue Einflussfaktoren auf die RIG-I-Signalkaskade zu ermitteln, wurden Proteine per Massenspektrometrie identifiziert, welche mit überexprimiertem RIG-I-flag in VSV-infizierten Zellen koimmunprezipitieren. In diesen Screeninguntersuchungen wurden CRIF1 und RBM10 als potentielle, mit RIG-I interagierende Proteine identifiziert. Ziel der vorliegenden Studie war es nun, herauszufinden, ob CRIF1 und RBM10 einen Einfluss auf die Virusabwehr haben, und wenn ja, über welchen Mechanismus.

In einem Zellkulturmodell wurde CRIF1 mittels RNA-Interferenz depletiert. Hierdurch kam es zu einer erhöhten Infektions- und Replikationsrate von RNA-Viren (VSV, Sendai Virus). Eine Infektion mit einem DNA-Virus (MVA) zeigte keinen solchen Effekt. Mechanistisch war die RIG-I- und MDA5-abhängige IFN-, IP-10- und IL-6-Induktion nach Depletion von CRIF1 reduziert, während die TLR-abhängige Aktivierung von NF-κB etwas erhöht wurde. Die Interaktion von CRIF1 mit der RLH-Signalkaskade schien oberhalb von TBK1, jedoch unterhalb von RIG-I stattzufinden. Eine direkte Interaktion zwischen CRIF1 und RIG-I konnte nicht bestätigt werden. Unsere Experimente legen stattdessen nahe, dass CRIF1 die antivirale Signalkaskade auf der Ebene von MAVS als gemeinsamem Adaptermolekül der RLH auf der äußeren Mitochondrienmembran beeinflusst.

Frühere Veröffentlichungen beschrieben CRIF1 als nukleäres Protein. Wir konnten dagegen zeigen, dass CRIF1 durch eine n-terminale Lokalisierungssequenz ausschließlich in Mitochondrien lokalisiert ist und die Lokalisation im Kern lediglich als Artefakt durch Überexpression oder N-terminales *tagging* entsteht.

Mitochondrien spielen mit dem Adapterprotein MAVS in der äußeren Membran eine essenzielle Rolle als antivirale Signalplattformen. Mitochondriale *reactive oxygen species*, das mitochondriale Membranpotential und die Dynamik von Aufbau und Fusion von Mitochondrien sind als Einflussfaktoren der antiviralen Signaltransduktion über RIG-I-*like* Helikasen beschrieben.

Unsere Ergebnisse lassen vermuten, dass CRIF1 einen Einfluss auf die antivirale Signaltransduktion auf der Ebene der Mitochondrien ausübt. Weitere Untersuchungen wer-

den nötig sein, um den genauen Mechanismus zu beschreiben, über den CRIF1-bedingte Veränderungen der mitochondrialen Funktion die beobachteten Effekte auf die antivirale Signalantwort verursachen.

List of Abbreviations

ADP adenosine diphosphate

AMP adenosine monophosphate

AscI arthrobacter species restriction enzyme I

APS Ammonium persulfate

ATCC American type culture collection

ATP adenosine triphosphate

bp base pair

CARD caspase-recruitment domain

cDNA complementary DNA

cGAS cGAMP synthase

CIAP calf intestine alkaline phosphatase

CKII casein kinase II

CLR C-type lectin receptor

CoQ coenzyme Q

CpG ODN cytosine phosphodiester guanine oligodeoxynucleotide

CRIF1 cytokine-responsive protein CR6-interacting factor 1

CRP C-reactive protein

CTD C-terminal domain

DAPI 4',6-diamidino-2-phenylindole

DMEM Dulbecco's modified eagle medium

DMSO Dimethyl sulfoxide

DNA deoxyribonucleic acid

dNTP deoxyribooligonucleotide

DpnI diplococcus pneumoniae restriction enzyme I

Drp1 dynamin related protein 1

dsRNA double-stranded RNA

EDTA ethylenediaminetetraacetic acid

ELISA enzyme linked immunosorbent assay

EBV Epstein-Barr virus

EMCV encephalomyocarditis virus

FA FseI-AscI

FBS fetal bovine serum

FSC forward scatter

FseI frankia species Eul1b restriction enzyme I

GADD45 growth arrest and DNA damage inducible protein 45

GADD45γ growth-arrest and DNA-damage inducible protein gamma

GFP green fluorescent protein

GL2 firefly luciferase

GPX glutathione peroxidase

HEK293 human embryonic kidney 293

HPRT hypoxanthine-guanine phosphoribosyltransferase

HRP horseradish peroxidase

HSP heat-shock protein

iE-DAP D-glutamyl-meso-diaminopimelic acid

IFN interferon

IFN-α interferon-α

IFN-β interferon-β

IFN-γ interferon-γ

IFN-λ interferon-λ

IFNAR IFN-α receptor

IκBα inhibitor of NF-κBα

IKK inducible IαB kinase

IL interleukin

IP-10 interferon gamma induced protein 10 kDa

IRF IFN regulatory factor

ISG interferon stimulated gene

ISGF interferon stimulated gene factor

ISRE interferon stimulated responsive element

JAK Janus kinase

kb kilobase

LB Luria Bertani

LGP2 laboratory of genetics and physiology 2

LMU Ludwig-Maximilians-Universität

LPS lipopolysaccharid

M matrix

MAL MyD88-adaptor like

MAPK mitogen-activated protein kinase

MAVS mitochondrial antiviral signaling protein

MDA5 melanoma-differentiation-associated protein 5

MEF mouse embryonic fibroblast

Mfn mitofusin

MOPS Morpholinepropanesulfonic acid

MPI Max von Pettenkofer Institute

MTS mitochondrial targeting sequence

MVA Modified vaccinia Ankara

Mx myxovirus resistance

NOD1 nucleotide-binding oligomerization domain-containing protein 1

MOI multiplicity of infection

mRNA messenger RNA

MSCV murine stem cell virus

MyD88 myeloid differentiation factor 88

NCBI National Center for Biotechnology Information

NEMO NF-κB essential modulator

NF-κB nuclear factor kappa B

NK cell natural killer cell

NLR NOD-like receptor

NLS nuclear localization signal

NRF2 nuclear respiratory factor 2

NUR77 nuclear receptor 77

OAS 2'-5'-oligoadenylate synthase

OD optical density

OXPHOS oxidative phosphorylation

PAGE polyacrylamide gel electrophoresis

PAMP pathogen associated molecular pattern

PBMC peripheral blood mononuclear cell

PBS phosphate buffered saline

PCR polymerase chain reaction

pDC plasmacytoid dendritic cell

PFU plaque forming unit

PI Propidium iodide

PKR protein kinase R

PMSF Phenylmethylsulfonyl fluoride

poly(I:C) polyinosinic:polycytidylic acid

PRR pattern recognition receptor

qRT-PCR quantitative real time reverse transcription PCR

RBM10 RNA binding motif 10

RIG-I retinoic acid-inducible gene

RLH RIG-I-like helicase

RNA ribonucleic acid

RNAi RNA interference

ROS reactive oxygen species

RRM RNA recognition motif

RT room temperature

SDS sodium dodecyl sulfate

SEM standard error of means

SeV Sendai virus

siRNA small interfering RNA

SOD superoxide dismutase

SSC side scatter

ssRNA single-stranded RNA

STAT signal transducer and activator of transcription

TAE tris-acetate EDTA

TBK1 TANK-binding kinase 1

TBS tris-buffered saline

TCR T cell receptor

TLR Toll-like receptor

TNFα tumor necrosis factor-alpha

TOM translocase of the outer membrane

TRAF TNF-receptor-associated factor

TRAM TRIF-related adaptor molecule

TRIF TIR-domain-containing adaptor protein inducing IFN-beta

TRIM25 tripartite motif E3 ligase

TUM Technical University Munich

TYK tyrosine kinase

UV ultraviolet

VSV Vesicular stomatitis virus

VSV M VSV mutant M51R

wt wildtype

Bibliography

[1] Ralph M. Steinman and Carol L. Moberg. "Zanvil Alexander Cohn 1926-1993 ". In: *Immunity* 179 (1994), pp. 1–30.

[2] M K Jenkins and R H Schwartz. "Antigen presentation by chemically modified splenocytes induces antigen-specific T cell unresponsiveness in vitro and in vivo." In: *Journal of Experimental Medicine* 165.2 (1987), pp. 302–19.

[3] Charles Janeway Jr. "Approaching the asymptote? Evolution and revolution in immunology ". In: *Cold Spring Harbor Symposium on Quantitative Biology* 54 (1989), pp. 1–13.

[4] Ruslan Medzhitov, P Preston-Hurlburt, and Charles Janeway Jr. "A human homologue of the Drosophila Toll protein signals activation of adaptive immunity ". In: *Nature* 388 (1997), pp. 394–7.

[5] RB Yang and MR Mark. "Toll-like receptor-2 mediates lipopolysaccharide-induced cellular signalling ". In: *Nature* 395 (1998), pp. 394–7.

[6] Janeway CA Jr and Medzhitov R. "Innate immune recognition." In: *Annual Review of Immunology* 20 (2002), pp. 197–216.

[7] Noah W. Palm and Ruslan Medzhitov. "Pattern recognition receptors and control of adaptive immunity ". In: *Immunological Reviews* 227 (2009), pp. 221–233.

[8] Kenneth Murphy. *Janeway's immunobiology, 8th edition*. Garland Science, Taylor & Francis Group, LLC, 2012.

[9] A. Isaacs and J. Lindenmann. "Virus interference. I. The interferon ". In: *Proceedings of the Royal Society of London. Series B, Biological sciences* 147 (1957), pp. 258–267.

[10] Volker Fensterl and Ganes C. Sen. "Interferons and viral infections". In: *Biofactors* 35 (2009), pp. 14–20.

[11] Kenya Honda, Akinori Takaoka, and Tadatsugu Taniguchi. "Type I Inteferon Gene Induction by the Interferon Regulatory Factor Family of Transcription Factors ". In: *Immunity* 25 (2006), pp. 349–360.

[12] Leonidas C. Platanias. "Mechanisms of type-I- and type-II-interferon-mediated signalling ". In: *Nature Reviews Immunology* 5 (2005), pp. 375–386.

[13] Otto Haller, Georg Kochs, and Friedemann Weber. "Interferon, Mx, and viral countermeasures ". In: *Cytokine & Growth Factor Reviews* 18 (2007), pp. 425–433.

[14] Akinori Takaoka et al. "Integration of interferon-alpha/beta signalling to p53 responses in tumour suppression and antiviral defence ". In: *Nature* 424 (2003), pp. 516–523.

[15] Daniel B. Stetson and Ruslan Medzhitov. "Type I Interferons in Host Defense ". In: *Immunity* 25 (2006), pp. 373–381.

[16] Otto Haller, Peter Staeheli, and Georg Kochs. "Interferon-induced Mx proteins in antiviral host defense ". In: *Biochimie* 89 (2007), pp. 812–818.

[17] Robert H. Silverman. "Viral Encounters with 2',5'-Oligoadenylate Synthetase and RNase L during the Interferon Antiviral Response ". In: *Journal of Virology* 81 (2007), pp. 12720–12729.

[18] Lucile Espert et al. "ISG20, a New Interferon-induced RNase Specific for Single-stranded RNA, Defines an Alternative Antiviral Pathway against RNA Genomic Viruses ". In: *The Journal of Biological Chemistry* 278 (2003), pp. 16151–16158.

[19] M. A. García et al. "Impact of Protein Kinase PKR in Cell Biology: from Antiviral to Antiproliferative Action ". In: *Microbiology and Moleculat Biology Reviews* 70 (2006), pp. 1032–1060.

[20] Richard E. Randall and Stephen Goodbourn. "Interferons and viruses: an interplay between induction, signalling, antiviral responses and virus countermeasures ". In: *Journal of General Virology* 89 (2008), pp. 1–47.

[21] Joel W. Graff et al. "Zinc-binding domain of rotavirus NSP1 is required for proteasome-dependent degradation of IRF3 and autoregulatory NSP1 stability ". In: *Journal of General Virology* 88 (2007), pp. 613–620.

[22] Maureen C. Ferran and Jean M. Lucas–Lenard. "The vesicular stomatitis virus matrix protein inhibits transcription from the human beta interferon promoter ". In: *Journal of Virology* 71 (1997), pp. 371–377.

[23] Antonio Alcami and Geoffrey L. Smith. "Cytokine receptors encoded by poxviruses: a lesson in cytokine biology ". In: *Immunology Today* 16 (1995), pp. 474–478.

[24] Krzysztof Brzozka, Stefan Finke, and Karl-Klaus Conzelmann. "Inhibition of Interferon Signaling by Rabies Virus Phosphoprotein P: Activation-Dependent Binding of STAT1 and STAT2 ". In: *Journal of Virology* 80 (2006), pp. 2675–2683.

[25] Jeremy Poppers et al. "Inhibition of PKR Activation by the Proline-Rich RNA Binding Domain of the Herpes Simplex Virus Type 1 Us11 Protein ". In: *Journal of Virology* 74 (2000), pp. 11215–11221.

[26] Reis e Sousa C. Osorio F. "Myeloid C-type lectin receptors in pathogen recognition and host defense ". In: *Immunity* 34 (2011), pp. 651–64.

[27] N. Inohara and G. Nunez. "NODs: intracellular proteins involved in inflammation and apoptosis". In: *Nat. Rev. Immunol* 3 (2003), pp. 371–382.

[28] Lijun Sun et al. "Cyclic GMP-AMP Synthase Is a Cytosolic DNA Sensor That Activates the Type I Interferon Pathway". In: *Science* 339.6121 (2013), pp. 786–791.

[29] Himanshu Kumar, Taro Kawai, and Shizuo Akira. "Pathogen Recognition by the Innate Immune System". In: *International Reviews of Immunology* 30 (2011), pp. 16–34.

[30] Daniel Kolakofsky, Eva Kowalinski, and Stephen Cusack. "A structure-based model of RIG-I activation". In: *RNA* 18 (2012), pp. 2118–2127.

[31] Takashi Satoha and Hiroki Kato et al. "LGP2 is a positive regulator of RIG-I– and MDA5-mediated antiviral responses". In: *PNAS* 107 (2010), pp. 1512–1517.

[32] Simon Rothenfußer et al. "The RNA Helicase Lgp2 Inhibits TLR-Independent Sensing of Viral Replication by Retinoic Acid-Inducible Gene-I". In: *The Journal of Immunology* 175 (2005), pp. 5260–5268.

[33] Leonid Gitlin et al. " Essential role of mda-5 in type I IFN responses to polyriboinosinic:polyribocytidylic acid and encephalomyocarditis picornavirus ". In: *PNAS* 103 (2006), pp. 8459–8464.

[34] Michaela U. Gack et al. "TRIM25 RING-finger E3 ubiquitin ligase is essential for RIG-I-mediated antiviral activity". In: *nature* 446 (2007), pp. 916–920.

[35] Osamu Takeuchi and Shizuo Akira. "MDA5/RIG-I and virus recognition". In: *Current Opinion in Immunology* 20 (2008), pp. 17–22.

[36] Andrea Ablasser et al. "RIG-I-dependent sensing of poly(dA:dT) through the induction of an RNA polymerase III-transcribed RNA intermediate". In: *nature immunology* 10 (2009), pp. 1065–72.

[37] Takumi Koshiba et al. "Mitochondrial Membrane Potential Is Required for MAVS-Mediated Antiviral Signaling". In: *Science Signaling* 4.158 (Feb. 2011), ra7.

[38] S Mehdi Belgnaoui, Suzanne Paz, and John Hiscott. "Orchestrating the interferon antiviral response through the mitochondrial antiviral signaling (MAVS) adapter". In: *Current Opinion in Immunology* 23 (2011), pp. 564–572.

[39] Sylwia Wasiak Heidi M. McBride Margaret Neuspiel. "Mitochondria: More Than Just a Powerhouse ". In: *Current Biology* 14 (2006), R551–R560.

[40] Lang BF. Gray MW Burger G. " Mitochondrial evolution ". In: *Science* 283 (1999), pp. 1476–81.

[41] Sankar Ghosh Phillip West Gerald S. Shadel. " Mitochondria in innate immune responses ". In: *Nature Reviews Immunology* 6 (2011), pp. 389–402.

[42] Vladimir Gogvadze Sten Orrenius and Boris Zhivotovsky. " Mitochondrial Oxidative Stress: Implications for Cell Death ". In: *Annual Review of Pharmacology and Toxicology* 47 (2007), pp. 143–183.

[43] P Wu et al. "Starvation and diabetes increase the amount of pyruvate dehydrogenase kinase isoenzyme 4 in rat heart." In: *Biochem. J.* 329.1 (1998), pp. 197–201.

[44] Tianzheng Yu, James L. Robotham, and Yisang Yoon. "Increased production of reactive oxygen species in hyperglycemic conditions requires dynamic change of mitochondrial morphology". In: 103.8 (2006), pp. 2653–2658.

[45] Takumi Koshiba. "Mitochondrial-mediated antiviral immunity". In: *Biochimica et Biophysica Acta (BBA) - Molecular Cell Research* 1833.1 (2013), pp. 225–232.

[46] Damien Arnoult et al. "The role of mitochondria in cellular defense against microbial infection". In: *Seminars in Immunology* 21.4 (2009), pp. 223–232.

[47] Richard J. Youle and Mariusz Karbowski. "Mitochondrial fission in apoptosis". In: *Nat Rev Mol Cell Biol* 6.8 (2005), pp. 657–663.

[48] K. Tanaka, T. Kanbe, and T. Kuroiwa. "Three-dimensional behaviour of mitochondria during cell division and germ tube formation in the dimorphic yeast Candida albicans". In: *Journal of Cell Science* 73.1 (1985), pp. 207–220.

[49] Kuang-Hueih Chen et al. "Dysregulation of HSG triggers vascular proliferative disorders". In: *Nat Cell Biol* 6.9 (Sept. 2004), pp. 872–883.

[50] Russell G. Jones et al. "AMP-Activated Protein Kinase Induces a p53-Dependent Metabolic Checkpoint". In: *Molecular Cell* 18.3 (2005), pp. 283–293.

[51] Rashu B. Seth and Lijun Sun. "Identification and Characterization of MAVS, a Mitochondrial Antiviral Signaling Protein that ActivatesNF-κB and IRF3". In: *Cell* 122 (2005), pp. 669–682.

[52] Fajian Hou et al. "{MAVS} Forms Functional Prion-like Aggregates to Activate and Propagate Antiviral Innate Immune Response". In: *Cell* 146.3 (2011), pp. 448–461.

[53] Xin-Yi Liu et al. "Tom70 mediates activation of interferon regulatory factor 3 on mitochondria". In: *Cell Res* 20.9 (Sept. 2010), pp. 994–1011.

[54] Kai Yasukawa et al. "Mitofusin 2 Inhibits Mitochondrial Antiviral Signaling". In: *Science Signaling* 2.84 (Aug. 2009), ra47.

[55] Kazuhide Onoguchi et al. "Virus-Infection or 5'ppp-RNA Activates Antiviral Signal through Redistribution of IPS-1 Mediated by MFN1". In: *PLoS Pathog* 6.7 (July 2010), e1001012.

[56] Céline Castanier et al. "Mitochondrial dynamics regulate the RIG-I-like receptor antiviral pathway". In: *EMBO reports* 11.2 (Feb. 2010), pp. 133–138.

[57] A. Salonen, T. Ahola, and L. Kääriäinen. "Viral RNA Replication in Association with Cellular Membranes". In: *Membrane Trafficking in Viral Replication*. Ed. by Mark Marsh. Vol. 285. Current Topics in Microbiology and Immunology. Springer Berlin Heidelberg, 2005, pp. 139–173.

[58] Anton Soucy-Faulkner and Esperance Mukawera. "Requirement of NOX2 and reactive oxygen species for efficient RIG-I-mediated antiviral response through regulation of MAVS expression." In: *PLoS Pathogens* 6 (2010), e1000930.

[59] Michal Caspi Tal et al. "Absence of autophagy results in reactive oxygen species-dependent amplification of RLR signaling". In: *Proceedings of the National Academy of Sciences* 106.8 (2009), pp. 2770–2775.

[60] L.C. Sutherland. "RNA binding motif (RBM) proteins: a novel family of apoptosis modulators?" In: *J. Cell. Biochem* 94 (2005), pp. 5–24.

[61] Hyo-Kyun Chung and Yong-Weon Yi. "CR6-interacting factor 1 interacts with Gadd45 family proteins and modulates the cell cycle". In: *Journal of Biological Chemistry* 278 (2003), pp. 28079–88.

[62] Nang-Soo Oh and Soo-Hyun Yoon. "Phosphorylation of CKBBP2/CRIF1 by protein kinase CKII promotes cell proliferation". In: *Gene* 386 (2007), pp. 147–53.

[63] Ki-Cheol Park. "CR6-Interacting Factor 1 Interacts with Orphan Nuclear Receptor Nur77 and Inhibits Its Transactivation". In: *Molecular Endocrinology* 1 (2005), pp. 12–24.

[64] Ji Ho Suh. " CR6-Interacting Factor 1 Represses the Transactivation of Androgen Receptor by Direct Interaction". In: *Molecular Endocrinology* 22 (2008), pp. 33–46.

[65] Hyo Jin Kang. "CR6-interacting factor 1 (CRIF1) regulates NF-E2-related factor 2 (NRF2) protein stability by proteasome-mediated degradation". In: *Journal of Biological Chemistry* 285 (2010), pp. 21258–68.

[66] Min-chul Kwon. "Essential Role of CR6-interacting Factor 1 (Crif1) in E74-like Factor 3 (ELF3)-mediated Intestinal Development". In: *Journal of Biological Chemistry* 284 (2009), pp. 33634–41.

[67] Min-chul Kwon. "Crif1 is a novel transcriptional coactivator of STAT3". In: *EMBO Journal* 27 (2008), pp. 642–653.

[68] Oliver Ebert et al. "Oncolytic Vesicular Stomatitis Virus for Treatment of Orthotopic Hepatocellular Carcinoma in Immune-competent Rats". In: *Cancer Research* 63.13 (2003), pp. 3605–3611.

[69] Oliver Ebert et al. "Systemic therapy of experimental breast cancer metastases by mutant vesicular stomatitis virus in immune-competent mice". In: *Cancer Gene Ther* 12.4 (Nov. 2004), pp. 350–358.

[70] Antonio Cosma et al. "Neutralization Assay Using a Modified Vaccinia Virus Ankara Vector Expressing the Green Fluorescent Protein Is a High-Throughput Method To Monitor the Humoral Immune Response against Vaccinia Virus ". In: *Clinical and Diagnostic Laboratory Immunology* 11 (2004), pp. 406–410.

[71] Andreas Schmidt et al. "5'-triphosphate RNA requires base-paired structures to activate antiviral signaling via RIG-I ". In: *PNAS* 106 (2009), pp. 12067–12072.

[72] Rüdiger Neef et al. "Phosphorylation of mitotic kinesin-like protein 2 by polo-like kinase 1 is required for cytokinesis". In: *The Journal of Cell Biology* 162.5 (2003), pp. 863–876.

[73] Sayda M. Elbashir, Harborth J, and Lendeckel W. "Duplexes of 21-nucleotide RNAs mediate RNA interference in cultured mammalian cells ". In: *Nature* 411 (2001), pp. 494–498.

[74] Michael Wenzel et al. "Cytosolic DNA Triggers Mitochondrial Apoptosis via DNA Damage Signaling Proteins Independently of AIM2 and RNA Polymerase III". In: *The Journal of Immunology* 188.1 (2012), pp. 394–403.

[75] Robert Besch et al. "Proapoptotic signaling induced by RIG-I and MDA-5 results in type I interferon–independent apoptosis in human melanoma cells". In: *The Journal of Clinical Investigation* 119.8 (Aug. 2009), pp. 2399–2411.

[76] Zhiguo Sun et al. "Phosphorylation of RIG-I by Casein Kinase II Inhibits Its Antiviral Response". In: *Journal of Virology* 85.2 (2011), pp. 1036–1047.

[77] Janina Görnemanna et al. "Interaction of Human Papillomavirus Type 16 L2 with Cellular Proteins: Identification of Novel Nuclear Body-Associated Proteins ". In: *Virology* 303 (2002), pp. 69–78.

[78] Hendrik Poeck et al. "5'-triphosphate-siRNA: turning gene silencing and RIG-I activation against melanoma". In: *Nat Med* 14.11 (2008), pp. 1256–1263.

[79] Brian Lichty et al. "Vesicular stomatitis virus: re-inventing the bullet". In: *TRENDS in Molecular Medicine* 10 (2004), pp. 210–216.

[80] Maryam Ahmed et al. "Ability of the Matrix Protein of Vesicular Stomatitis Virus To Suppress Beta Interferon Gene Expression Is Genetically Correlated with the Inhibition of Host RNA and Protein Synthesis". In: *Journal of Virology* 77 (2003), pp. 4646–4657.

[81] Camilla Foged. "siRNA Delivery with Lipid-based Systems: Promises and Pitfalls". In: *Current Topics in Medicinal Chemistry* 12.2 (2012), pp. 97–107.

[82] M.G. Claros and P. Vincens. "Computational method to predict mitochondrially imported proteins and their targeting sequences". In: *European Journal of Biochemistry* 241 (1996), pp. 770–786.

[83] Kathryn A. Whitehead et al. "Silencing or Stimulation? siRNA Delivery and the Immune System". In: *Annual Review of Chemical and Biomolecular Engineering* 2 (2011), pp. 77–96.

[84] Sung Jung Kim and Min-chul Kwon. "CRIF1 is essential for the Synthesis and Insertion of Oxidative Phosphorylation Polypeptides in the Mammalian Mitochondrial Membrane". In: *Cell Metabolism* 16 (2012), pp. 1–10.

[85] Ohad Yogev and Ophry Pines. " Dual targeting of mitochondrial proteins: Mechanism, regulation and function". In: *Biochimica et Biophysica Acta* 1808 (2011), pp. 1012–1020.

[86] Sharon Karniely and Ophry Pines. " Single translation—dual destination: mechanisms of dual protein targeting in eukaryotes". In: *EMBO reports* 6 (2005), pp. 420–425.

[87] Min Jeong Ryu et al. "Crif1 Deficiency Reduces Adipose OXPHOS Capacity and Triggers Inflammation and Insulin Resistance in Mice". In: *PLoS Genet* 9.3 (Mar. 2013), e1003356.

[88] Di-Feng Fang et al. "RAD23A negatively regulates RIG-I/MDA5 signaling through promoting TRAF2 polyubiquitination and degradation". In: *Biochemical and Biophysical Research Communications* 431.4 (2013), pp. 686–692.

[89] Juhee Shin et al. "Cardiomyocyte Specific Deletion of Crif1 Causes Mitochondrial Cardiomyopathy in Mice". In: *PLoS ONE* 8.1 (Jan. 2013), e53577.

[90] Jessica I. Cohen, Xiaocong Chen, and Laura E. Nagy. " Redox Signaling and the Innate Immune System in Alcoholic Liver Disease". In: *Antioxidants and Redox Signaling* 15.2 (2011), pp. 523–534.

[91] Kitti Pazmandi et al. "Oxidative modification enhances the immunostimulatory effects of extracellular mitochondrial {DNA} on plasmacytoid dendritic cells". In: *Free Radical Biology and Medicine* 77 (2014), pp. 281–290.

[92] Ralf Schreck, Kaj Albermann, and Patrick A. Baeuerle. "Nuclear Factor Kb: An Oxidative Stress-Responsive Transcription Factor of Eukaryotic Cells (A Review)". In: *Free Radical Research* 17.4 (1992), pp. 221–237.

[93] Katherine Green, Martin D. Brand, and Michael P. Murphy. "Prevention of Mitochondrial Oxidative Damage as a Therapeutic Strategy in Diabetes". In: *Diabetes* 53.suppl 1 (2004), S110–S118.

[94] J Loscalzo. "Oxidant stress: a key determinant of atherothrombosis". In: *Biochemical Society Transactions* 31 (2003), pp. 1059–1061.

[95] HENRY M. HONDA, PAAVO KORGE, and JAMES N. WEISS. "Mitochondria and Ischemia/Reperfusion Injury". In: *Annals of the New York Academy of Sciences* 1047.1 (2005), pp. 248–258.

[96] Josephine S. Modica-Napolitano and Keshav K. Singh. "Mitochondrial dysfunction in cancer". In: *Mitochondrion* 4.5–6 (2004), pp. 755–762.

[97] Robert S. Balaban, Shino Nemoto, and Toren Finkel. "Mitochondria, Oxidants, and Aging". In: *Cell* 120.4 (2005), pp. 483–495.

[98] María Monsalve et al. "Mitochondrial dysfunction in human pathologies". In: *Frontiers in Bioscience* 12 (2007), pp. 1131–1153.

Acknowledgements

First of all, I would like to thank my supervisor, Prof. Simon Rothenfußer, for giving me the opportunity to do research in this fascinating field and in a stimulating environment. Thank you also to Dr. Andreas Schmidt, who was always there and ready to give expert guidance.
Also, I am grateful to Prof. Stefan Endres for allowing me to perform this research in his department of clinical pharmacology and as a member of graduate college 1202 "Oligonukleotide in Zellbiologie und Therapie".
Thank you as well to the whole working group and department of clinical pharmacology, who created a fun and inspiring working atmosphere.
Last but not least a big thanks to my parents and my sister Britta for their endless love, support and helpful feedback, and to my friend Hong-Khoan for his technical support and patience.

Eidesstattliche Versicherung

Ich, Debra Stefanie Lietke, erkläre hiermit an Eides statt, dass ich die vorliegende Dissertation mit dem Thema

CRIF1 and its Function in Anti-Viral Immunity

selbständig verfasst, mich außer der angegebenen keiner weiteren Hilfsmittel bedient und alle Erkenntnisse, die aus dem Schrifttum ganz oder annähernd übernommen sind, als solche kenntlich gemacht und nach ihrer Herkunft unter Bezeichnung der Fundstelle einzeln nachgewiesen habe.
Ich erkläre des Weiteren, dass die hier vorgelegte Dissertation nicht in gleicher oder in ähnlicher Form bei einer anderen Stelle zur Erlangung eines akademischen Grades eingereicht wurde.

Ort, Datum	Unterschrift